PHYSICAL MECHANISM OF SILK STRENGTH AND DESIGN OF ULTRA-STRONG SILK

WU XIANG

(B.Sc., University of Science and Technology of China)

A THESIS SUBMITTED

FOR THE DEGREE OF DOCTOR OF PHILOSOPHY

DEPARTMENT OF PHYSICS

NATIONAL UNIVERSITY OF SINGAPORE

2010

I would like to dedicate this doctoral dissertation to my father, who taught me that the broadness of scientific knowledge best equips a researcher because it provides him the perception and adaptability toward a new field. Meanwhile, I also dedicate this doctoral dissertation to my mother, who taught me that simultaneous tasks need be put in order before starting any of them, and even the toughest can be accomplished bit by bit.

Acknowledgements

I am most indebted to my supervisor Professor Li Baowen and co-supervisor Professor Liu Xiang-Yang, for their invaluable advices, patience, kindness and encouragement throughout my Ph.D. candidature. I cannot grow up to be an independent researcher without their help. Professor Li provided me a global insight of a research topics, and acted as a captain guiding the direction of my research. Besides, he also shaped my mature personality, which benefits and will benefit me in my later lifetime. Professor Liu took care more of the details of my research works, such as logic, expression, and presentation. He taught me the magic to transform an experimental report to a publishable manuscript, and at the same time pushed me to better understand the motivation and the flow of my research.

I would also like to express my appreciation to Prof. Liu Zonghua, Prof. Wang Jian-Sheng, Prof. Lai Ying-Cheng, Prof. Yan Jie, Prof. Yang Huijie and Prof. Wang Wei for their guidance and help on my thesis project and my investigation of complex networks; Prof. Feng Yuan-Ping, Prof. Wang Xuesen for their support of my society works during my Ph. D. life.

Meanwhile, I would like to thank my seniors Dr. Li Nianbei, Dr. Yang Nuo, Dr. Du Ning, Dr. Wang Hui, Dr. Yuan Bing, Dr. Pan Haihua, Dr Xie Rongguo and Dr. Dario Poletti, as well as my colleagues Ms Xu Gangqin, Mr Zhao Xiaodan, Ms Yin Jianwei, Ms Diao Yingying, Ms Yang Zhen, Mr Deng Qinqiu, Mr Tan Chek Kiang Joel, Mr Toh Guoyang William, Mr Li Yang, Mr Luo Yuan, Ms Ye Dan, Ms Tang Jingwen, Mr Ren Jie, Mr Chen Jie, Mr Zhang Lifa, Ms Shi Lihong, Ms Zhang Kaiwen, Ms Ni Xiaoxi, Mr Zhang Xun, Ms Ma Jing, and all members in Prof. Li Baowen and Prof Liu Xiang-Yang's research groups. I cannot enjoy myself so much in the past four fruitful years of my Ph. D. life without them.

Finally I would like to express my deepest thankfulness to my father and mother. They are always there to encourage me whenever I was trapped in trough, and ask me to remain humble when I am faced by a contemporary success. I cannot express more of gratitude to my parents who always keep the greatest faith in me.

Table of Contents

Abstract

Natural silk fiber spinning, as one of the mainstays of the economy centuries ago, continues to exert its power in various fields nowadays. As the biggest silk provider, silkworm has a long history of domestication, and their high production volume makes it an irreplaceable stay in textile market. Besides of common role as the raw material in apparel industry, the silkworm silk has been dedicated to biomedical and military applications in recent decades. The spider silk, hailed as super fiber, is the toughest silk among natural silk family, marked by the combination of both its great strength and extensibility.

Despite of extensive studies of silkworm silk and spider silk, they remain not fully understood, especially concerning the undergoing mechanism of their good performance. Current studies ranging from micro-structure probing to mechanical measurements still have not formed a solid relation between the mechanical properties and the structures of silk materials.

Hence the general aim of my doctorial dissertation is to uncover the mystery of the mechanical properties of silk through the way of decoding the conformation of its hierarchical structures. Theoretical modeling, hand in hand with experimental

measurements and probing, turns out to be the principal method I adopted in most of the research topics to achieve the ultimate goal.

To understand the structure-property relation of silk, the structural origin of the mechanical stress-strain profiles was investigated in the first place. It was found that the existence of the β-crystallites plays an important role in the occurrence of the yield point of silkworm silk, whereas the work-toughness region of spider dragline silk was attributed to the fully dissolution of small-sized β-sheets into the amorphous matrix. Besides, the increased reeling or extruding speeds enhanced the mechanical performance of both silks, and elevated the level of the splitting force of crystallites. Such change of the mechanical strength by fast reeling was then interpreted by the properties of β-crystallites, most important of which was their orientation. It showed that better alignment of the crystallites became more efficient in resisting external stress, thus reinforcing the backbone of silk fibers. This finding also provided the engineering insight that the mechanical properties of silks, generally speaking, those of semicrystalline biomaterials, could be optimized by fine tuning of their nano-structures.

The time-resolved mechanical behavior of silks was also taken into account. Abnormal stress relaxation behavior was measured, and a bipartite pattern of stress relaxation by fixing at various strains was found with the separation strain around the yield point. More importantly, in comparison with rubber and kevlar, a much higher level of viscous energy dissipation was detected for silkworm silk at its moderate and high strain ranges, which was quantified by the Differential Relaxation Index defined in the study. Meanwhile, the linearly increased energy dissipation ratio was interpreted by the mechanism of local strain induced thickening, via the

viewpoint of the conformational change of fibrils.

The last but not least topic is the extensive investigation of the influence of twisting on the change of longitudinal mechanical properties. An optimal initial modulus of the silkworm silk was acquired by a proper extent of twisting. From a simplified elastomeric model, the threshold of massive breakage of the crystallites within the silkworm silk corresponded to the optimally twisted extent. An inferior tendency of properties at failure was detected but the twisting manner could still enhance the energy absorbability in the low-strain range.

The general aim was finally achieved by synthesizing the aforementioned topics through various dimensions, scales and domains. The high strength of silk is attributed to the highly entangled protein macromolecules,and the semicrystalline conformation of the silk molecules plays a key role in shaping its mechanical profiles, which is reflected in the stress-strain profile, stress relaxation behavior and cross-dimensional coupling. The amorphous matrix gave rise to the high extensibility of silk material while the interspersed crystalline domains reinforce the backbone of silk. The method of combining theoretical prediction and experimental verification always turned out to be a powerful strategy for soft biomaterial design. Meanwhile, by revealing the mechanism of the super-strength of silk and implementing it with feasible experimental methods, important insights were provided in the improvement of silk quality, which could further benefit the development of silk engineering and widen the application of silk.

Publications

[1]: Xiang Wu, Xiang-Yang Liu, Ning Du, Gangqin Xu, and Baowen Li, "Unraveled mechanism in silk engineering: Fast reeling induced silk toughening", *Appl. Phys. Lett.*, **95**, 093703(2009).

[2]: Zonghua Liu, Xiang Wu, Huijie Yang, Neelima Gupte, and Baowen Li, "Heat Flux Distribution and Rectification of Complex Networks", *New J. Phys.*, **12**, 023016 (2010).

[3]: Gangqin Xu, Xiang Wu (parallel first author), Xiang-Yang Liu, Ning Du, Yang Li, and Baowen Li, "Will Silkworm Silk Match Spider Silk?", submitted to *Biophys. J.*(2010). (*Gangqin Xu and Xiang Wu share equal contirubtions in this work.*)

[4]: Xiang Wu, Bing-Hong Wang, Tao Zhou, Wen-Xu Wang, and Hui-Jie Yang, "Synchronizability of Highly Clustered Scale-Free Networks", *Chin. Phys. Lett.*, **23**, 1046(2006).

[5]: Chuan-Long Tang, Wen-Xu Wang, Xiang Wu, and Bing-Hong Wang, "Effects of Average Degree on Cooperation in Networked Evolutionary Game" , *Eur. Phys. J. B*, **53**, 411(2006).

List of Tables

List of Figures

Chapter 1

Introduction

Natural silk spinning was one of flourishing economies since the technological revolution, and continued to act as a pillar industry during the last several centuries until massive manufacturing of man-made fibres obtained from feedstocks of petrochemical became popular.

Nowadays, thanks to the advancing of biotechnology and bio-mimicking methods, industries of natural silk fibers still shed light on the economy and people's daily life. Apart from the traditional application of silk, for instance, the costume production of silkworm silk, the advanced and future potential applications are more of engineering concern. Thus the fabrication of ultra-strong and multi-functional silk materials have been put on researchers' agenda. To achieve this goal, the underlying mechanism whereby silk possesses good properties, mechanical, chemical and thermal, is contemporarily most urgent task to be accomplished.

1.1 General Description of Natural Silk

Polymer composites, along with other soft materials, can be considered as a big family with similar viscoelastic properties and diversified structural features. Polymer products have been widely used in human life, ranging from costume industry to polymeric high-tech engineering. Such extensive applications of these materials can most be attributed to their high diversity of properties, especially the mechanical, chemical and thermal properties. The unique mechanical and chemical properties of polymers are highly determined by their molecular structures and conformation[1]. Polymer composites can be crudely divided into two types based on their origins: conventional polymers and biopolymers. Conventional polymers are constituted of short repeated organic monomers, and biopolymers are composed normally of longer, comparatively irregular or functional units that are originated or reproduced from living creatures. Different from conventional polymers of simply repeated blocks, biopolymers retain a great variety of the properties, including strength and extensibility.

As the most ancient biomaterial comprised of protein molecules served for human beings, silkworm silk has been in use for thousands of years by spinning from its provider - silkworm. However, silkworm (e.g. *Bombyx Mori*, in the insect order of *Lepidoptera*) is not the only provider of silk; numerous animals in the classes *Insecta* and *Arachnida* are able to produce silk, including most of the $113,000$ species in the insect order *Lepidoptera* and more than $30,000$ species of spider known up to present[2], though different kinds of silks may have various chemical composition and mechanical qualities[3–5]. Nonetheless, the silk extruded from

spiders have an excellent combination of extraordinary strength and toughness[6–9]. In this respect, spider draglines, the breaking stress of which can reach 1.4GPa, are superior to all the other kinds of silks[10]. Despite the superiority of spider draglines in strength and toughness, the aggressive nature of spider prohibits the commercial massive production of spider draglines. As a result, the high production of silkworm silk may take the role of a promising alternative to spider silks, although mechanical strength of silkworm silk is inferior to spider draglines under the current framework of processing technique.

In addition, natural silk fibers, such as silkworm and spider silks, attain good biocompatibility and environmental friendliness besides their biological or physiological functions[11, 12]. As environmental protection has become increasingly important, it is reasonable to see the increasing attention of biomaterials received from both the scientific and the engineering fields in the last decade. As a result, biomaterials have become one of the most promising candidates of conventional organic polymer product substitutes[13, 14]. Because of attractive features of biomaterials, bio-functional materials and bio-mimicking devices have started to be developed in the past few years, which boost up the relevant industries by transferring the laboratory-technology advance to their massive production. To fulfill the demand of bio-functional material and devices, the synthesized biomaterial based on bio-mimicking technology has gradually emerged; Silk engineering, as one of the principal components of the biomaterial industry, besides the endeavor of silk synthesis, has been put intensive efforts on the strengthening and functioning of the natural silk fibers.

One contemporary task is to reinforce the native silkworm fiber supported by its

high production in order to meet the social and industrial demands of silk fibers, best by the ways that are easily to be commercialized or industrialized. In that sense, several issues need to be pre-addressed in advance: 1) the structures of silkworm and spider silk in different scales; 2) the influential factors of the silk strength from the perspective of composites and micro- or nano-structure; 3) the relation between different structural factors, and their combined effects on mechanical responses; 4) probable recipes varying molecular structures or synthesizing similar protein material for the improvement of the mechanical properties of silk. Continuous efforts have being devoted on the above issues in the past century; however, the mystery of the silk strength remain unclear, and only a few experimental recipes with rare and coarse theoretical support have been proposed to date. Therefore, the study of silk started from ancestor has not yet approached an end; in turn, the silk investigation and engineering are becoming more and more broadened, deepened and diversified.

1.2 Silk Structure, Properties, and Applications

1.2.1 Hierarchical Nano-structure

Natural silk fibers are composed of protein macromolecules that are connected by amino-acid polypeptides sequentially. The most carefully characterized silks are the cocoon silk of silkworm *Bombyx mori*, and the silks from orb-weaving spiders, *i.e.* the capture and dragline threads. Among thousands of species of spiders, *Nephila clavipes, Nephila pilipes* and *Nephila antipodiana* which are famous for their woven golden orbs and hailed as "golden web spider", attract the highest attention from both the scientific and silk engineering field. Nevertheless, the two groups, silkworm silk and spider silk, share a high similarity even from its primary structure, as both of them contain high portion of Glycine ($\mathbf{NH_2CH_2COOH}$, Gly, G) and Alanine ($\mathbf{NH_2CHCH_3COOH}$, Ala, A)[15, 16]. Silkworm silk has mainly two kinds of proteins, heavy and light protein macromolecular chains, which are also termed as "Fibroin I and Fibroin II", respectively. C -Z. Zhou and S -W Ha have studied in detail the amino-acid sequence of the heaving chain. The $5,263$-residue (391-kDa) polypeptide chain comprises 12 very simple Gly-X (**GX**) repeated blocks, covering 94% of the whole sequence, where X is Alanine in 65%, Serine in 23%, and Tyrosine in 9% of the repeats[17, 18]. Broadening the scanning window, the heavy chain sequence can be further classified, among which the largest group is the **GAGAGS** repeat blocks while the irregular but evolutionarily conserved **GX** repeats are secondly dominant. The whole sequence starts and ends with completely nonrepeating sequences, and all the amino acid sequence information was obtained from the genetic decoding rather than a direct observation[18].

However, fibroin light chain is composed of very different portions of amino acids, i. e. 11% glycine, 14% alanine, 11% serine[19, 20]. On the other hand, spider draglines, functioning as the framework and scaffold of the orbs woven by spiders, are also composed of two kinds of proteins, *i. e.*, Spidroin I and Spidroin II[21]. Different from silk fibroins, spidroins are rich in Poly-Alanine domains[22]. Typically for spider draglines, the content of glycine is 37%, that of alanine and that of serine are 21% and 5%, respectively[23].

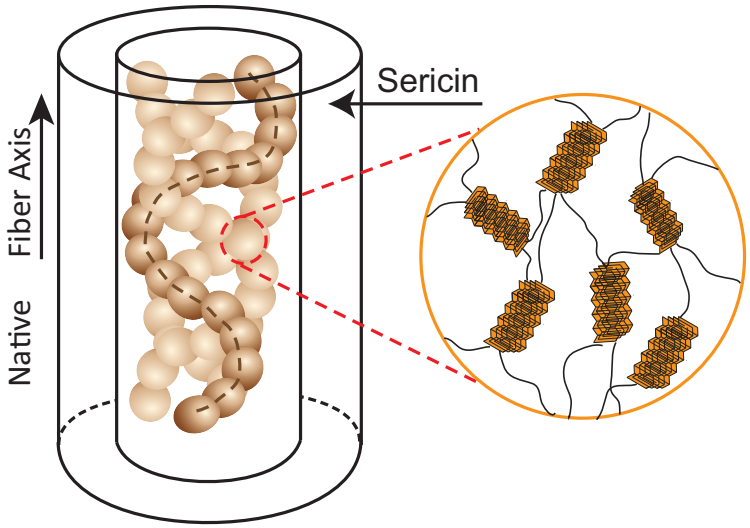

Figure 1.1: **Hierarchical structure of silkworm silk**(*Bombyx mori*). The left panel shows the conformation of the silkworm silk fibers, and the fibrilar structure composed of nano-fibrils is coated with sericin. The right zoom-in panel shows the semi-crystalline structure within each "sphere" of a strand of nano-fibril, which consists of interspersed nano-crystallites and their embedded amorphous matrix.

Beyond the primary structures of silk, X-Ray Diffraction measurements provide evidences that different segments of protein macromolecular chains may form different secondary structures, including α-helices, β-sheets, β-turns, random coils, *etc.* The pepptide crystalline repeats are mainly contributed by the heavy chain

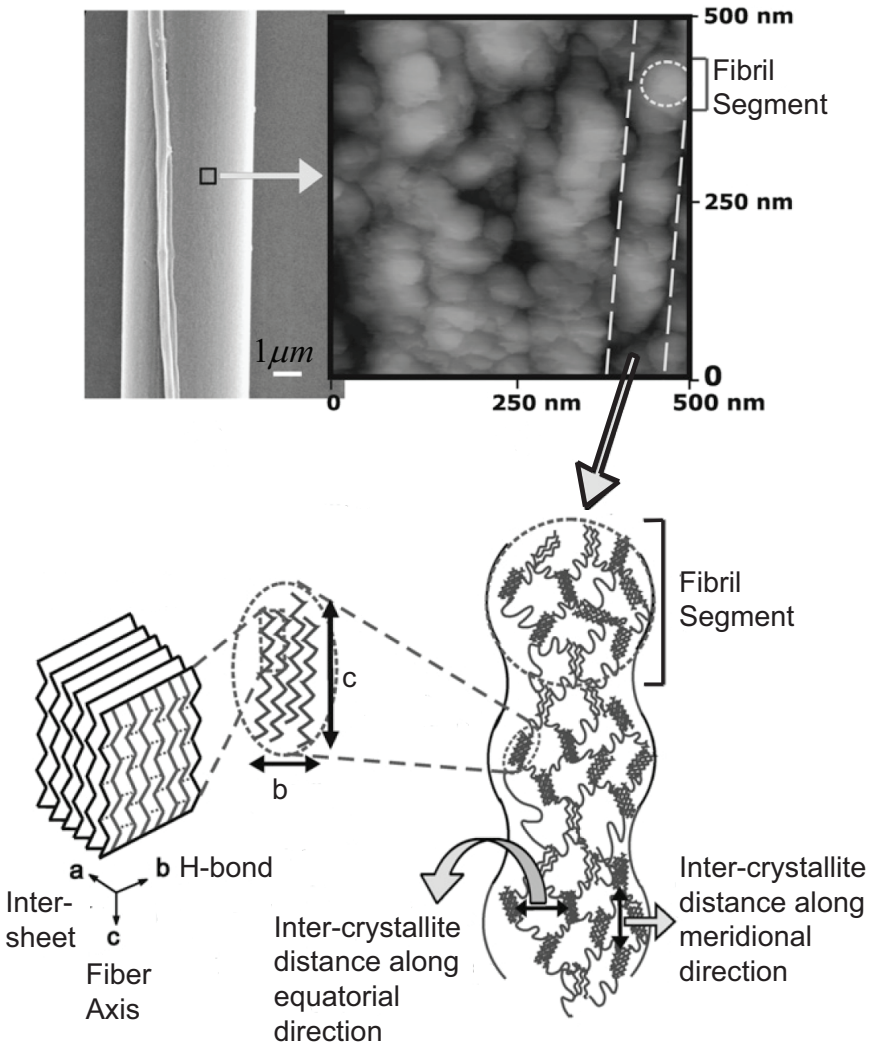

Figure 1.2: **Hierarchical structure of spider dragline silk**(*Nephila pilipes*). (Redrawing of Fig. 1 from ref[10]) The Scanning Electron Microscopy(SEM) image of spider dragline silk located at the upper-left corner shows its surface; The zoom-in Atomic Force Microscopy (AFM) image located at the upper-right corner shows the fibrilar structure as indicated by the bright dashed straight lines. The lower-right panel shows an inter-connected pattern of amorphous matrix and crystallites. The mesh size of the network can be characterized by the inter-crystallite distances. The crystallites in each fibril are composed of multiple β-sheets shown in the lower-middle panel. The unit cell of crystallites has an antiparallel β-sheet configuration, shown in the lower-left panel.

fibroin of silkworm silk, which are regarded as $\mathbf{GAGAGSGAAG[SG(AG)_2]_8Y}$ (S=Serine, Y=tyrosine), while the amorphous matrix is not specifically defined, but generally it includes the less ordered β-sheets, turns and coils[24]. However, from the Wide Angle X-ray Scattering halos, the α-helices are rarely seen for bio-spinning silkworm silk. During the process of spinning, the concentration of silk proteins in glands gradually increases, and metallic ion content, as well as the pH value in the solution are well controlled. An elongational stress is then applied near the "spigot" to extrude the semi-crystalline and insoluble fiber threads, rich in β-sheet crystallites[25–30]. The detailed structure of β-sheet crystallites of silkworm silk was characterized by Nicholson *et al.*, by Marsh *et al.*, by Takahashi *et al.* and by Shen *et al.* most recently[31–34]. The β-sheet crystallites are formed by the adjacent protein molecule segments folded into β-sheets within individual molecules, and their lateral size was measured to be 1 to 24nm, and their axial size varies from 20 to 170nm[34]. An illustration of hierarchical structure of silkworm silk is shown in Fig. 1.1. The sericin is coated on the undegummed silk fibers. Besides, each strand of undegummed silk is constituted of two filaments, each of which have a semi-circle shaped cross section. A number of studies characterizing the secondary structures of spider dragline silk were carried out by groups of researchers, and it was found that different from *Bombyx mori* silk which contains a high portion of β-sheet crystallites, the crystallinity within spider dragline silk is lower[35–37]. In both kinds of silks reeled or extruded from silkworms and spiders, the crystalline structures are interspersed in the amorphous matrix. The hierarchical structure of spider dragline silk is illustrated in Fig. 1.2. The fibrilar structure is constituted of interconnected "fibril segments" as indicated by the dashed circles in the lower-right panel of Fig. 1.2, sized from 40 to 80nm. They consist of

several intra-molecular β-sheets and inter-molecular β-sheet crystallites, which are inter-connected by amorphous matrix. The size and orientation of inter-molecule β-sheet crystallites can be determined by X-Ray Diffraction (XRD) measurements. The structural differences between the two kinds of silks refer to the existence of intra-molecular β-sheets, and the size and orientation of the inter-molecular β-sheet crystallites. Such structural differences look minor to the whole construction of silk conformation, but will lead to the difference of their mechanical responses. This issue will be discussed in Chapter 2 in details.

1.2.2 Mechanical Performances

Besides the ubiquitous hierarchical structures in silk materials, the properties of different species of silk deviate from each other. Cocoon silkworm silk fibers from domesticated *Bombyx mori* have been used in the textile industry for thousands of years due to their good mechanical properties, lucidus appearance, lithe texture and dye-ability. Recent studies explored their excellent tissue compatibility, high oxygen permeability and ready availability for increasing interests in biomedical and biotechnological applications[13]. On the other hand, spider silk fibers attract more and more practical interests not only because of their superior mechanical properties, but also many unique features such as supercontraction and torsional shape-memory effect[38–41]. Among all the features of natural silks, mechanical properties, including the high strength and toughness of some kinds of silk, are most worthwhile for investigation, because they may provide the insight to man-made fiber engineering by biomimetic synthesis. The comparison of mechanical

properties of silks and some good-performance man-made fibers from the view of failure characteristics is presented in Table. 1.1.

Table 1.1: Mechanical Properties of Polymeric Materials

Material	Strength(GPa)	Extensibility(%)
Dragline Silk	1.4 [10]	35 [10, 43, 44]
Cocoon Silkworm Silk	0.5 [45]	15 [45]
Forcibly Reeled Silkworm Silk	$\sim$ 0.8 [46]	35 [46]
Kevlar	4[43]	4 $\sim$ 5[43]
Rubber	1×10^{-3} [43]	600 [43]
Tendon	1 [43]	5 [43]

From that table, one can easily distinguish that the failure features of silks and other polymeric materials, by their modest combination of breaking strength and extensibility. Kevlar® family (e.g. 29, 47, 49) have a high strength about 4GPa, but a low extensibility less than 4%[42]. On the contrary, rubbers have a high extensibility from 300% to 500%, depending on their composites; however, their breaking strength are usually 3 orders of magnitude lower than Kevlar. Neither brittle nor weak, as silk materials are referred to, the combination of high strength, though inferior to Kevlar, and the high extensibility make them highly energy dissipative material, as they possess high toughness[6–9]. One highlighted remark tells that one strand of pencil thick spider dragline silk can stop a Boeing 747 in flight[47]. Besides of the rupture behaviors of silks, a typical mechanical profile (stress-strain curve) of the spider dragline silk is illustrated in Fig. 1.3. Zemlin pioneered the mechanical property investigation of numerous species of orb-weaving spiders, including *Nephila Clavipes, Nephila Antipodiana, etc*[48]. For *Nephila Clavipes*

spider major ampulate (MA) dragline silk, the elastic modulus was measure as 12.0 ± 5.2GPa, the tensile strength as 0.950 ± 0.381GPa, and the tensile strain as 16.9%. These quantities are inferior to *Nephila Pilipes*, which were measured by Du *et al.*[10].

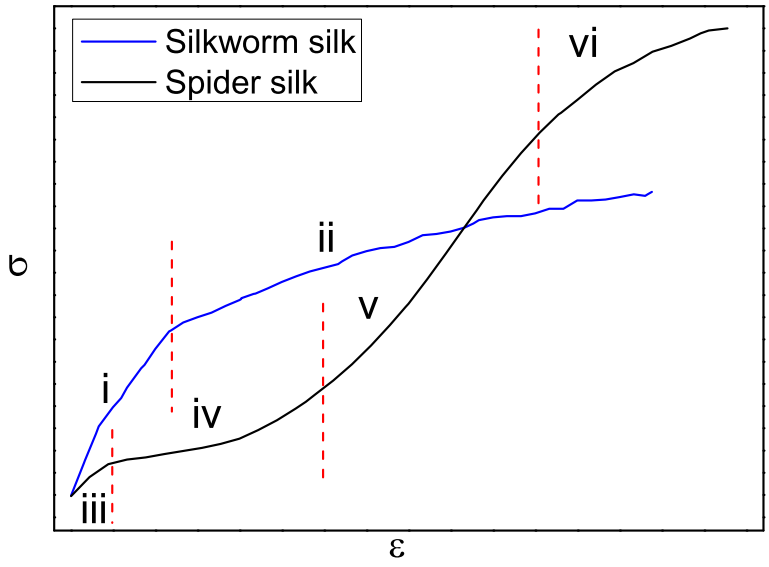

Figure 1.3: **Mechanical Profiles of Silkworm and Spider Silks**. Stress-strain relation is shown for both silkworm and spider dragline silks, where σ represents the tensile stress, and ϵ represents the tensile strain of silks. (i) and (ii) respectively denote the linear and post-yield region of stress-strain profile for silkworm silk; for stress-strain profile of spider silk, (iii) and (iv) denote the linear and first post-yield regions; tensile strength increases in region (v), and (vi) denotes the "second post-yield" region.

Attracted by the superiority of spider dragline silks, researchers are dedicated into spider-silk-like fiber synthesis since the last decade. One feasible way is biomimetic regeneration and recombination of spider silk and silkworm silk. Zhou *et al.* and

Yan *et al.* extruded silk (*Bombyx mori*) fibers from aqueous silk fibroin solution, subjected to different spinning conditions[49, 50]. Zhou showed a superiority of regenerated silk fibers from fibroin solution with respect to their mechanical properties through the extruding fashion to native cocoon silk fibers[49]. Slower extruding rate brought about a higher mechanical response. The influential factors of the mechanical properties of regenerated silk fibers were comprehensively discussed in Yan's work, including the effect of dope concentration, coagulation bath, extrusion rate, and postdraw treatment on the morphology and mechniacal properties of regenerated silk fibers[50]. An optimal dope concentration will cause a morphology of the regenerated silk fibers closest to the native ones, and a postdraw manner enhances the mechanical performance significantly. However since an earlier age, silk fibroin solution has been extruded to filmy structures, i. e. fibroin thin films[51–53]. The dynamic mechanical and thermomechanical behaviors of silk fibroin film were explored, where an increased thermal stability is found to be attributable to the β-sheets formation. The factor of drawing rate was examined by Kameda (Hornet Silk Gel Films) and Jiang (ultra-thin fibroin film)[52, 53], and better aligned crystallites and helices, as well as an increased crystallinity is the most probably reason for high rate reinforcement.

Besides, physical methods are more accessible and economic than the regeneration or recombination ways. The mechanical strength of silkworm silk and spider dragline silks are both subjected to the reeling or extruding speed from silkworms and spiders respectively, as can be seen in Fig. 1.4. The higher the reeling/extruding rate, the higher the breaking strength; Du *et al.* also measured the change of structural properties, such as crystallite size, crystallinity and crystallite

orientation[10]. However, the undergoing mechanism of this mechanical universality remained unknown at that time. Interestingly, from the measurements of the mechanical strength of both species, the breaking strain with high reeling rates does not drop dramatically, shown in panels (a) and (b) in Fig. 1.4(panel (b) shows an obvious decrease of the breaking strain for higher reeling rate, but the later repeated experiment by averaging over 24 samples per data plot conducted by us supports my statement(details will be shown in Chapter 3).) The toughness, defined as the under area of the stress-strain profile, of both silks will be enhanced by increasing the reeling rate. In other words, silk materials are good energy absorbing materials against high-speed collision.

Other chemical and genetic methods are also available now though either the experiment conditions require very fine control or the silk sample experiences a harsh solution or radiation during the experiment. One of these is the birth of transgenic goat or "spider goat", which can produce silk by refining its milk[54, 55]. The strength of such silk is comparable to that of steel. Lee *et al.* demonstrated that metals can be intentionally infiltrated into inner protein structures of biomaterials through multiple pulsed vapor-phase infiltration performed with equipment conventionally used for atomic layer deposition (ALD)[56]. Through infiltrating metallic particles, such as zinc, titanium and aluminum, combined with water from corresponding ALD precursors, into spider dragline silks, greatly improved strength and toughness of the treated silk, has been observed. The strength of treated *Araneus* spider silk is about 4 times of the native silk while the toughness of the treated spider silk may reach $6 \sim 8$ times of the native toughness. The aforementioned two methods play roles like the shining stars among the extensive

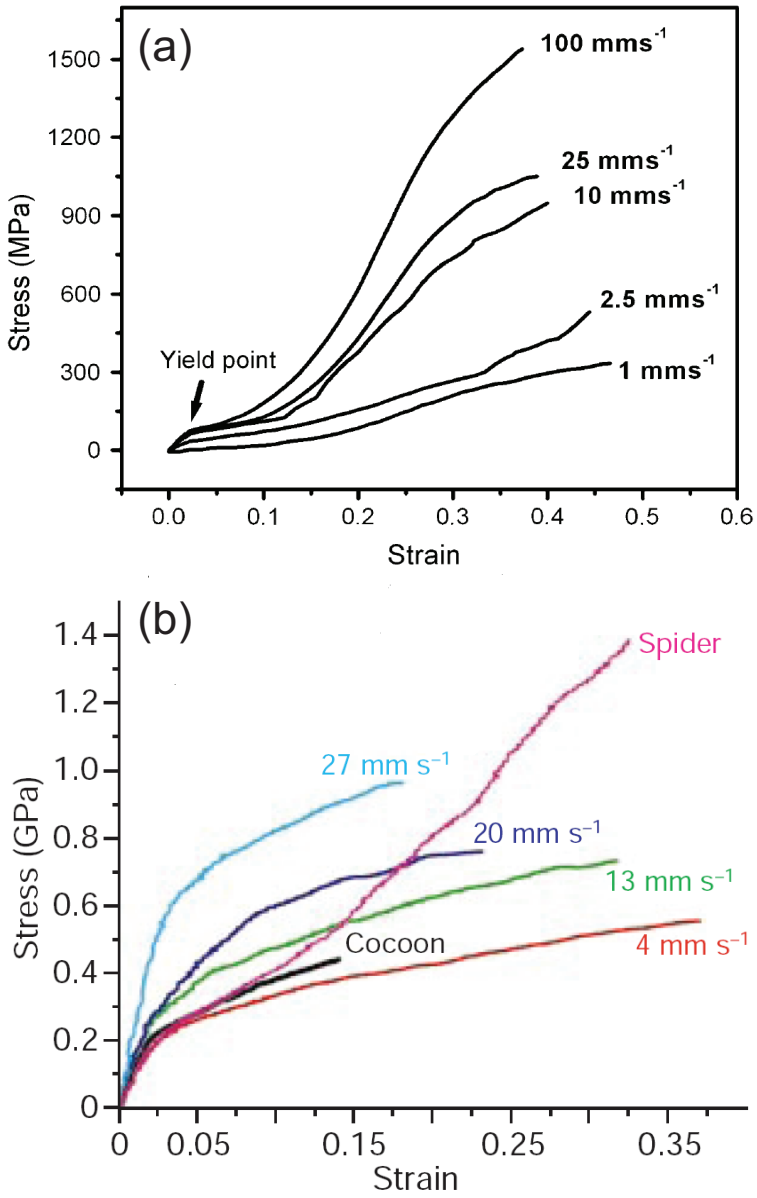

Figure 1.4: **Mechanical Profiles of Silks under Various Reeling Rates.** (a): Stress-strain profile of spider dragline silk under extruding rate from $1mms^{-1}$ to $100mms^{-1}$(*Nephila Pilipes*)(Fig. 8 of ref[10]); (b): Stress-strain profile of spider dragline silk under extruding rate from $4mms^{-1}$ to $27mms^{-1}$(*Bombyx mori*)(Fig. 8 of [46]).

endeavors of silk engineering and decoration, but there is still a long way to go for its industrialization or commercialization despite the greatness of the enhancement of silk quality.

Besides of the aforementioned excellent mechanical performances of synthetic or natural silks and the various ways for their elevation, the dynamic time-resolved behaviors were widely studied as well. Previous results suggested that the mechanical properties of silks deviated only a little in the limit of high strain rate and quasi-static (strain rate$\approx$ 0) process. Cunniff *et al.* displayed a comparison between the a ballistic and quasi-static static measurements for spider silk in Table 1.2. From that table, one can see the similar values of initial modulus and breaking strain of *Nephila clavipes* spider silk, but there is no convincing evidence of the time resolution for ballistic test and justification of the modeling which roughly estimated high-strain rate properties of the relaxed state.[6]. On the other hand for silkworm silk, similar conclusion was drawn that changing the stretching rate could vary its mechanical strength but only by less than 15%, which was very minimal compared to other elastomers like collagen and elastoidin[57, 58]. Parthasarathy *et al.* determined the viscoelastic properties of silkworm (*Bombyx Mori*) silk by distinguishing the contributions from the elasticity, plasticity and viscosity, respectively[57]. Very recently, a shape-memory effect was solely found in the time-resolved torsional behavior of spider dragline silk. Such unique property, as a result of nature selection, is distinguished from other metal strings or organic fibers, which prevents the spiders from a non-preferential spinning when the silk was used as a lifeline attached to a fixture[40, 41].

This section briefly introduced the mechanical properties of silkworm and spider

Table 1.2: Mechanical properties for High and Low Strain Rates (Table 3 of Ref[6])

Properties	Quasi-static	Ballistic
Initial Modulus (GPa)	22	22.3
Secant Modulus (GPa)	13	10
Ultimate Tensile Stress (GPa)	1.1	N. A.
Ultimate Tensile Strain (%)	9	10

dragline silks. Spider draglines process high strength and toughness, which is superior to silkworm silk and other fibers. Worthwhile endeavors have been dedicated in improving silk quality to be ultra-strong or ultra function, as well as drawing silkworm silk closer to spider silk, with respect to its mechanical performances. Such extraordinary properties of silk, including with the potential of their continuous improvement, open them multiple channels to their extensive applications, which will be reviewed in next section.

1.2.3 Existing and Potential Applications

Since 1980s, the unique balance of material properties, i.e. good tensile strength, extensibility, and the energy absorbing capability, is the principle driving force behind of continuing interest in silk engineering. The *Bombyx mori* silkworm was domesticated for more than five thousand of years, and their silk has continued to be used for costume industry[59]. The quality of silk is highly dependent on the species, the living environment, as well as the food the silkworm takes. The spider silk, attributed to its extraordinary mechanical properties, has been more and

more attractive for its various potential applications. As widely known, silkworm silk was firstly initiated to for costume industry and "Bo"(which was used for write substrate before the invention of contemporary paper). The Silkworm silk's absorbency makes it comfortable to wear in warm weather and while active, and its low conductivity keeps warm air close to the skin during cold weather. The costume manufacture family includes the clothing such as shirts, ties, blouses, formal dresses, high fashion clothes, negligees, pajamas, robes, skirt suits, sun dresses and kimonos[60]. The silk industry, referring to the aspect of costume manufacture is still flourishing nowadays, and it will continue to be an irreplaceable stay of the social economy in the foreseeable future.

Dating back to the era of Ghengis Khan, the silkworm silk, combined with leather, were started to make the body armor of warriors, preventing the injury and death from arrows[61]. Such kind of extension of silk application was not *ad hoc* but was conducted in various places and dynasties. Due to the high strength and extensibility, silks can be made into ropes and cables, which outperform the ones fabricated by nylon. One example is the high extensibility and possibility of encoding saltwater protection into a silk-based fibrous material[62]. Besides, the strength combined with the light weight of silk fibers may arise the substitution of fish net/cable material, as well as a new generation of parachutes, gliders or sailing boats. The dyed silk, which has been demonstrated in conventional textile silk industry though technically it has yet been popularized, has great advantages to other man-made costume materials.

In recent decades, thanks to the development of the degumming technique, the biocompatibility and bio-degradability were recognized of silk fibroin which is the primary component under the sericin coating. Altman *et al.* reviewed the bio-medical applications of silk from 1990s onwards[13]. Among those newly developed biomedical applications, one of the most popularized applications is surgical suture. Sutures require the following characteristics for general surgical applications[63, 64]:

I. Tensile strength − to match the clinical repair.
II. Knot strength − the amount of force required to cause a knot to slip.
III. Elasticity − the ability to conform to the current stage of wound repair.
IV. Memory − change in stiffness over time; the better the suture,the less memory.
V. Degradability − ability to be metabolized by the host once its repair function has been completed.
VI. Tissue Reactivity − non-irritant.
VII. Free from infection − related to the materials geometry.

The silkworm silk turns out to be good candidate for its satisfaction of the above concerns to a large extent. Besides, silk matrices are now being rediscovered and reconsidered (due to the technique of sericin removal which recovers the biocompatibility of silk) as potentially useful biomaterials for a range of applications in clinical repairs and in vitro as scaffolds for tissue engineering[65]. These applications, including the role as surgical sutures, are beneficial from the properties of silk, while there remain concerns where precautions may be paid, listed as follows:

Advantages:

I. Novel mechanical properties of some silks (e.g. *Bombyx mori* silk), outperforming other natural fibers and rivaling many synthesized fibers.

II. A long standing history and the tradition of usage of natural silk fibers in clinical applications.

III. A mild processing way of natural fibers in aqueous solutions for subsequent formation of films and other material formats, with relatively simple insolubilization via exposure to alcohols and other environmental factors.

IV. Capability of easy chemical modification with surface decorations,such as adhesion sites or cytokines, due to the availability of amine and acid side chains on some of the amino acids.

V. Genetically tailorable composition and sequence to moderate specific features,such as molecular weight, crystallinity, solubility.

VI. Slow rates of degradation both in vitro and in vivo; Particularly useful in biodegradable scaffolds desiring slow tissue ingrowth.

VII. No risk of bioburden.

Concerns:

I. Adequate removal of contaminating sericin from silkworm silk to avoid biocompatibility problems.

II. Slow degradation of crystalline (β-sheet) regions.

III. Aborted proteolytic attack by macrophages and giant cells leading to encapsulation and the formation of a granuloma.

IV. Potential sensitization to silk fibroin resulting in an allergic response upon exposure to the biomaterial.

Tissue engineering required diversified portfolio of biomaterial to follow the pace of the development of *in vitro* and *in vivo*. Silk may play a role of the matrix which assists communicating or transducing the environmental information, minerals and cell feedstock from the external to cell located on it. The function of the silk matrix is actually promote the biologically feasible cell-environment functions, and the silk matrix is appropriate for cell attatchment, diffusion, growth, differentiation. Meanwhile, after the removal of sericin coated on the silk, silk matrix is also possible to be bio-degradable by the host cells while the rate of biodegradation must be slower than that of the cell growing rate.

Quite of a few groups have demonstrated that either silk fibroin film or wire/rope-like fibroin matrix as scaffold is feasible in cell culture for certain species of cells. Inouye *et al.* and Minoura *et al.* compared the silk fibroin film with the sericin matrix and the traditional used collagen, and found that the degummed silk fibroin film turned out to be a good candidate as cell culture matrix[65, 66]. Altman *et al.* chemically decorated the fibroin film with the RGD peptide, and found that the bone formation rate with the seeding of bone-forming cell (Osteoblasts) was significantly enhanced by tracking the increased alkaline phosphatase and calcification levels, as well as the up-regulation of the relevant transcripts[67]. They proposed that the utility of silk as a tissue engineering scaffold is attributed to two reasons: 1. the extraordinary mechanical properties and biocompatibility; 2. diversified coupling sites for selective chemical coupling. The superiority of silk fibroin matrix emerges comparing with collagen when they are used for ligament formation. Dunn *et al.* clarified that the poor performance of collagen in ligament cell formation was because of the dynamic and mechanically demanding features[68, 69].

Besides, they seeded anterior cruciate ligaments (ACL) using a patients own adult stem cells *in vivo*, as well as seeded Human bone marrow stromal cells (BMSCs) *in vitro*. Additionally, one point need to be highlighted is the long-term absorbtion of silk material, which matches the growing rate of quite a number of host cells.

Besides of the boom of the biomedical application of silks or silk fibroin, the role in military application as a body armor continues. Different from Ghengis Khan's time that body armor was used to prevent the attack from arrows, the body armor refers to the modern bullet-proof vest. Currently most of the bullet-proof vest is made of Kevlar, which is strong and brittle (Table 1.1); however, the cost of such a vest is extremely costly. The high strength and toughness of silk made it an alternative material in fabricating the "soft proof vest" which has a comparable protection level against shooting bullets[70, 71]. Moreover, the cost of fabricating silk bullet-proof vest is far more economic than the Kevlar one, and its comfortableness is better than that as well.

High-tech applications of silks do not fully rely on the strength and toughness of silks. In turn, many new development applications are based on silks' other eye-catching properties. For instance, supercontraction is one specific property of spider dragline silk, and this may make impact on sensitive impact systems[72]. The absence of the kink-band structure of silk which leads to a high compressive strength may apply to certain structural components to prevent impact damges[73]. Function silks are nowadays popularized by coating, depositing or penetrating nano-sized clusters or particles onto the silk/silk fibroin film surface or into their fibrillar structures, such as $\mathbf{TiO_2}$, $\mathbf{TiO_2/Ag}$ and **FePt** nano-particles. These works are carried by our group and in progress currently.

Last mentioned in this section but not least the patterning and templating on silk fibroin films or matrix. Lotus effect with superhydrophobicity has been achieved by patterning the silk fibroin film analogous to the lotus leaf. Enhancement of luminescence have been acquired by nano-structured patterning by Ganesh and Zhang[74, 75], and such dramatic increment of the luminescence density is purely caused by structural reason. In this sense, silk fibroin matrix turns out to be a kind of excellent patterning material for structure induced enhancement of luminescence and structure color[76].

The section summarizes the traditional, contemporary and future applications of silks. The diversity of silks provides a big pool for choosing demanding material candidate, and excellent mechanical performance stands a basis where silk applications can be branched into various fields. Supercontraction, wettability, patterning variability, together with their bio-compatibility and bio-degradability give of silks give rises to an increasingly broadened application scope, such as sensitive composites, luminescence enhancement, biomedical applications including surgical sutures and scaffold of tissues, as well as the costume industry which still flourishes nowadays.

1.3 Theoretical and Computational Modeling of Silk

Benefited from their extraordinary mechanical properties, silkworm and spider silks have been receiving extensive attention thus continuous applications are brought about, which is presented in section 1.2. From the biomimetic viewpoint, to understand the mechanism why silks have such high strength comparing with other protein polymeric biomaterials turned out to be an imperative task, which generations of researchers, including physicists, chemists and mechanical engineers have made efforts on. Theoretical frameworks and computational simulations carried out for explaining the silk strength are generally divided into two groups according to the studied scales: 1): microscopic molecular modeling of silk protein macromolecules; 2): meso/macroscopic study, including coarse-grain modeling and thermodynamic analysis.

1.3.1 Molecular Modeling of Silk Proteins

Molecular modeling of silk fibroin dates back to Marsh's work who proposed the first detailed structural model for Silk II, the conformation of fibroin in spun silk comparing with the one dried without mechanical stimulus from silk solution/gel[31, 77]. The basic feature of silk II conformation was proposed to be the β-pleated, which was later widely accepted as one important secondary structural domain. Zimmerman, Chou and Fossey calculated the conformational energies of single or multiple-stacked β-sheets using **ECEPP1/2**(Empirical Conformational Energy

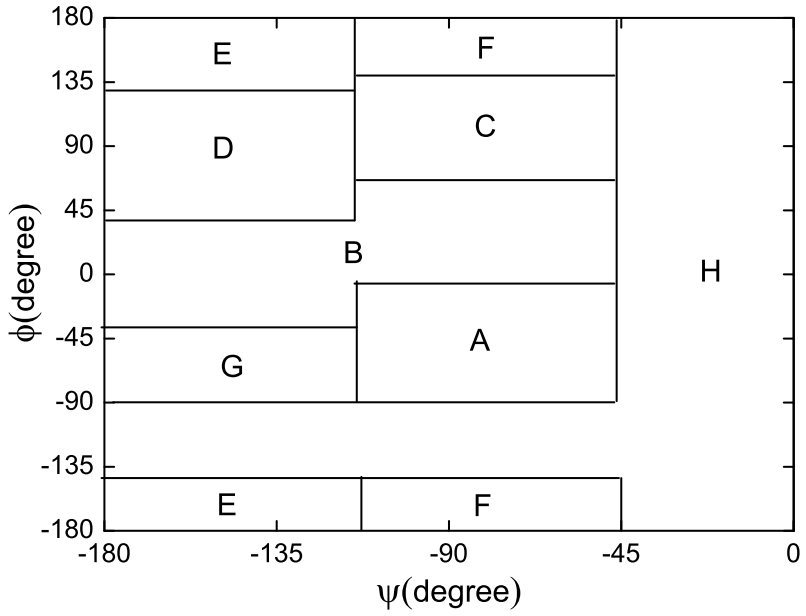

Figure 1.5: **Dihedral Angles of Fibroin Side Chain at Energy Minima**(Redrawing of Fig. 1 from Ref[78]). Region A is the contains the right-handed α-helical conformation at minimal energy; Region A, C, D, E, G contain the five local lowest-energy minima of alanine; Region F contain some energy minima of amino acids (not glycine and alanine); Region B and H denote the moderate energy bridge and high energy region, respectively.

Program for Peptides 1 or 2)[78–81]. The dihedral angles of the side chains within silk fibroin were calculated at the same time. A typical ϕ-ψ map was shown in Fig. 1.5. The Ala residues in β-sheet crystallites show the dihedral angel(ϕ, ψ) of $(\pm 135°, \mp 150°)$, and the Gly residues in amorphous region show that of $(\pm 60°, \mp 135°)$, which is a criteria in later molecular modeling simulation[82]. Moreover, the dimensions of the unit cell were determined for both forms existing the Silk I as $a = 0.894nm$, $b = 0.646nm$, $c = 1.126/1.213nm$[78].

Accompanying with rapid development of computer power including the doubled

speed of CPU every 18 months and dramatically increased capacity of memory, computational simulations are feasible to be performed on large-scale systems. Effective force field (EFF) methods, as applied to calculate the conformation and dynamics of macromolecules (e.g. DNA, proteins) started developing since 1980s. **CHARMM** (Chemistry at HARvard Macromolecular Mechanics) pioneered to embed the various force-field sets into molecular dynamics simulation package written in Fortran 77/95[83], which is suitable for the EFF simulation for kinds of macromolecules. This package is still updating nowadays by incorporating newly pop-up and widely accepted force fields into it. **GROMACS** (GROningen MAchine for Chemical Simulations), **AMBER** (Assisted Model Building with Energy Refinement), **NAMD** (Not (just) Another Molecular Dynamics program) were the recently developed packages/softwares implementing force fields like Charmm++ and OPLS (Optimized Potentials for Liquid Simulations), satisfying various molecules, conditions and dynamic concerns[84–87]. The differences between these packages are not restricted to the force fields; more importantly, they applied different computational methods according to different target problems, which cause their different simulation efficiency.

The EFF method was applied to the conformation of silk fibroin before spinning using **AMBER**, typically for individual Gly, Ala and Ser in water solution, as well as a short chain of repeated GA blocks or GAS tri-peptide[88]. The dihedral angle of Gly, Ala and Ser were most concerned in validating the advances of their simulation method. Recent works done using **NAMD** and **CHARMM** by Keten and Nova investigate the fibroin and spidroin in native silk fibers[82, 89–91]. They attributed the strength and toughness to the β-crystallites of silk, which play

the role of molecular junction. The dependence of mechanical properties on the dimensions of crystallites was well characterized. Meanwhile, the simulation of a crystalline-amorphous complex turns out be an important mark since it represents the experimentally detected nano-structure of silk fibers, an amorphous matrix interspersed with β-crystallites. The molecular simulation scale has now been extended to the level shown in Fig 1.6(c).

Conformational energies calculation of peptide residues cannot provide sufficient information to meet the contemporary desires due to the loss of the molecular structures or conformation under different micro-circumstances. The development of molecular dynamics and EFF packages give rise to the feasibility of protein molecular properties with respect to its conformation. Although such modeling cannot easily go to macroscopic scale and does not incorporate the high-level structures into account, the mechanical responses of the secondary structural elements somehow are consistent with the high strength and toughness of silk materials.

1.3.2 Coarse-grain modeling and Thermodynamics

Macro/mesosopic modeling is an alternative way to interpreting the mechanism of the high silk strength with respect to its hierarchical structures. Elastomeric theories (e.g. kinetic theory) are well applied for spider dragline silk after supercontraction, since supercontracted silk behaves like rubber due to the water penetration, which breaks its ordered nano-structures to be coiled ones[59, 92, 93]. Non-gaussian model was first proposed by Treloar, with a description of finite-sized random-walk network[94]. It was found from the non-gaussian modeling that the

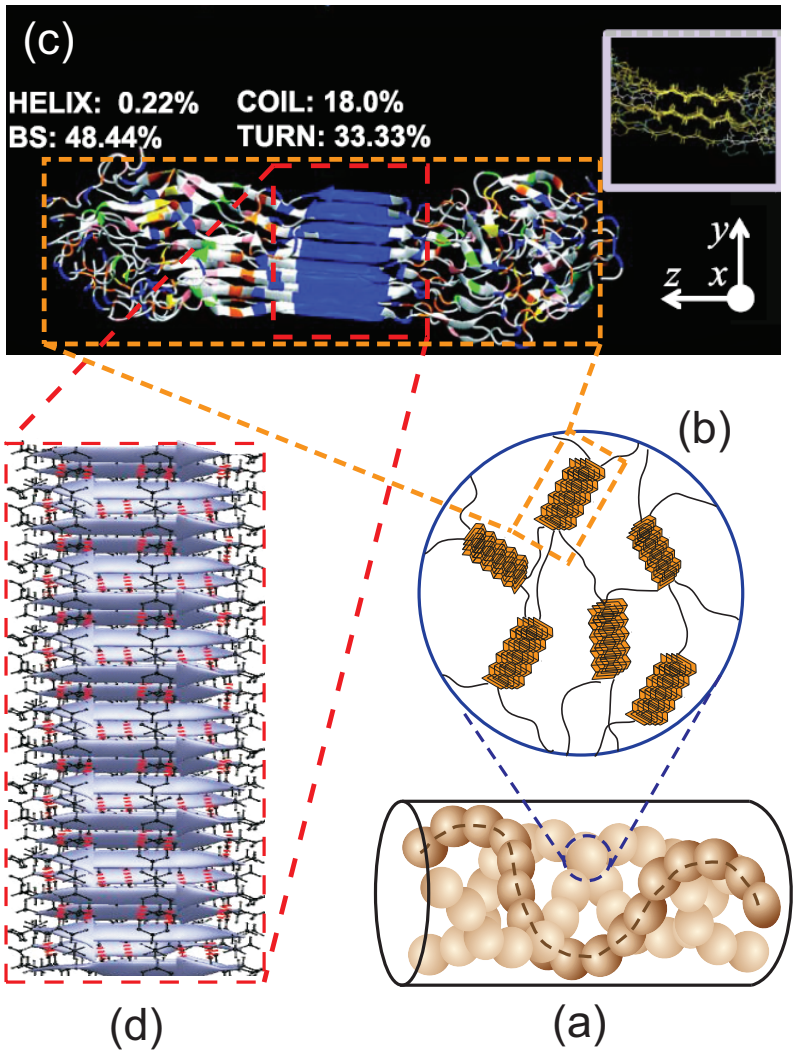

Figure 1.6: **Molecular Simulation Levels in Structural Hierarchy of Silk** (a) Illustration of silk fibers, composed of bundled nano-fibrils. (b) An ellipsoidal unit of a nano-fibril; the fibrils are constituted sequentially by these units (non-branching). (c) A simulated crystalline-amorphous complex composed a crystallite and attached amorphous fibroin chains. (d) A simulated conformation of β-crystallite; it is stacked by layers of β-sheets within which the β-strands are closely packed by hydrogen bonds.

dramatic increase of supercontracted spider dragline silk causes a small value of step size of random walk. The modeling parameter "links per chain", which fits the force-extension profile of supercontracted silk and equivalent to the random walk size was determined to be $0.4 \sim 2.86$ with various strain amplification strategy. The shear modulus (G) was also estimated which made it possible to obtain the average molecular weight of the network chains between crosslinks[94, 95]. This method using random walk theory is to consider spider dragline silk as a kind of elastomer while the supercontracted dragline silk was found to be the modeling counterpart. Group interaction modeling method was developed from later 1980s to early 1990s by Porter, and some of the theory are applicable to silks, such as glass transition and the "yield-break" stress relation, the latter of which is referred to the domain size within materials[1].

The network relevant theory and modeling mentioned above was made a breakthrough by Termonia, for the novelty of incorporating a simplified secondary structural conformation of spider silk[96]. Although that modeling was termed as "molecular modeling" as discussed in section 1.3.1, it is, to our present understanding, more suitable to be grouped into coarse-grain modeling. This model discussed conformation with secondary structural domains, i. e., crystalline and non-crystalline (amorphous) domains. The crystallites were interspersed in the amorphous matrix, of which the "junctions" in the amorphous matrix were assigned at the lattice sites as crystallites (Fig. 1.7(a)). By setting the two domains satisfying different mechanical responses, the collective stress-strain profile was well reproduced[97]. This is the first work integrating the nano-mechanics and nanostructures to produce the mechanical properties of the whole construction of spider

silk material. Another extension of the elastomeric modeling was carried by Zhou *et al.*, as was illustrated in Fig. 1.7(b). The focus of the model was shifted from the nano-mechanical behaviors of the semicrystalline domains to the structural hierarchy of the viscid spider silk (capture silk)[98]. The hierarchical structure of spider silk makes the presence of the dramatic increased elastic modulus in their mechanical profile, whereas the order of the hierarchy was not specified. Interestingly, the model is robust to the very form of the nano-mechanical responses.

Porter *et al.* proposed a nanostructured polymer model of spider dragline silk. Imposing the mean field theory for polymers in terms of chemical composition and the degree of orderliness in their polymeric structure, the full range of thermo-mechanical properties of spider draglines were predicted, such as elastic and lost modulus, as well as the stress-strain profile[99]. The cohesive energy difference and the fraction of ordered structure turn to be two most important factors determining the mechanical and thermal properties of silk polymeric material, and the modeled envelop meets the experimental data well(Fig. 1.8). This model was reviewed by Vollrath, who asserted that spider silk is an archetypal model for elastomeric protein material study[100, 101].

Attempts of multiscale modeling of silk material have been made in recent years. By synthesizing the MD simulation results in atomic or residual (or C^{α}) level for a single crystallite composed of several β-sheets, or for a confined region of amorphous matrix, the collective mechanical response is possible be to integrated on a larger structural scale of silks, typically for crystalline-amorphous constitution[91, 102]. The development of the "bottom-up" method is crucial for

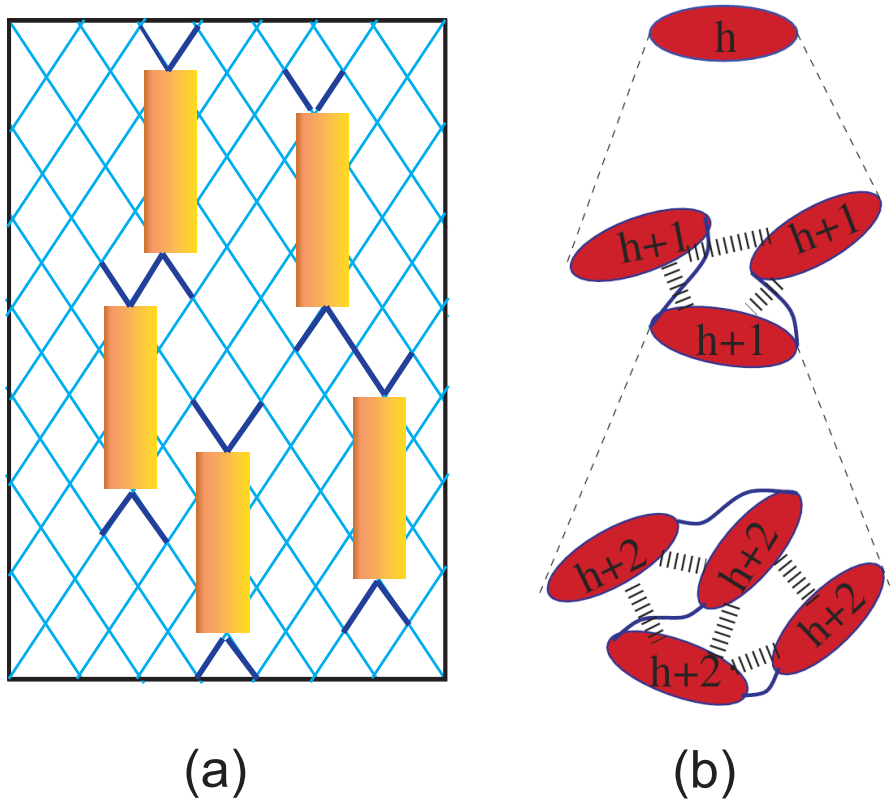

Figure 1.7: **Elastomeric and Hierarchical Structural Modeling**. (a) Schematic representation of the elastomeric model for spider dragline silk: the amorphous chains have been denoted by the cross-linked solid cyan thin lines; the crystallites are denoted by the brown squares; thickened dark blue lines indicate the high-modulus layer in the amorphous matrix. (b) Schematic representation of the hierarchical chain model for spider capture silk. $h/h+1/h+2$ are the level indices, and the dotted line means the inclusion relation of level $h+i+1$ structure and a subunit in level $h+i$.

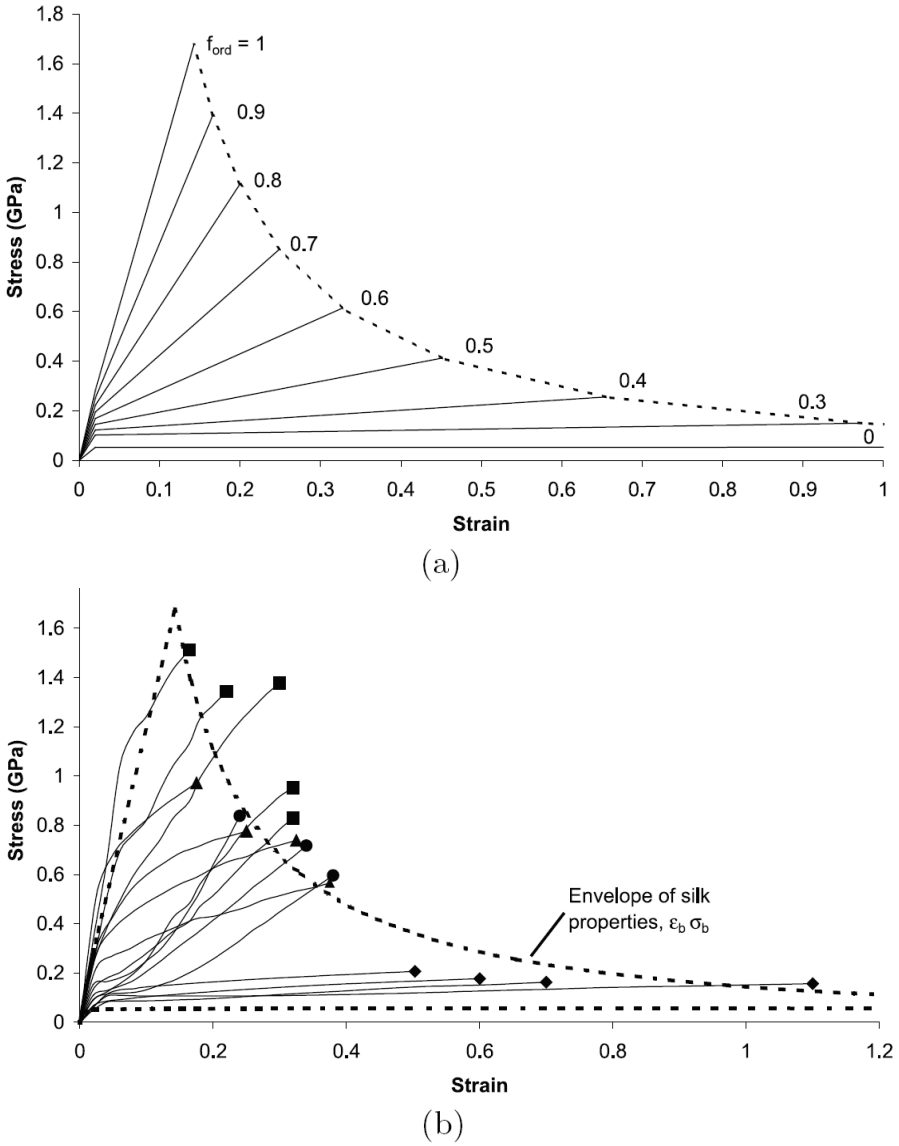

Figure 1.8: **Stress-strain Profiles for Various Crystalline Orderliness Fraction**(Fig. 4 from Ref[99]). (a) Stress-strain profiles of silks with different crystalline orderliness fraction f_{ord}. (b) Experimental stress-strain curves for silks comparing with the predicted envelope of properties shown in dashed line; Markers of experimental curves at breaking point: ■ various dragline silks; ▲ *Bombyx mori* drawn evenly at different rates; • *Argiope Trifasciata* dragline silk; ♦ Laboratory spun recombinant silk based upon Spidroin II.

revealing the mechanism of silk strength, because there are less assumptions in simulating their mechanical behavior, and more realistic conformation in reproducing the multiscale structures. However, to the most recent progress of this channel, it is yet evident to fully mimic the structural hierarchy of silk material by a single crystallite, a confined amorphous region, or their simple combination.

This section briefly introduces primarily the theoretical and computational ways studying the undergoing mechanism of silk strength, as well as other mechanical properties. Macroscopic mechanical or thermodynamic modeling turns out to be computational inexpensive and efficient in integrating various themomechnanical properties and their semi-empirical formulae. On the other hand, Molecular modeling, originated from studying the conformation of a single macromolecule or molecular formation/aggregation in solutions, has been well implemented into the investigation of silk properties. Multiscale modeling of silk, as a joint of the macroscopic and molecular modelings has started being established. Direct expanding the simulation size to approach the realistic silk conformation is beyond contemporary computation capacity. Nonetheless, this trend is still highly appreciated, as it has made clear of mechanical dependance on the nano-structures of silks, which provides the cues of the silk quality improvement through nano-manipulation.

1.4 Research Motivation and Objectives

In section 1.2, we reviewed the nano-structure, properties and applications of silk fibers. Excellent mechanical performances of silks, combining with their biocompatibility and environmental friendliness, make all the dedications of the silk investigation to be worthwhile. A few empirical works have revealed the relation between the mechanical properties of silks and their structure or external controls[10, 46]. Theoretical and computational endeavors, discussed in section 1.3, were devoted including thermodynamic analysis, elastomeric network and coarse-grain modeling, EFF molecular dynamics simulation, as well as the integration of the available theoretical and computational methods, *i. e.*, multiscale modeling of silk structures. The aim of these studies is to unravel the structure-property thus to interpret the origin of the high strength and toughness of silks. However, very few studies to date can conclude a convincing mechanism whereby silk possess such properties from currently available methods and tools, and few study could interpret the yielding behavior or the work-hardening phenomenon by the hierarchical semicrystalline characteristics of silk fibers. Besides, mechanical or thermomechanical studies of silks have not yet taken their time-resolved dynamic behavior into account, and the transverse mechanical responses were only investigated for silk fibroin solution, such as shearing response. However, all these topics are extremely important in understanding the nature of silks which may guide the orientation of their applications.

Therefore, the general aim of my Ph. D. research project of silks is to unravel the relation between the nano-structure and mechanical responses against various

external stress. Note that the structures within silk fibrils are widely considered to be hierarchical, all structural levels may respond to external forces. However, previous studies show that the secondary structures, such as β-sheets, α-helices and amorphous coils may start to change their conformation while the chemical composites remain unchanged against elongation stress, which provides me the standing point of my study. Particularly, in order to effective achieve the general aim of this investigation, several topics are refined in line with the general aim, listed as follows:

I) The relation between the secondary structure variation and mechanical responses along fiber axis and the mechanical differences induced by structural diversity for different species of silks.

II) The influence of crystallite properties, including orientation and crystallinity, on the mechanical strength and toughness of silks.

III) The time-dependent, strain-dependent relaxation behavior, and the mechanism of conformational varied viscosity of silks.

IV) Torsion induced enhancement of elastic properties of silk and the origin of longitudinal and transverse coupling.

In addressing the above issues, both theoretical and experimental expertise are required, and a set of results combined with experimental measurements and theoretical prediction or verification are expected to conclude convincing mechanisms. The general approaches adopted in my project include theoretical, computational

and experimental aspects. Theoretical modeling is to propose quantitative relations refined from existing empirical observations, and computational simulation is imposed to implant the derived relation to obtain experimentally comparable data. Experiments need to finely designed and conducted in comparison with the computational results, and act as the validating strategy of the proposed theories. All the experiments, including the conventional mechanical measurements, were conducted by collaborators, they will be credited in their contributed chapters, respectively.

1.5 Outline of Thesis

The dissertation is divided into 6 chapters.

Chapter 1 provides the background information, including silk structure, properties, and its applications. The modeling information, which voices more of theoretical and computational concerns, was indented to an individual section, in order to furnish a systematic reserve knowledge for better digesting the contents of rest chapters.

Chapter 2 to Chapter 5 represent the initiative and originality of the topics relevant to my Ph. D. research project. The collaboration of the presented topics, if any, will be credited to the specific collaborators at the end of respective chapters.

Chapter 2 proposes a low-dimensional model of two species of silks - silkworm silk and spider dragline silk, explaining the mechanism whereby silk possesses supra-strength.

Chapter 3 examines the relation between silk structure, property and experimental strategy. By structurally unraveling the nano-mechanics and experimentally varying the structure, optimal mechanical performance can be achieved by a mechanism guided effective strategy.

Chapter 4 investigates the time-resolved dynamic behavior of silks. Abnormal dynamic mechanical responses of silk has been observed, different from other conventional natural or synthetic materials. Mechanism referring to silk behavior in

space-time domain is proposed and verified through the comparison to other materials. The implication of the novelty of silk will be proposed at the end of this chapter.

Chapter 5 starts with a new angle of the mechanical response of the silkworm silk and the spider dragline silk - transverse direction. Transverse movement, referring to the torsion of silk, makes the impact on the longitudinal direction. Such impact will be attributable to the cross-dimension coupling of silk material, after which potential applications according to this characteristics will be foreseen.

Chapter 6 concludes the whole dissertation by summarizing the individual chapters (Chapter 2 to Chapter 5), and draws a general conclusion of my Ph. D. research project. Main points will be highlighted, and further studies, either on agenda or still in mind, will be proposed at the end of my dissertation.

Chapter 2

Low Dimensional Modeling of Silk

In this chapter, we studied theoretically and experimentally the mechanical response of silkworm and spider silks against stretching and the relationship with the underlying structural factors. It was found that the typical stress-strain profiles were predicted in good agreement with experimental measurements by implementing the "β-sheet splitting" mechanism we discovered and verified, primarily varying the secondary structure of protein macromolecules. The functions of experimentally observed structural factors responding to the external stress were clearly addressed, and optimization of the microscopic structures to enhance the mechanical strength would be pointed out, which turns out benefit their biomedical and textile applications.

Spider silk, superior to most of the other biomaterials, has extraordinary strength

comparable to steel, and the highest toughness in the whole natural silk market[6–9]. On the other hand, the high production of silkworm silk makes its irreplaceable stay in silk engineering, despite its relatively inferior properties to spider silk[46, 103]. Other *lepidoptera* larvaes, such as scorpions, mites, flies, bees and ants are also silk providers, whose protein polymers are assembled into fiber forms[3–5]. Silks spun from silkworms and spiders, benefited from their high strength and biocompatibility, serve a wide range of applications, from costume manufacture to clinical treatment, as well as the recently developed biomedical implementations, such as artificial tendon, polymeric scaffold, and nerve grafts in tissue engineering[11, 13, 14, 104–109].

2.1 Silk Structure and Property

Although spider and silkworm silks share a high degree of similarity in their Ala- and Gly-rich composition and nano-structure, they behave differently in their mechanical responses, typically the work-toughening process in the post-yielding region of spider draglines[98, 110, 111]. This remains an open question for years and very few works have been exposing the mechanism from the view of the nano-structural conformation to date.

Let us start from recalling the hierarchical structure of the spider dragline silk and silkworm silk, which are primarily comprised of GA or poly-A repeated polypeptides in their respective fibrils, of the weight percentage above 70%[111–113]. The small residues allow a spatial possibility for the secondary structure formation, *e. g.*

β-sheets, β-turns, α-helices, random coils, *etc*[114, 115]. The secondary structure of silks can divided into crystalline(β-sheeted) and non-crystalline(amorphous) domains, as illustrated in Fig. 2.1. For the *Bombyx mori* silkworm silk, the primary two composites, heavy chains and light chains, and the **GAGAGX** repeats are dominant in the formation of β-sheets[116]. Due to the hydrophobic nature of the surfaces β-sheets, as well as driving of the entropic force, the β-sheets from adjacent protein macromolecule chains may aggregate to form inter-molecular β-sheet crystallites. Compared with other secondary structures, β-sheet crystallites are more compact in structural formation, and more rigid in mechanical responses (high Young's Modulus). The portion of β-sheet crystallites is quantified by crystallinity, which can be calculated from the experimentally measured data of X-ray Diffractroscopy (XRD). The crystallinity of the *Bombyx mori* silk is about 40%. For the spider dragline silk, despite their similarity of nano-structural hierarchy, the amino acid sequences of silkworm silk and spider draglines differ, which results in the difference of their secondary structures. Different from silkworm silk, the crystallinity of spider dragline silk is lower than 20%[10]; however, the total amount of β-sheet structures is 40%, the rest of which are referred to as the inter-molecule β-sheets. The tertiary and higher level of structures, composed of the folded secondary structure, inter-connected hydrogen bonds and hydrophobic interactions, are similar for both silks except the sericin coating of the *Bombyx mori* silk.

X-ray diffraction and AFM probing provide direct evidence on the molecular level that subtle deviation in amino acids assembly sequence may lead to significant difference in mechanical properties[10]. However, direct links between the composites and mechanical difference are not feasible to be established. In contrast, it

is more straightforward to bridge the relation between the mechanical properties to their high-order structures of protein macromecules[103, 117, 118]. They are similar in both kinds of silk fibers except the lower crystallinity and the solely observed β-sheets in the amorphous region of spider draglines[10, 118]. Such β-sheets are referred to the "*intra-protein β-sheets*", and those in the crystalline region are referred to "*inter-protein β-sheet crystallites*".

2.2 Mechanism of Plasto-elastic Behavior

In this section, the connection between the mechanical properties of spider dragline and silkworm silk and their nano structures will be investigated. To this end, theoretical model will be built. A quasi-periodic structure is adopted with repeated segments of massive rigid bodies and elastic springs, and they are aligned along fiber axis with one dimensional confinement, as indicated by Raman spectrum experiments[119]. More importantly, definition before or after the transition from rubber-like to glass state needs to be addressed.

2.2.1 β-sheet crystallite Splitting Mechanism

The elasticity of silk fibers is contributed mostly by the amorphous matrix before approaching the yielding point, thus the linear responded entropic force dominates in this region. In addition, β-sheet crystallites, previously regarded as rigid bodies, were report actually elastic with about 4 times high strength of the amorphous

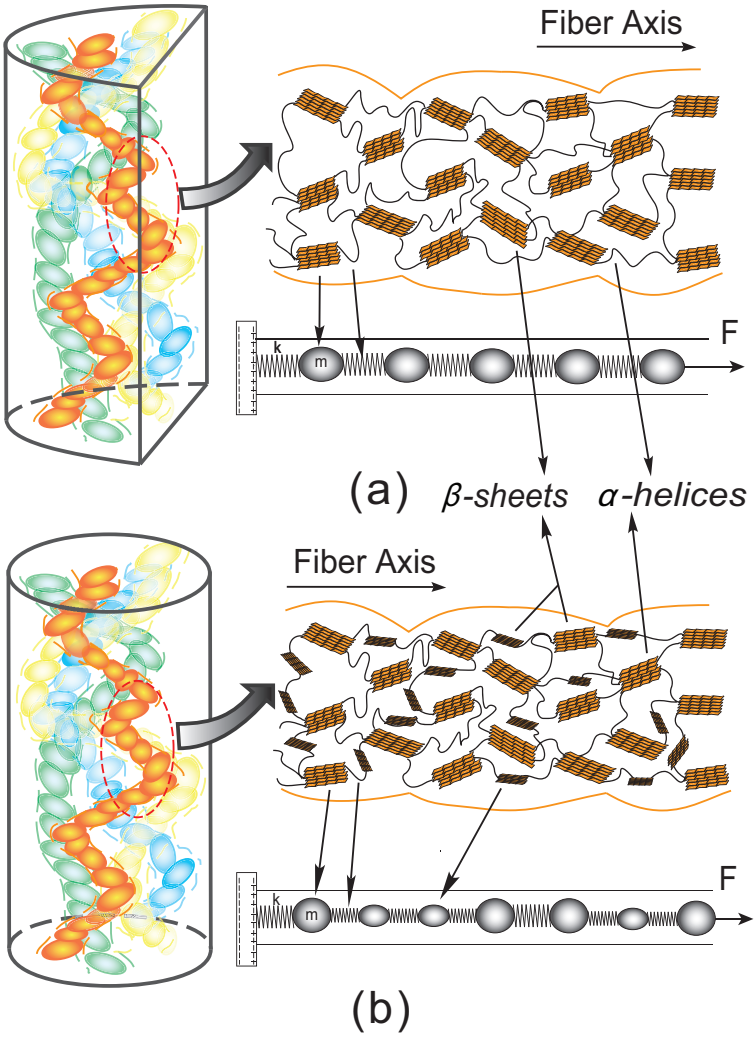

Figure 2.1: **Secondary Structure of Silks and Modeling**. The left panels are several strands of fibrils aligning along silkworm silk and spider dragline fibers in (a) and (b) respectively; native silkworm silk is double-stranded with semicircular cross-section for each strand and spider dragline is almost cylindrical. The upper-right sketches are the nano-structures of each fibril; the larger blocks denote the inter-protein β-sheet crystallites, and the smaller beads denote the intra-protein β-sheets; the flexual lines in-between denote helical or random structures in the amorphous matrix. The lower-right parts is the model construction based on their nano-structures, and the element correspondence is directed by the thin solid arrows.

matrix[110]. However, this rigidity can still be counted into the constant elasticity of the whole silk fiber within linear region. Herein we imposed Hooke's springs describing the linear elastic behavior before the yield point.

More importantly, definition before or after the transition from rubber-like to glass state needs to be addressed. Taking into account the facts of the transverse size of β-sheet crystallites shrinking and the irreversible process of elasticity measurement for the pre-stretched silk fibres, the splitting of the"β-sheet crystallites" turns out to be very probable mechanism in characterizing the post-yielding behavior[110].

2.2.2 Modeling Elements and Model Construction

Based on aforementioned facts, the silk fibres can be modeled as a serially connected system of N segments, each of which is comprised of massive body with mass m and light spring with original elasticity k_0. The segment at one end is stretched by an applied force F and the other boundary one is fixed immobile. During the stretch process, for an arbitrary crystalline segment i of the quasi-periodic structure, the extension linearly increases with the responsive force $F(i)$ in the linear region until $F(i)$ reaches the threshold force $F_{th}(i)$, after which the β-sheet crystallites start to split. The collective behavior of splitting at $\{F_{th}(i)\}$ characterizes the critical behavior around the yielding point. The splitting of β-sheet crystallites is intrinsically the breakage of dens hydrogen bonds, and a larger force F is more likely to retrieve longer free molecules from the compactly stacked β-sheet crystallites by breaking more bonds. Hereby, a simple linear relation between applied force F and the released molecule length $\Delta L(i)$ can be presumed as:

$$\Delta L(i) = \begin{cases} 0 & F < F_{th}(i) \\ (F - F_{th}(i))/E_0 & F \geq F_{th}(i) \end{cases} \tag{2.1}$$

Therefore, the relation between applied force F and observable extension Δx ($= \sum_{i=1}^{N} \Delta x_i$) yields:

$$\begin{aligned} F &= k_{\text{eff}} \cdot (\Delta x - \Delta L) \\ &= \frac{1}{\sum_{i=1}^{N} \frac{1}{k_i}} \cdot (\Delta x - \sum_{i=1}^{N} \Delta L(i)) \\ &= \frac{k_0 E_0 L_0 \Delta x - N k_0 L_0 \cdot \int_0^F (F - f)\rho_{th}(f)\mathtt{d}f}{N E_0 L_0 + N \int_0^F (F - f)\rho_{th}(f)\mathtt{d}f} \end{aligned} \tag{2.2}$$

where $\rho_{th}(\cdot)$ is the distribution of the threshold force $\{F_{th}(i)\}$, and L_0 is the original length of each segment. Mapping three dimensional reality to our one dimensional model, the scaling is governed by $F \sim \sigma$(set the area of cross section $\Delta S = 1$), and $\Delta x \sim \epsilon \cdot N L_0$, where σ and ϵ denote the tensile stress and tensile strain respectively. Without loss of generality, Gaussian random function is chosen for the distribution of threshold forces concerning the heterogeneity of biomaterials.

To mimic the dynamic process of silk stretching, extensive numerical simulations based on Molecular Dynamics (MD) were carried out in comparison with the corresponding experiments. MD numerical results of the stress-strain profiles predict very well with experimental data for proper values E_0/k_0 and $\langle F_{th} \rangle$, as shown in Fig. 2.2. It is found that the ratio E_0/k_0 determines the relative steepness of the two segments of stress-strain profiles. We also found that the stress-strain profile is

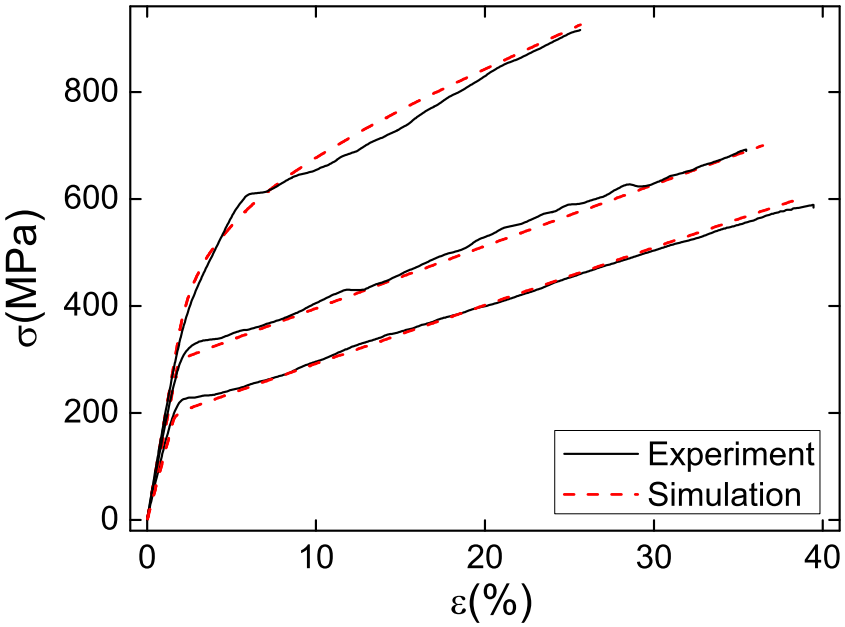

Figure 2.2: **Modeling and Experimental Results for Silkworm Silk**. The relation between stress σ and strain ϵ of silkworm silk fibers is shown for various artificial reeling speeds: the black solid line is the experimental curve, and the red dashed line is the simulation results. The scaling constant in simulation $S_c = 20$, the corresponding parameters k_0, E_0, and $\langle F_{th} \rangle$ increase with the reeling speed.

relatively robust to the form of distribution function of threshold forces, as general gradually varying and centralized functions give out similar profiles. Therefore, the breakage of β-sheet crystallites in silkworm silk fibrils weakens the linkage between protein molecules.

2.3 Work-toughening Process of Spider Silk

2.3.1 Influence of Intra-protein β-sheets

To extend the model to describe structure of spider dragline silk, we took into account the intra-protein β-sheets(Fig. 2.1(b)). Analogous to the silkworm silk modeling, the linear presumption still holds for intra-protein β-sheets. Due to the morphological inperfectness and stacking incompactness of intra-protein β-sheets, they are split before the inter-protein β-sheet crystallites. Besides, their limited sizes give rise to the complete destruction during stretching at forces $\{F_{tr}(i)\}$, after which the intra-protein β-sheets are fully resolved into the amorphous matrix.

2.3.2 Extended Modeling for Spider Dragline Silk

Hereby, the lengthening response relation of spider draglines can be analogously derived as that of silkworm silk, as shown in Eq. 2.3.

$$\Delta L(i) = \begin{cases} 0 & F < F'_{th}(i) \\ (F - F'_{th}(i))/E_1 & F'_{th}(i) \leq F < F_{tr}(i) \\ (F_{tr}(i) - F'_{th}(i))/E_1 & F \geq F_{tr}(i) \end{cases} \tag{2.3}$$

where E_0 and E_1 are the proportional constant of applied force and the released molecular length for inter-protein β sheet crystallites and intra-protein β-sheets, respectively. Concerning the above statements, qualitative relation can be derived as $E_1 < E_0$, and $\langle F'_{th} \rangle < \langle F_{tr} \rangle < \langle F_{th} \rangle$. Hence, the explicit force-extension expression of spider silk writes:

$$F \approx \frac{k_0 L_0 \Delta x - N k_0 L_0 \cdot \Omega(F)}{N L_0 + N \Omega(F)}, \tag{2.4}$$

where $\Omega(F)$ denotes:

$$\begin{aligned} \Omega(F) &= \frac{p}{E_1} \left(1 - \int_0^F \rho_{tr}(f) \mathtt{d}f \right) \int_0^F (F - f) \rho'_{th}(f) \mathtt{d}f \\ &+ p \cdot \int_0^F \int_0^{f_2} \left(\frac{f_2 - f_1}{E_1} \right) \rho_{tr}(f_2) \rho'_{th}(f_1) \mathtt{d}f_1 \mathtt{d}f_2 \\ &+ \frac{1 - p}{E_0} \int_0^F (F - f) \rho_{th}(f) \mathtt{d}f. \end{aligned} \tag{2.5}$$

Therein, p is the fraction of intra-protein β-sheets to overall β-sheeted structures; $\rho'_{th}(\cdot)$, $\rho_{tr}(\cdot)$ and $\rho_{th}(\cdot)$ respectively characterize the distribution of the threshold forces, the destruction forces of the intra-protein β-sheets, and the threshold forces

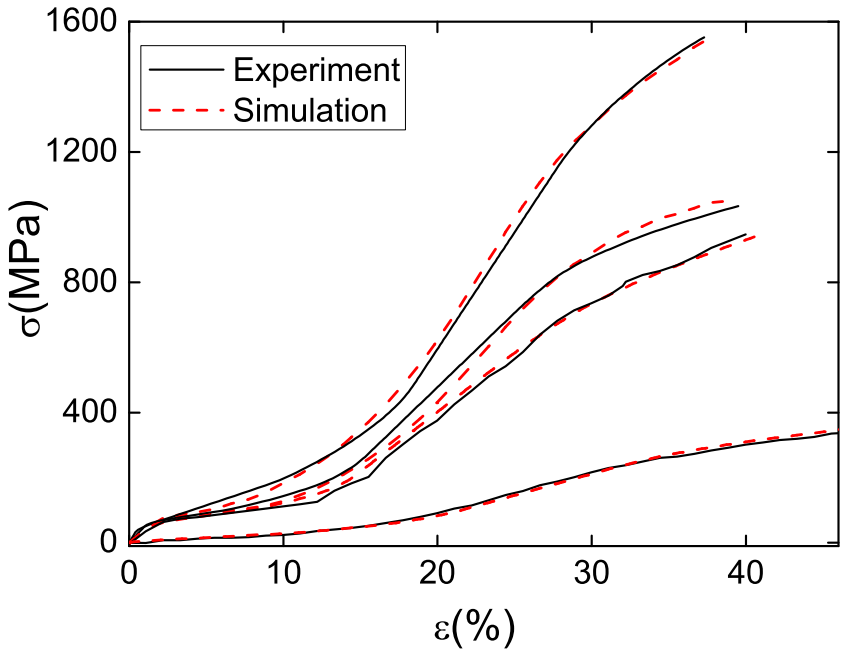

Figure 2.3: **Modeling and Experimental Results for Spider Dragline Silk.** The black solid lines denote the stress-strain profile for spider silk under different reeling speed, see Ref[10]. The red dashed lines are the computational results, where scaling constant $S_c = 20$, the preserved fraction of intra-molecule β-sheet $p = 0.5$, and parameters k_0, E_0 and E_1 are varied for different reeling speeds.

for inter-protein β-sheet crystallites, as the turning-on of each mechanism is reflected in different segments of stress-strain profile of spider draglines.

By simulating the dynamic stretching process, we found that the ratio $E_1/(pk_0)$ and $E_0/((1-p)k_0)$ are dominant in characterizing the relative steepness of stress-stain profile. The proper choices of adjustable parameters ratio $E_1/(pk_0)$ and $E_0/((1-p)k_0)$ make the MD numerical results best fit the experimental stress-strain profiles, which were measured for spider draglines artificially extruded under different speeds, as can be seen in Fig. 2.3.

Moreover, it follows that linear elasticity k_0 and proportional constant E_0 and E_1 increases with reeling speed, indicating their dependence of initial conformation of nano-structures. Comparing with the increasing profile for silkworm silk in Fig. 2.4, we found that both threshold forces $\langle F_{th} \rangle$ for spider draglines increase monotonously with reeling speed as well. It coincides with the fact that the initial formation of β-sheet crystallites have better alignment for higher reeling speed, according to the higher splitting threshold. The intra-protein β-sheets are less compact, and split at low stress region with slight variation. Therefore, the mechanism of spider dragline mechano-profile has been distinguished that the destruction of intra-protein β-sheets lead to the work-toughening process in the post-yielding region. To be more generalized, the diverse high-order structures of protein molecules for silk fibers of different species bring about their distinct mechanical complexity.

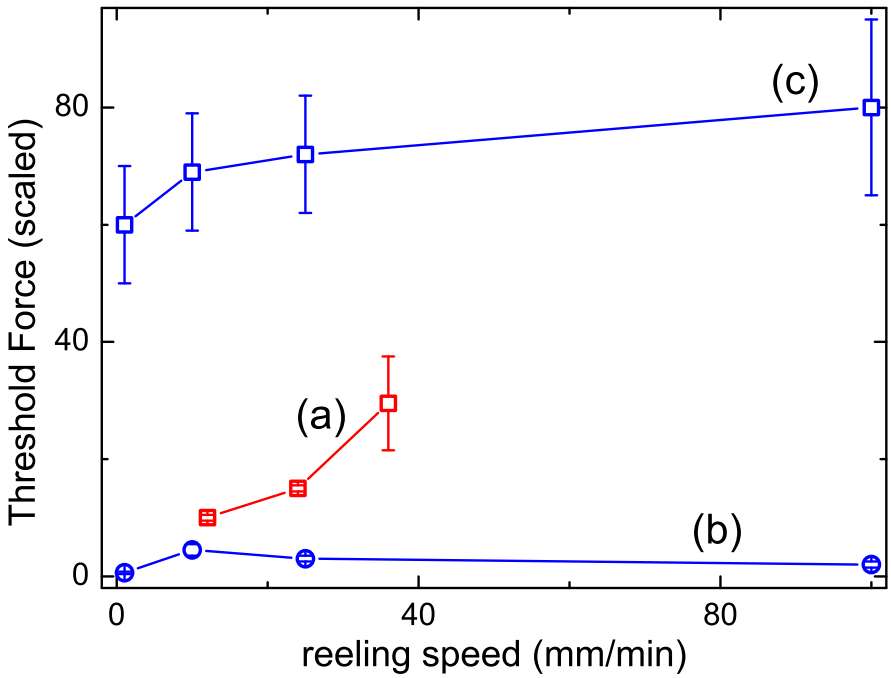

Figure 2.4: **Threshold Forces in the Modeling of Silks**. (a) The relationship between reeling speed and splitting threshold forces of inter-protein β-sheet crystallite for silkworm silk; (b) and (c) The relationship between reeling speed and splitting threshold forces of intra-protein β-sheets and inter-protein β-sheet crystallites for spider dragline silk respectively.

2.4 Remarks and Limitations of the Modeling

We have observed the enhancement of the initial modulus for both silkworm silk and spider dragline silk by direct fast artificial reeling from their glands, which is reflected by the increase of elasticity in the amorphous region of silk fibres. It implies that the protein macromolecules in amorphous state are better aligned under higher reeling speed, and more efficient resisting external stress. Meanwhile, the yield points for both species of silks appear at higher stress for faster reeling manner. This finding refers to the better orientation along the fibre axis which can also be realized by high dimensional simulation, essentially due to increase of the threshold force of β-sheet splitting by summing over all those on the same cross-section. Such improvement of mechano-properties of silks may give rise to their sustainable application, combining with its stability against circumstance variation, such as scaffold and tendon substitute in tissue engineering.

Besides, following the monotonic tendency of the modeling parameters, we are able to expect an enhanced strength and toughness for artificially reeled silkworm silk, and a lower-strain-shift of the work-toughening region for spider dragline silk by increasing their reeling or extruding speeds. Therefore, by accurate control of reeling speed in order to tune the properties of the intra- and inter-protein β-sheet structure (orientation, size and portion), mechanical profiles fulfilling various functional desires can be attained. Mechanically tunable materials may acquire high opportunity broadening the scope of applications in future.

However, our one dimensional modeling of silkworm silk and spider silk did not take account into the detailed information of secondary structures. The amorphous

matrix was simplified as linear response elastomer, driven by the entropic forces; The size, orientation and the content of β-sheet structures were not considered in this work, but embedded in the parameters E_0, E_1 and threshold forces of β-sheet splitting. Regarding the increase of such threshold forces of crystallites and the increase of the reeling or extruding speeds of silks, a self-consistent logic is still valid, as a higher orientation of crystallites increases the force at rupture. The influences of the properties of the β-sheet crystallites will be detailed in Chapter 3.

2.5 Summary

In summary, we have established the correlation between the nano structures and mechanical properties of silk fibers. It is found that the splitting of inter-protein β-sheet crystallites gives rise to the weakening the linkage among protein molecules while limited capacity of intra-protein β-sheets results in the lengthening and the work-toughening of spider draglines. Fast reeling increasing the elasticity in the amorphous region of silks, implies that the protein macromolecules in amorphous state are better aligned for higher reeling speed, and more efficient resisting external stress. The exploration from microscopic mechanical properties by combining the theoretical modeling and experimental measuring turns out be a brand new probing method to investigate the subtle structural differences among biomacromolecules. Meanwhile, feasible improvement of the silk properties have been pointed out, potentially satisfying wide ranges of robust biomedical and biotechnological functions[1].

[1]This work is supported by ARF funds: T206B1114 and R-144-000-212-112. The artificial reeling, processing of *Bombyx mori* silkworm silk, and the mechanical measurement were conducted by Ms Gangqin Xu; The artificial reeling, processing of *Bombyx mori* silkworm silk, and the mechanical measurement were conducted by Dr Ning Du.

2.6 Methodology

2.6.1 Computational Methods:

Velocity Verlet algorithm was applied in the MD simulation for respective modelings. Each site in the one-dimensional chain represents a confined crystallite, thus the equation of motion for crystallite i yields:

$$M\Delta\ddot{x}_i = -F(\Delta x) - \mu\Delta\dot{x}, \tag{2.6}$$

where μ is the viscosity of silks. As silk materials are viscoelastic, viscosity in the both simulated silks does exist. Here the implantation of viscosity μ is also aimed to damp the system to its equilibrium, thus the stress and strain may be explicitly derived. Eq. 2.6 was scaled by M, which leads the scaling $\tilde{\mu} = \mu/M$, $\tilde{k_0} = k/M$ and $\tilde{E}_i = E_i/M$.

The simulation parameters for both kinds of silks are detailed in Table 2.1:

The scaled viscosity was properly adopted, by satisfying two conditions: 1): overdamping pattern, with no oscillatory motion shown in crystallites; 2): no significant influence of transient state on final results. The stress-strain profiles thus obtained by tracking the strain and simultaneously calculating the stress of the simulated silk at equilibrium. The adjustable parameters are threshold forces and the ratios mentioned in section 2.2.2 and 2.3.2.

Table 2.1: Parameters in Models of Silk

Parameter Name	Notation	Value
Size	N	100, 500, 1000
Original Inter-crystallite Distance	L_0	1.0
Time Step	Δt	0.01, 0.005, 0.001
Scaling Constant	S_c	20
Maximum Strain[a]	ϵ_{max}	40%
Viscosity	$\tilde{\mu}$	2.0
Spread of $F_{th}(\cdot)$ [b]	σF_{th}	$0.2 * \langle F_{th} \rangle$
Spread of $F_{th}(\cdot)$ [c]	σF_{th}	$0.05 * \langle F_{th} \rangle$
Spread of $F'_{th}(\cdot)$	$\sigma F'_{th}$	$0.05 * \langle F'_{th} \rangle$
Spread of $F_{tr}(\cdot)$	σF_{tr}	$0.2 * \langle F_{tr} \rangle$

[a] The breaking point cannot be predicted from the simulation, and the artificial cut-off fulfills the comparison of all available experimental data.

[b] The threshold force of β-sheet crystallites of silkworm silk.

[c] The threshold force of β-sheet crystallites of spider dragline silk.

Detailed MD simulation method, the practical way of stress calculation, and the equation of motions for inter-protein β-sheet crystallites and intra-protein β sheets can be found Section A.1 in the appendix chapter.

2.6.2 Experimental Methods:

Sample Preparation: Immobilized silkworms (Bombyx mori) were forcibly silked on a computer-controlled motorized spindle at different speeds at $25°C$, and the relative humility of 55%. And all the silk reeled from the silkworms was degummed by washing the fibers for 30 minutes in a $1wt\%$ solution of Marseille soap and $0.5wt\%$ of Na_2CO_3 in water at about $96°C$, followed by rinsing with deionized water. The process was repeated several times with fresh solutions and the degummed silk fibers were air dried.

Adult female *Nephila pilipes* spiders were anaesthetized by CO_2 and fixed to a black hard cardboard with tape. A plastic column attached to the computer controlled motor was used to collect the single major ampullate (MA) silk at the speeds of $2.5mm/sec$, $10mm/sec$, $25mm/sec$ and $100mm/sec$. The temperature and relative humidity were kept at $25°C$ and RH 55%.

Mechanical Measurement: Silk samples of gauge length $10cm$ were mounted on the Instron MicroTester (Model 5848). The machine controlling parameters and conditions are listed in Table 2.2:

The tensile stress, tensile strain and elapsed time were recorded during the whole process of mechanical measurements.

Table 2.2: Parameter Controls and Conditions of Instron Microtester

Parameter/Condition	Value
Force Resolution	0.5% (unit of indicated load)
Position Resolution	$0.02\mu m$
Strain Rate	$50\%/min$
Temperature	$20 \pm 2°C$
Humidity	$60 \pm 5\%$

Chapter 3

Effect of Crystallite Properties on Silk Strength

In this chapter, in order to predict the strength limit of silk, a series-connected parallel-responded model was proposed to establish the correlation between the mechanical properties and the structures of *Bombyx mori* silk. It is found that both the orientation of β-sheet crystallites and the crystallinity of silk have highly positive adjustability on the strengthening and toughening of silk. The upper limit of the strength of *Bombyx mori* silk is predicted to be 1.2GPa when the embedded crystallites are perfectly aligned. This is comparable with the strength of spider silk on average. To verify this prediction, a direct forcibly manner of reeling the silkworm silk was adopted. It follows that a higher reeling speed results in a higher degree of alignment of the β-sheet crystallites and simultaneously an increased crystallinity of silk, which indeed gives rise to the enhancement of the strength of

Bombyx mori silk. The results show that the silk strength is greater at faster reeling speed with a higher degree of orientation and crystallinity, in good accordance with our theoretical prediction. The method designated to acquire ultra-strong silks by making a multi-scale structure-response linkage can be served as a general guide for the enhancement of the performance of animal silks, and a general reference both for our study and future investigation.

3.1 Motivation and Objective

3.1.1 Brief Description of Silk Superiority

As mentioned in previous chapters, spider dragline silk, known as a kind of lithe and light weighted biomaterial, protein fiber has become one of the most versatile materials due to its extraordinary strength and toughness against stretching, superior to most synthetic high-performance fibers[6–9, 25]. Besides, silks including that extruded by spiders possess high environment-friendliness, for its biocompatibility and the mild processing condition, compared to man-made polymeric materials which are processed either from harsh solvents or high temperature and pressure[25, 120]. Beneficial from its exceptional mechanical properties and biocompatibility, silk family covers a broad range of applications, such as bullet-proof vests, surgical sutures, reinforced composites, *etc.*

3.1.2 Motivation of Improvement of Silk Quality

Although spider silk is superior to other natural fibers with respect to its unusual combination of strength and extensibility, the extremely high cost of spider silk fabrication has become the major obstacle for its commercialization due to the spiders' aggressive nature and the practical difficulty in their domestication. In addition, the massive production of biomimetic silk, including the solvent spinning of both regenerated silk protein and recombinant spider silk/analogues, remains a challenge, particularly due to the unique features embedded in the hierarchical structures of silk through precise control of the spinning process[49, 55, 121–124]. On the other hand, the high production volume of commercial mulberry silkworm (*Bombyx mori*) silk ensures itself a potential substitute of spider silk. Furthermore, the similarities in the spinning process and the hierarchical structures of spider and silkworm silk provide the feasibility that the strength of silkworm silk may approach spider silk in spite of its native mechanical inferiority[45, 46].

Natural silks are comprised of protein molecules(e.g. silkworm and spider silks are constituted of fibroins and spidroins, respectively), stored in the silk glands of their providers in the aqueous state. During the spinning process of silks, an elongational stress is applied near the spigot to the silk protein solution of increased concentration, to extrude the semi-crystalline insoluble fiber threads[25–30, 125]. Above the level of their chemical composites, semi-crystalline domains were found in both silkworm and spider silk(Fig. 3.1), where antiparallel β-sheet crystallites are embedded in an amorphous matrix. The antiparallel β-sheet crystallites are compactly stacked by the highly conserved poly Gly-Ala or poly Ala motifs, and

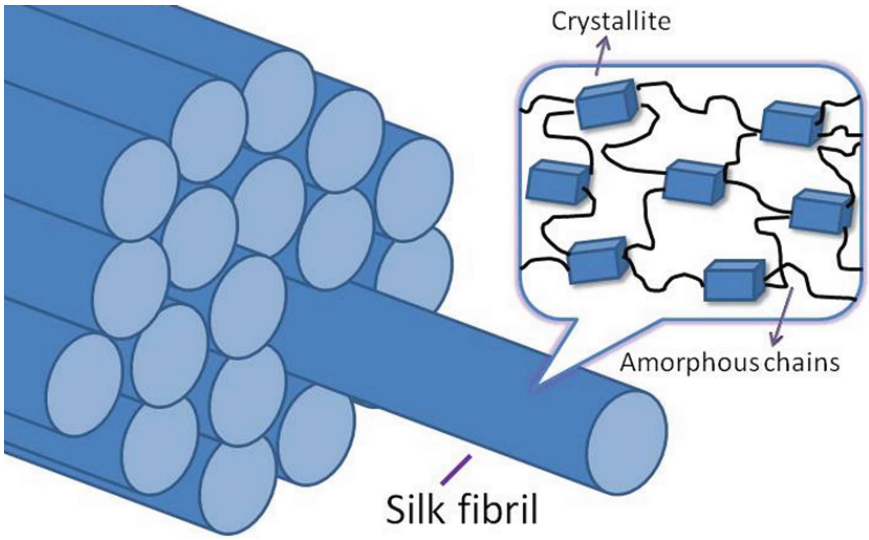

Figure 3.1: **Bundled Fibrillar Structure of Silk**. Schematic illustration of the bundled fibrillar structure of silkworm and spider silks. Both silk threads are composed of numerous bundled nano-sized fibrils, consisting of interspersed crystalline and amorphous domains.

the matrix are rich of -helices, less ordered -structures[8, 126–128]. The crystallites play a key role in determining the mechanical properties of silk. β-sheet crystallites act as the interlocking to transfer the load between the partially extended macromolecular chains[126], enabling the uniaxial extension of the amorphous matrix till the rupture of the crystallites. Furthermore, silk proteins (spidroins and fibroins) may self-assemble into nano-sized fibrils according to the recent Atomic Force Microscope (AFM) observations[129].

In general, the mechanical properties of silks are determined by the hierarchical structures at all levels. The toughness of silk is attributed to its nano-fibrillar structures with their strong inter-fibrillar interactions, as well as the fine channels described for probable energy dissipation[25, 130]. The strength of silk is attributed to the presence of the compacted β-sheet structures which bind molecules with

the "inter/intra-molecular junctions"[8, 131]. Reducing the crystallite size and increasing their alignment along the fiber axis have been adopted to increase the mechanical strength and toughness of silks[10, 132].

In addition, Lee *et al.* acquired the silks of better quality than their natural counterparts in terms of mechanical strength by infiltrating metallic atoms to form reinforced backbones of silk fibers[56]. They acquired the silks of better quality than their natural counterparts in terms of mechanical strength and proposed possible mechanism of the reinforcing of silks, whereas the relation between the silk strength and its semi-crystalline features has yet been taken into account. Besides, the above methods require harsh experimental conditions, as well as their fine controling. Apart from those bio/chemical engeering approaches, some mild physical approaches, i.e. controlling the reeling manner, have been proposed in order to enhance the mechanical properties without changing the molecular primary structure of silks[10, 46, 132, 133]. Nevertheless, the governing mechanisms behind these approaches remain to be addressed. Computationally, Keten *et al.* employed molecular dynamics simulation, targeting the crystallite nanostructure for difference species of silks[82, 89]. They figured out the length dependence of the crystallite strength, as well as the detailed information including dihedral angles and H-bond length. Yet the directionality of crystallites, and a collective behavior of crystallites and their embedded matrix, which turn out to have significant influence on the mechanical response of silk, have not been revealed.

3.1.3 Objective of Improvement of Silk Strength

Hence, the purpose of this chapter is to determine the structural factors influencing the mechanical properties of silk to identify the way to acquire ultra-strong silk. We start from the theoretical modelling to explore the dependence of the strength of silkworm (*Bombyx mori*) silk on the collective properties of crystallites, including their size and directionality. The predicted structure-property relation is verified experimentally by controlling the reeling manner of silkworm silk, which is imposed to tune its nano-structure. Besides, we are also able to predict the strength limit of silkworm silk achieved by implementing this mild processing method. Meanwhile, based on our ultra-strong silk design, a guideline-destination protocol is proposed for efficient design of functional or ultra-strong soft material.

3.2 Modeling of Crystallite Properties and Mechanical Responses

We proposed a series-connected and parallel-responded model in order to unravel the dependence of silk strength on the characteristics of crystallites. As is widely regarded, the yield point implies the microstructure change caused by the massive hydrogen bond breakages within hydrogen-bond (H-bond) rich structures during the stretching process, including a translational distortion among neighboring protein molecules[99, 110]. We noticed that the splitting force of protein molecules highly depends on the orientation of unfolding domains[134], and such phenomenon

has been confirmed for the α-helices in natural fibroin by Single Molecule Force Spectroscopy (SMFS) experiments, where the splitting force ranges from 200pN to $1,500$pN[135]. β-sheet crystallites, but not α-helices in native silks reeled from *Bombyx mori* are commonly observed, as indicated by the halo of Wide-Angle X-Ray Scattering (WAXS) pattern[136] (also available in the inset of Fig. 3.4).

Hence, the unfolding occurs at molecular level due to the breakage of β-sheet crystallites, of which H-bonds are $3 \sim 4$ times denser than that of α-helical structure[34]. Besides, a recent work shows that the elasticity of β-sheet crystallites is about 4 times larger than that of amorphous matrix by synchrotron radiation x-ray diffraction experiments[110]. Therefore, the upper bound of splitting force of a single β-sheet crystallite is approximately estimated to 5000pN, corresponding to the perfect oriented situation. All-atom simulation based on effective force field is a convincing way to reveal the dynamic process of the β-sheet crystallite unfolding[89, 90]. Nevertheless, the unfolding rate ranges in seconds/milliseconds, and the inter-molecular entanglement rises up the burden of at least tens of thousands of amino-acid residues, which is far beyond the computation capacity in time and size aspects. Besides, currently computational stretching speed in simulation of molecular chains is about 10^{10} higher than the experimental one.

In order to overcome this difficulty, a general coarse-grain method by approximating the splitting force was adopted for the arbitrarily oriented crystallites, abiding by two facts: (1) β-sheet crystallites in an arbitrary orientation split at force thresholds between F_{min}(200pN) to F_{max}(5000pN); (2) splitting force decreases dramatically when the β-sheet crystallites slightly deviate from the perfectly oriented case, since less H-bonds will respond to the external stress, as illustrated in

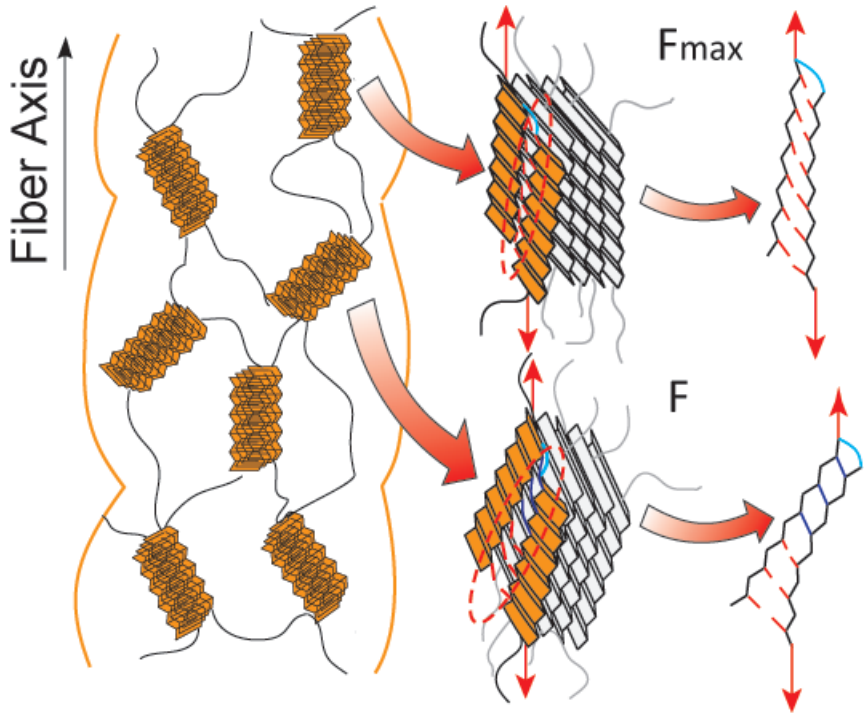

Figure 3.2: **Microscopic Mechanism of Silk Yielding Behavior**. The left panel shows the interspersed β-sheet crystallites in fibril with their orientations deviated from the fiber axis. The middle panel illustrates the splitting of β-sheet crystallites for an arbitrary direction. The right panel is a sketch presenting the number of H-bonds engaged in the splitting dynamics, as indicated in red-dashed line.

Fig. 3.2. Based on the aforementioned facts, a simple expression of the splitting force in terms of the orientation angle ϕ of a single crystallites can be written as:

$$F_{th}(\phi) = F_{min}p(\phi) + F_{max}(1 - p(\phi)), \tag{3.1}$$

where $p(\phi)$ is general function ranging from 0 to 1. By applying the boundary condition, $p(\phi)$ is set to be following forms, with an adjustable parameter $\alpha \in (0, 1)$:

$$p(\phi) = \begin{cases} \sin^{\alpha}(\phi) \\ (\frac{2\phi}{\pi})^{\alpha} \end{cases} \tag{3.2}$$

The orientation function $f(\sigma)$ reads:

$$f(\sigma) = \frac{1}{2}(3\langle\cos^2(\phi)\rangle - 1) \tag{3.3}$$

$$= \frac{1}{2}(\frac{3\int_0^{\pi/2} N_\phi(0,\sigma)\cos^2\phi\sin\phi d\phi}{\int_0^{\pi/2} N_\phi(0,\sigma)\sin\phi d\phi} - 1), \tag{3.4}$$

where $N_\phi(0,\sigma)$ is the normal distribution of zero mean and standard deviation σ. The stress and strain at the yield point are termed as "yield stress " σ_Y and "yield strain" ϵ_Y respectively, and the slope of the stress-strain curve below the yield point is Young's modulus[25, 137]. Noticing that the yield point locates at where vast H-bonds breaking, the parallel-responded mechanism give rise to σ_Y as a summation form of the splitting force of β-sheet crystallites within the same cross section.

$$\sigma_Y = \frac{F_Y}{S} = \frac{2n}{S}\int_0^{\pi/2} N_\phi(0,\sigma)F_{th}(\phi)\sin\phi d\phi, \tag{3.5}$$

where S is the cross section area of one fiber strand, and n denotes the number of crystallites within the cross section. n is determined by $S(C\%)^{2/3}/(ab)$ for a uniform distribution of interspersed crystallites, where a and b are the transverse dimensions of crystallites perpendicular to the crystallite axis ($\vec{c}$ axis), and $C\%$ is the crystallinity.

Hence, the relation between the yield stress σ_Y and the orientation function $f(\sigma)$ can be established. In polymer theory, the mechanical energy can be calculated by counting in the contribution of six free surfaces of a domain sized d^3, where d denotes the average inter-domain distance. Thus, the breaking stress σ_b governs:

$$\sigma_b \approx \sqrt{\frac{12\Gamma\sigma_Y}{\epsilon_Y d}}. \tag{3.6}$$

Herein, $\Gamma \approx 0.15 J/m^2$ is a good approximation for most polymers[1, 138]. The domains are regarded as the compact and deformed clusters in response to external stress, and their inter distance can be determined around $45nm$ for silkworm (from available *Bombyx mori* silkworm silk data of stress-strain profile), which is larger than that of spider draglines ($= 4nm$)[138]. The larger the domains, the less space the inter-domain matrix occupies. Since H-bonds are the principal way of the intra/inter-domain connection in silks, qualitative calculation of elasticity can be estimated as follows, by setting the volume ratio of domains:

$$\begin{cases} k' = pk_d + (1-p)k_m \\ k'' = \frac{k_d k_m}{pk_m + (1-p)k_d}. \end{cases} \tag{3.7}$$

In Eq. 3.7, k' and k'' are the elasticity in parallel and series connection respectively, and k_d/k_m is the elasticity of domains/matrix (k_d/k_m). Herein, we combine the shear modulus of the matrix into its elasticity , and the orientation of the domain-matrix connect is omitted. However, Eq. 3.7 is to show that the larger the domain size or inter-domain distance, as in the larger the value of p, the higher the stiffness

no matter what manner of the domain-matrix is (parallel/series/the combination). Besides, the nano-scaled domains provide important evidence that the softening of silk is mainly attributed to the variation of the secondary structures in the scale of nanometer.

As shown in Fig. 3.3, one can see that higher breaking stress can be achieved by better alignments of β-sheet crystallites for various values of α, which is related to the compactness of crystallites. In particular, the breaking stress can be enhanced substantially once $f(\sigma) > 0.92$. The general trend with a steep increasing end is robust to both the mathematical forms of $p(\phi)$, as well as the value selection of the parameters in respective forms. These guidelines acquired to implement the idea of "design-and-production" will be confronted with our experiments, which will be discussed in the following part. This designing guideline will also be verified by the comparison to the structural and the mechanical properties measurements.

3.3 Experimental Results and Discussion

3.3.1 Modification of Structure by Tuning the Reeling Speed

We have shown in our theoretical modeling calculation that a higher strength can be achieved by better aligning the crystallites and increasing the crystallinity. Hence, the problem lies on how to experimentally modify the nano-structure of silk, and whether the modeling prediction can be verified by the according mechanical measurements. Noticing that there have been reports on tuning silk mechanical

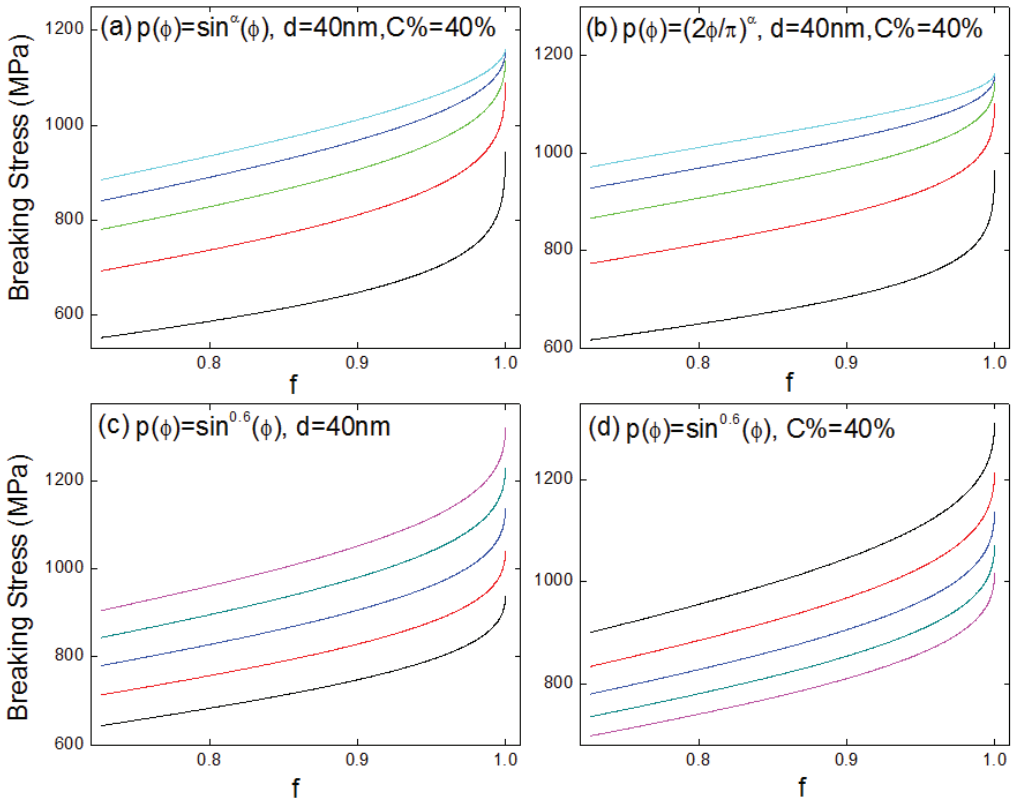

Figure 3.3: **Breaking Stress Dependence on Crystallite Orientation**. (a) and (b) take different forms of $p(\phi)$, and the model parameter α ranges 0.2 to 1 with interval of 0.2 from the bottom up; (c) the influence of crystallinity $C\%$ on the breaking stress of silk, from 30% to 50% bottom up spaced at 5% interval; (d) the influence of domain size on the breaking stress, from $30nm$ to $50nm$ top down spaced at 5nm interval. The average sizes in the dimension of $\vec{a}$ and $\vec{b}$ are set to $2.5nm$ and $3.0nm$.

performance by altering of spinning conditions[10, 46, 132]. In this regard, we will first identify the structural change of silkworm silks by altering spinning condition from its native figure-of-eight spinning to forcibly reeling from insects with constant speeds. Simultaneous mechanical test will be carried out for various spinning conditions. The detailed procedure concerning the treatment of silkworms and silks are elucidated in the experimental section. WAXS was employed to characterize the crystallinity, size and orientation of crystallites, examining the alignment of the β-sheet crystallites in the silk fibers[10, 35]. The size of crystallites in each dimension can be extracted by the radial integration of intensity as a function of azimuth angle along the equator and meridian of the WAXS pattern, which gives out the radial peak width for the (200), (120) and (002) reflections. According to Scherer's formula[139], the crystallite size in one dimension yields:

$$L = \frac{0.9\lambda}{FWHM\cos\theta}, \tag{3.8}$$

where FWHM means Full Width at Half-Maximum of the peak at the diffraction angle θ and the wavelength of incident ray λ equals to $1.5418\mathring{A}$. The equatorial data were deconvoluted into four crystalline peaks corresponding to the (100), (200), (120) and (300) Bragg reflections and an amorphous halo. Similarly, integration along meridian gives another two crystalline peaks (002) and (102)[136]. The crystallite sizes along $\vec{a}$, $\vec{b}$ and $\vec{c}$ directions are determined by the position and $FWHM$ of these peaks, and the crystallinity is determined by the ratio of the under area of crystalline peaks to that of the total reflection pattern.

Table 3.1 lists the crystallinity and crystallite size of silk fibers for different reeling

Table 3.1: Crystallinity and crystallite sizes of silks for various reeling speeds

Reeling speed (mm/s)	Crystallinity(%)	a^1	b^2	c^3
1	43	2.39	3.02	8.93
2.5	45	2.55	3.12	7.56
4	45	2.46	3.09	8.10
13	49	2.41	2.93	7.67

[1] The size of crystallites along $\vec{a}$ axis.

[2] The size of crystallites along $\vec{b}$ axis.

[3] The size of crystallites along $\vec{c}$ axis.

speeds. We found that the crystallinity of silk fibers slightly increases, and the size of the crystallites remains almost the same as the reeling rate increases. It indicates that apart from the orientation and the crystallinity of the β-sheet crystallites, other properties referring to the secondary structure maintains for various reeling speeds. In this sense, such changes embedded in the reeling fashion points out a feasible way to verify our theoretical prediction.

The orientation of the crystallites about the fiber axis is calculated from the $FWHM$ of (120) and (200) peaks. We apply the Herman's orientation function Eq. 3.4, where ϕ is the angle between the $\vec{c}$ axis of crystallites and the fiber axis. $f(\sigma)$ is 0 for no preferential orientation and 1 for perfect alignments of crystallites. For two reflections, (200) and (120), which are not orthogonal but have a known geometry in the equatorial plane, the expression of $\langle \cos^2 \phi \rangle$ reads:

$$\langle \cos^2 \phi \rangle = 1 - A\langle \cos^2 \phi_{200} \rangle - B\langle \cos^2 \phi_{120} \rangle. \tag{3.9}$$

Since (120) is 65° from the (200), $A = 0.8$ and $B = 1.2$. $FWHM$ of (200) and (120) peaks are measured perpendicular to the fiber axis (e.g. $\phi_{120} = \pi/2 - \varphi_{120}$), thus $\langle \cos^2 \phi_{200} \rangle = 1 - \langle \cos^2 \varphi_{200} \rangle$, where $\langle \cos^2 \varphi_{200} \rangle = \cos^2 0.4FWHM$.

Fig. 3.4 shows the orientation function $f(\sigma)$ of the β-sheet crystallites of silk fibers obtained from the WAXS patterns as a function of the reeling speeds. Silks drawn at faster speed lead to a narrower span of WAXS peaks. And $f(\sigma)$ has an approximately logarithmic dependence on reeling speed. It indicates that the structural features are varied by the shearing strength for crystallization under different longitudinal flow rate, and a fast reeling manner may turn out to be an efficient strategy to align the internal nano-scaled crystallites.

3.3.2 Enhancement of Mechanical Strength by Modification of Structure

We carried out the mechanical measurements simultaneously for the silks spun with indicated reeling speeds, and one-to-one correspondence of the structure and property is established, in order to verify modeling conclusion. Stress-strain profile is a proper way describing the stretching response of material, and silkworm silk, like most polymers, experiences stretch-softening beyond the yield point, which is reflected by the deviation from linear response at threshold. Stress-strain mechanical profiles of *Bombyx mori* silkworm silk was shown in Fig. 3.5. A general

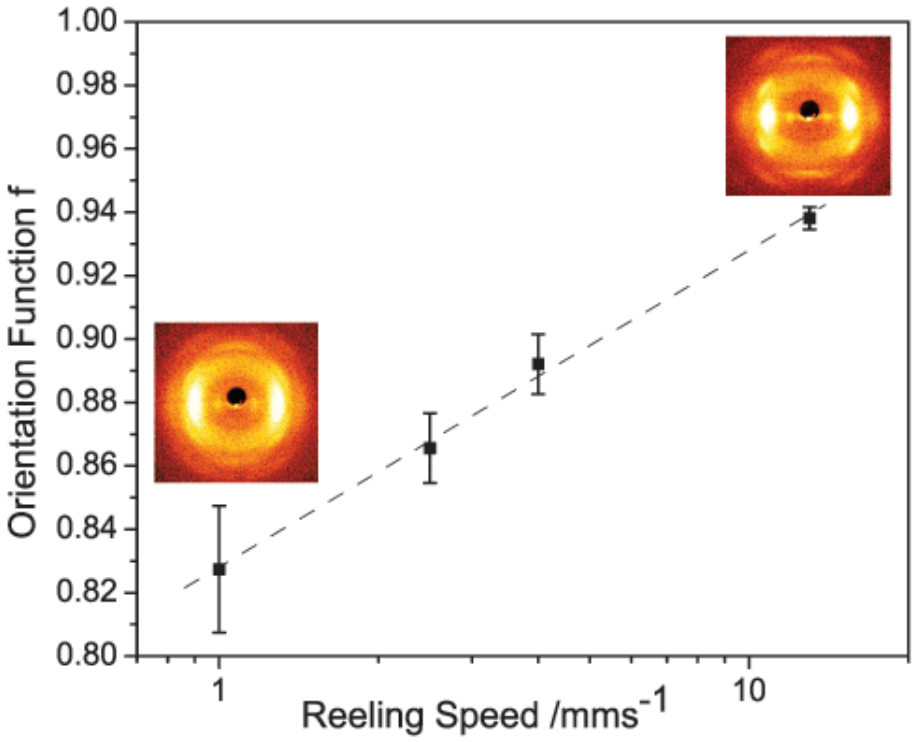

Figure 3.4: **Impact of Reeling Speed on Crystallite Orientation**. The relation between the orientation function of the crystallites within the silk fiber and the corresponding reeling speeds. The upper-right and lower-left insets are the WAXS pattern illustrating the structural difference. The dashed line directs the data deviation from linearity.

toughening trend was observed for high reeling speed. To analyze the mechanical characteristics in detail, the relation between the yield/breaking stress and reeling speeds was plotted in Fig. 3.6(a)/(b). It is apparent from the two figures that both the yield and the breaking stress increase with reeling speed of fibers, while the yield and the breaking strain do not exhibit much difference in respective experiments.

Referring to the mechanical properties, our results show that silkworm silk acquires higher Young's modulus and higher breaking energy reeled at higher reeling speed. This indicates that a faster reeling fashion not only produces stronger, but also stiffer and tougher silks at the same time.

3.3.3 Comparison of Experimental and Predicted Relation

At the molecular level, several structural factors interactively affect simultaneously the glass-state transition and the rupture of the silk[99]. The discrete points in Fig. 3.7 show experimentally the positive dependence of breaking stress on crystallite orientation function $f(\sigma)$ of the β-sheet crystallites controlled by reeling speeds. Simultaneously, the increased crystallinity also reinforces the backbone of the silk threads, but the breaking stress undergoes a sub-linear dependence of it, as indicated by the exponent of 2/3 implicitly in Eq. 3.5. Moreover, the size in the transverse dimension of the crystallites does not change significantly within the experimental range. Substituting the structural quantities in Eq. 3.5 and taking the form of $p(\phi) = \sin^{\alpha}(\phi)$, as indicated in Section 3.2, the adjustable parameter was chosen to be 0.4, where the predicted profile coincides with the experimental

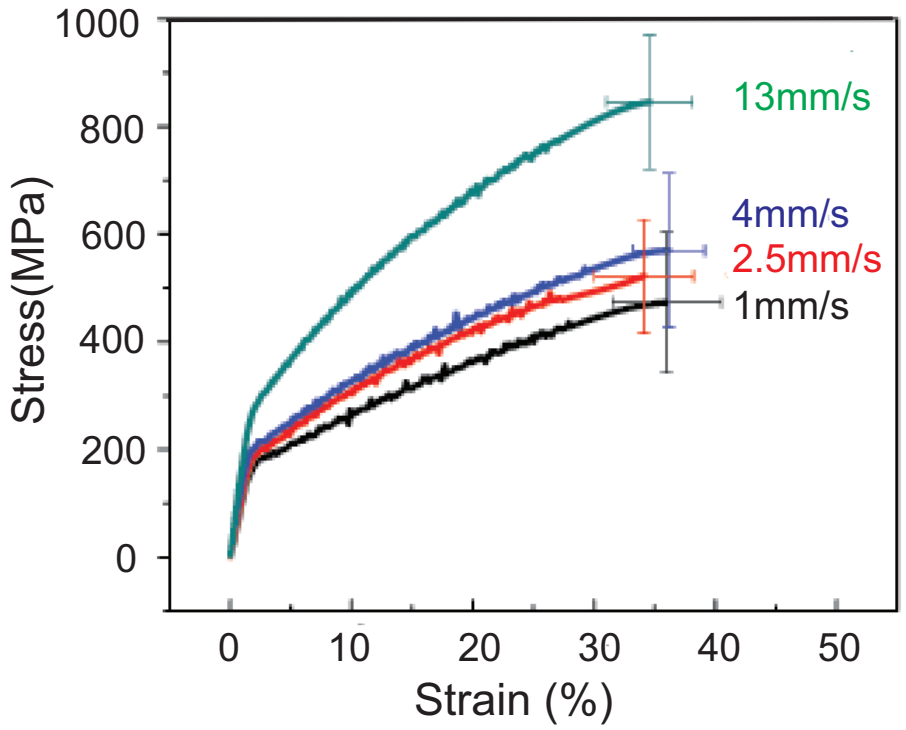

Figure 3.5: **Silk Mechanical Profile for Various Reeling Speeds**. Stress-strain profiles of silkworm silk are obtained by averaging over 12 samples; The reeling speeds are indicated at the side of the diagram with color correspondence. The error bar of each curve denotes the standard deviation of breaking strain (horizontal) and breaking stress (vertical). The data points from the breaking of the first sample to the average breaking point were interpolated by $2nd$ or $3rd$ order polynomials.

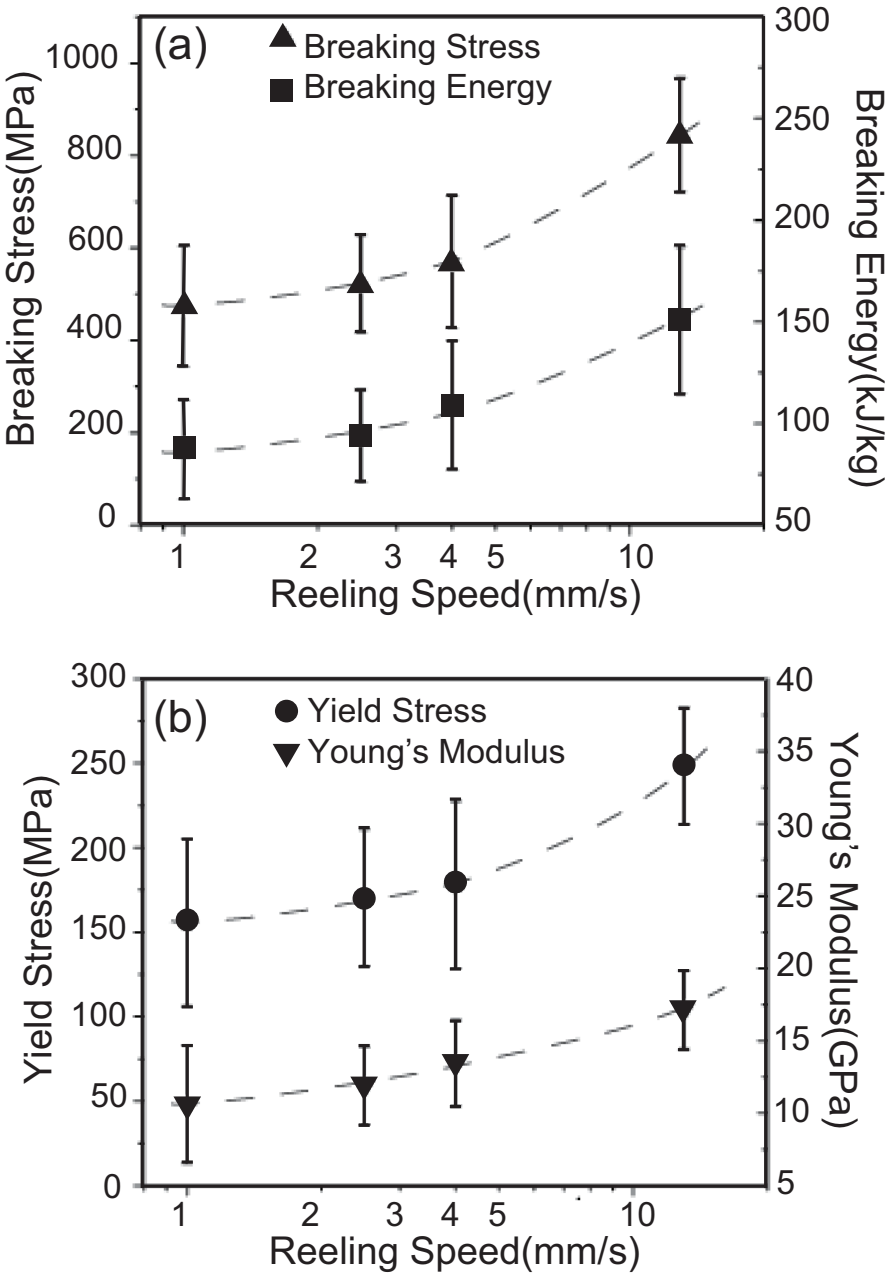

Figure 3.6: **Characteristic Silk Quantities for Various Reeling Speeds**. (a) The dependence of breaking stress (▲) and breaking energy (■)of silk on reeling speed; (b) The dependence of yield stress (●) and Young's modulus (▼) on reeling speed. The dashed line is for eye direct, and the error bars indicated the standard deviation for each measured characteristic mechanical quantities.

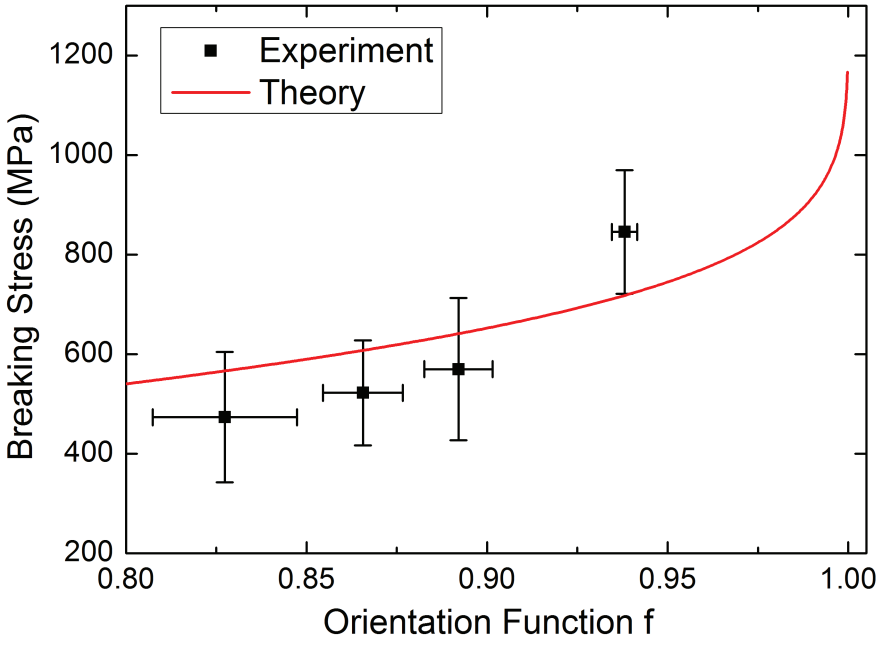

Figure 3.7: **Comparison of Computed Breaking Stress vs Crystallite Orientation Relation with Experiment**. Red solid line is the theoretical prediction by implementing the parameters measured by experiments, i. e. a, b, $C\%$; d is calculated as $45nm$ mentioned in section 3.2. The form of $p(\phi)$ is $p(\phi) = \sin^{\alpha}(\phi)$ and model parameter $\alpha = 0.4$. The black dots denote the experimental measurements, and the horizontal and vertical error bards represent the standard deviation of orientation function and breaking stress respectively.

measurements, as can be seen in Fig. 3.7. Therefore, it verifies the modeling of the structure-property relation, based on the β-sheet crystallite splitting mechanism, and the factors including structural properties of crystallites are entangled by the control of reeling fashion, which consequently influence the strength and toughness of silk fibers.

As shown in the theoretical scheme and demonstrated by the stress-orientation

relation from measurements, we know that a higher degree of orientation between crystallites and external forces will lead to greater yield and breaking stress. This implies that the most effective way to resist the external stress is to align all crystallites within the fibrils in parallel along with fiber axis/ the direction of applied force. The breaking stress experiences a dramatic increase when the crystallite orientation approaches the ideal perfectly aligned situation. In that sense, apart from the crystallinity and crystallite size, the alignment of crystallites turns out to be the dominant factor of the silk stiffening, revealing the potential of ultra-strong silk fabrication. Furthermore, standing upon the current experimental condition, the highest theoretically achievable strength of silkworm silk can be estimated around 1.2GPa, by perfectly aligning the crystallites and maintaining the slight increasing trend of the crystallinity. The upper bound of the silk strength is still 30% higher than the best experimental values reported and our results[46]. This finding indicates a very important fact that *Bombyx mori* silk has the potential to acquire an impact equivalent to that of spider draglines if the β-sheet crystallites are perfectly aligned[10]. Note that the approach we imposed is merely facile physical control, rather than harsh and costly biochemical treatments to silk glands or fibers[56]. Different from the other currently developed methods, the method by varying the reeling speed is more feasible to be massively applied and environmentally friendly to optimizing the nano-structure of silk. Additionally, we would like to point out that we have recently filed a patent of fabricating super silkworm silk fibers on the basis of this understanding, where the silkworms are exposed to an electromagnetic field. Under the treatment, the dispersed β-sheet crystallites of *Bombyx mori* silkworm silk fibers were better aligned than native ones, which directly give rise to the enhancement of the breaking stress.

3.3.4 Discussion of Modeling Assumption and Limitation

As discussed in section 3.2, the relation between the orientation of a single crystallite and its mechanical response is presumed in various mathematical forms. But generally speaking, they need to satisfy several conditions, which are expanded in detail of the previous mentioned two facts.

I. The maximum splitting force F_{max} of a crystallite occurs when its crystallite axis ($\vec{c}$ axis) perfectly aligned to the force direction. For uniaxial extension, one can assume that the elongation force is in the direction of fiber axis. In this case, all the H-bonds are initially perpendicular to the force direction, thus all these bonds will contribute to the rigidity of the crystallite. Previously studies have shown that the most probable H-bond density for α-helix is 3 residue/bond; on the other hand, from structure description of β-sheets, the linear density of H-bonds of β-sheet crystallites are 3 times higher than the helical structure. Hence it is rational to set $F_{max} = 5000pN$ for β-sheet crystallites.

II. The minimum splitting force F_{min} of a crystallite occurs when its crystallite axis ($\vec{c}$ axis) is perpendicular to the applied elongation force. Note that the force acts on the ends of crystallites so that only one H-bond will contribute the rigid of the crystallite. A zip-like cascading will take place once one bond is split. Here we took the lowest value of experimental data for α-helices splitting from AFM observation[135].

III. For the case a crystallite is slightly deviated from the perfectly alignment with the force direction, the H-bonds at the other end of the crystallite cannot respond

to the force. But the decrease of the non-responded bonds will be alleviated, as can be analyzed from simple geometry.

The above three evidences may support and rationalize the mathematical form of the relation between crystallite orientation and its splitting force we set.

The work of Keten *et al.* simulated a crystallite-like structure by aligning 6-residue β-strand in to a bundle. We don't take the computed value there because there are some issues unsolved. The crystallites in their work has a different size with that is widely accepted, and the effect of crystallite orientation on the β-crystallite breakage is not mentioned. Besides, the stretching rate in their simulation is highly deviated from the experimental one. Following Keten's work, the influence of the crystallite orientation on the β-crystallite splitting force cannot be computed. A slower stretching rate, together with a structure with residues close to the crystallite is required in the future study.

3.4 Summary

We were dedicated to making ultra-strong silk by tuning the structural characteristics from inverse engineering, and a theoretical series-connected parallel-responded model is proposed to quantify this design, as well as to predict the upper bound of the silk strength by implementing the idea. Hence, nano-structure and mechanical response of *Bombyx mori* silkworm silk are bridged, and the role and relative importance of each factor is clearly elucidated. Experimentally, physical alternation in spinning fashion from silkworm's uncontrolled figure-of-eight style to forcibly

reeled process is introduced in order to tune the structural factors by modifying the nano-structure of silk. Meanwhile, we tracked the variance of the mechanical strength and toughness of silk. We succeeded in achieving a higher degree of orientational ordering and crystallization simultaneously by speeding up the reeling, both of which are beneficial factors in silk strengthening.

Remarkably, this work develops a new inverse engineering method to design ultra-strong material by implementing the guideline extracted from our proposed theoretical model. This guideline-destination protocol gives rise to an efficiency leap in functional semi-crystalline material design. Particularly in our study, we aimed at and achieved finding methods on aligning the crystallites and reinforcing the backbones of silk fibers[1].

[1]This work is supported by ARF funds: T13-0602-P10. The artificial reeling, processing of *Bombyx mori* silkworm silk, the mechanical measurement, and the structural characterization by WAXS were conducted by Ms Gangqin Xu; The analysis of crystallite orientation from WAXS data was done by Dr Ning Du. Part of technical issues were supported by Mr Yang Li.

3.5 Experimental

Sample Preparation:

Immobilized silkworms (Bombyx mori) were forcibly silked on a computer-controlled motorized spindle at different speeds at $25°C$, and the relative humility of 55%. And all the silk reeled from the silkworms was degummed by washing the fibers for 30 minutes in a $1wt\%$ solution of Marseille soap and $0.5wt\%$ of Na_2CO_3 in water at about $96°C$, followed by rinsing with deionized water. The process was repeated several times with fresh solutions and the degummed silk fibers were air dried.

Mechanical Measurement:

To obtain the mechanical properties of the silk sample, Instron Micro Tester (Model 5848) was used to measure their stress-strain profiles. The force resolution is 0.5% of indicated load, position resolution is $0.02\mu m$, and strain rate is 50% per minute. The whole tests were performed at $22°C$ and the Relative Humidity is 60%.

Structure Characterization:

Wide Angle X-ray Scattering Patterns (WAXS, Bruker NanoSTAR) of a bundle of degummed silkworm silk filaments were collected to characterize the structure of crystallite and amorphous region including the crystallite size, crystallinity and orientation of crystallites. The sample-to-detector distance rearranged to $4.3cm$.

The beam size was $0.15mm$. The radiation wavelength is $1.5418\mathring{A}$ for Cu K_α. And the sample was tested under vacuum condition with exposure time 2 hours. The generator was operated at Voltage $40kV$ and Current $35mA$.

Chapter 4

Abnormal Stress Relaxation of Silk

In this chapter, we studied experimentally and theoretically the stress relaxation of the *Bombyx mori* silk, and investigated the micro-structural factors influencing its relaxation behavior. Abnormal stress relaxation behavior of silkworm silk was observed, including the bipartite pattern of the stress relaxation profiles under various extension. This pattern was separated by the yield point despite the stretching speeds. Besides, an extremely high degree of stress relaxation in moderate and high strain regions was detected in our step-relaxation experiments, different to the previously findings regarding a minimal influence of viscosity on the silk strength. The highly dissipated strength is probably attributable to the increased viscosity, which was interpreted by the mechanism of "local strain induced thickening". This mechanism was introduced and verified consistently by both our

theoretical modeling and experimental results. It tells that the deformation of the macromolecular segments within silk fibrils enhanced the viscosity of the internal environment. Moreover, we derived the upper and lower bounds of the strength of silkworm silk on one hand, and pointed out the potential applications regarding its envelop of mechanical profile on the other.

4.1 Introduction to Silk Stress Relaxation

4.1.1 Background Knowledge of Stress Relaxation

Stress relaxation of viscoelastic polymeric materials has been widely studied during the past centuries. Polymers comprised of monomer repeats exhibit various stress relaxation profiles according to their diversified components and microstructures[140]. Extensive efforts have been invested into interpreting the stress relaxation of polymeric materials by relating it to the viscoelasticity, where numerous phenomenological models were proposed, including the Maxwell model, Voigt model and many of their generalized variants[141, 142].

Illustrations of the Maxwell model, Voigt model, and the generalization Zener model (Standard Linear Solid Model) are shown in Fig. 4.1. All of them are constituted of Hooke linear springs ($F_e = -k\Delta x$) and linear dashpots ($F_v = -\mu\Delta\dot{x}$). The Voigt model can be applied to describe the retraction of a free-end material, and the Maxwell model can describe the stress profile of exponential decay as follows:

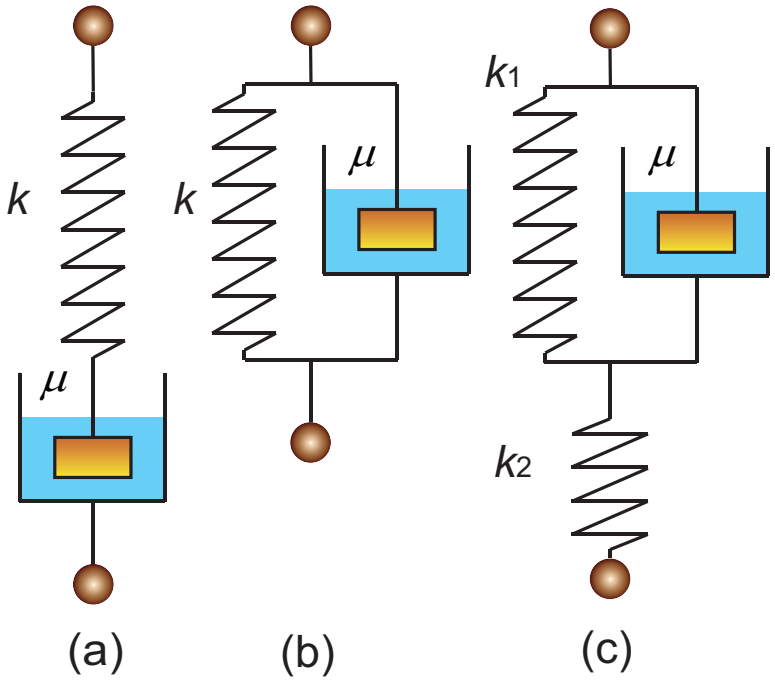

Figure 4.1: **Models of Material Viscoelasticity**. (a) Maxwell model; (b) Kelvin-Voigt model (Voiget model); (c) Zener model (Standard Linear Solid model). The zig-zag black solid line component is elastic spring with elasticity k in (a) and (b), k_1 and k_2 in (c); the yellow block immersed in cyan fluid is the dashpot with viscosity μ.

$$\frac{d\Delta x}{dt} = \frac{d\sigma(t)/k}{dt} + \sigma(t)/\mu. \tag{4.1}$$

Hence, $\sigma(t)$ yields an exponential decay with relaxation time $\tau = \mu/k$ by setting $d\Delta x/dt = 0$. Some of the generalized forms of these models developed in later stages have velocity-dependent viscosity $\mu(\Delta\dot{x})$, which can still be numerically solved. These models properly interpret the interplay between the elasticity and viscosity of certain materials by connecting the model elements in series, parallel or mixed manner. However, they might only be suitable for uniform materials because no information of the micro-structures of materials are provided in these model. Besides, there are lack of evidence that the "elasticity" and the "viscosity" can be connected in such simple ways. Since hierarchical nano-structures of materials may respond to external force differently, the current theoretical framework based on these models may not be sufficient to link the relation between stress relaxation behavior and the hierarchical nano-structured materials.

4.1.2 Motivation of Study of Silk Stress Relaxation

As a prominent family of viscoelastic materials, natural silks reeled from silkworms(*Bombyx Mori*) have attracted scientific and engineering attention for their unusual combination of high strength and extensibility, as well as their high capacity of energy absorbability[45, 46, 133, 143]. The underlying mechanism whereby silk possesses such high strength was proposed by attributing its mechanical properties to its hierarchical structures, including the phenomenological models and atomistic molecular dynamics simulation[89, 98, 102, 143], as was discussed in

Chapter 2 and Chapter 3.

Benefitted from its exceptional mechanical performance, environmental friendliness and biocompatibility, the applications of silkworm silk nowadays have been extended to military and clinic disciplines while it still flourishes in the traditional textile industry[11, 12].

The increasing variety of silk applications and the fabrication of functional silk require a comprehensive understanding of its mechanical responses in different regimes, where its stress-strain profile alone might not provide sufficient mechanical information. For instance, the surgical suture requires a reliable durability of material strength while the bullet proof-vest requires a high level of resistivity against high-speed thrust. From this viewpoint, the responses in the time domain are also important.

Parthasarathy *et al.* determined the viscoelastic properties of *Bombyx Mori* silkworm silk by distinguishing the contributions from elasticity, plasticity and viscosity, respectively[57]. It was claimed that changing the stretching rate could vary the mechanical strength of silkworm silk but only by less than 15%, which was very minimal compared to other elastomers like collagen and elastoidin[57, 58]. Besides, stress relaxation behavior for silks from different species was characterized under low tensions, and the inverse stress relaxation phenomenon was observed when the subsequent retraction was sufficiently large[144]. To alleviate the retarded response due to the silk viscoelasticity, a stepwise strategy was adopted in later studies for their mechanical measurements[110]. Based on the established models, the relaxation profile of silkworm silk may be best-fitted by giving the models sufficient

number parameters[141, 142]. However, the stress relaxation behavior of silkworm silk under large tensions, as an important benchmark of the energy absorbability of silk, which may guide the orientation of further developments in its applications, is yet to be investigated and accounted for under the current theoretical framework.

4.1.3 Objective of Study of Silk Stress Relaxation

In this study, we aim at uncovering the abnormal stress relaxation behavior of *Bombyx mori* silkworm silk and revealing its nature by correlating it with the variation of the secondary structures through a combined method of theoretical modeling with experimental verification. Phenomenological behavior of silk stress relaxation was first figured out throughout the strain range before silk rupture. Meanwhile, a quantitative characterization was carried out to identify the level of stress relaxation at preset strains. The same experiment was also conducted for kevlar and rubber, in order to compare their stress relaxation behavior with that of silkworm silk, as well as to verify the corresponding mechanism. We then tried to reveal the origin of the stress relaxation of silkworm silk by modeling the silk "thickening" during the stretching process, and incorporating into it the "β-sheet splitting" mechanism, which was discussed in Chapter 2.

4.2 Stress Relaxation at Various Strains

4.2.1 Stress Relaxation Profiles

In order to uncover the characteristics of its time-resolved mechanical behavior, stress relaxation experiments of the single-stranded silkworm silk were carried out throughout its extensible strain range. The stress relaxation profiles were tracked for different stretching rates($6\%/min$ or $50\%/min$), as shown in Fig. 4.2(a) and (b). The profiles display robust bipartite patterns for respective stretching rate despite their large difference. The stress relaxation profiles for strains at $\epsilon = 1, 1.5\%$ belongs to one group (fast relaxed), and those of $\epsilon = 5, 10, 15, 20\%$ belong to the other (slow relaxed). To figure out the characteristics of the stress relaxation behavior of silk, one may impose the relaxation time(RT) spectrum analysis, through which the time-dependent stress $\sigma(t)$ can be expanded in the following(Eq. 4.2):

$$\sigma(t) = \sigma(0) \int_0^\infty L^*(\tau) e^{-t/\tau} d\tau, \tag{4.2}$$

4.2.2 Characteristic Relaxation Time Spectra

Since the high instability of Inverse Laplace Transform in deriving the spectrum $L^*(\tau)$, the calculated RTs and their coefficients may diverge for the fluctuating stress profiles[145–147]. The detailed stress relaxation spectrum analysis by using Inverse Laplace Transform and the discussion of instability of this method can be

found in Section A.2 in the appendix chapter. Hence, we would rather examine the dominant RTs from the relaxation profiles while best maintaining their accuracy. A third-order exponential function ($\sum_{i=1}^{3} E_\epsilon(\tau_i)e^{-t/\tau_i}$) turns out to be a good estimator to characterize the discrete RT Spectrum, where τ_i denotes the value of characteristic RTs, and $E_\epsilon(\tau_i)$ the corresponding coefficients of each mode(Fig. 4.2(c) and (d)). It was found that the three RTs τ_i for various strains located in the magnitudes of $10s$, $100s$ and $1000s$ respectively, with comparable $E_\epsilon(\tau_i)$s.

The RTs for stress relaxation at strains $\epsilon = 5, 10, 15$ and 20% almost overlap with each other, but they apparently deviate from that at strain $\epsilon = 1\%$ and 1.5%. Despite the equal-importance of the three characteristic RTs in the stress relaxation profiles, the coefficients of them $E_\epsilon(\tau_i)$ increase with τ_i at strain $\epsilon = 1\%$, but they decrease at other strains. It implies that the the stress-relaxation at strain $\epsilon = 1\%$ is long-RT dominant while it is short-RT dominant at other higher strains. Interestingly we found that the transition from the long-RT to short-RT dominance occurs approximately at the yield point($\sim 2-3\%$), which quantitatively reconfirm the result shown in Fig. 4.2. From the analysis of the stress relaxation profiles of silkworm silk, one may foresee that different relaxation pattern is probably induced by the structural transition below and above the yield point, specifically the variation of the secondary structures.

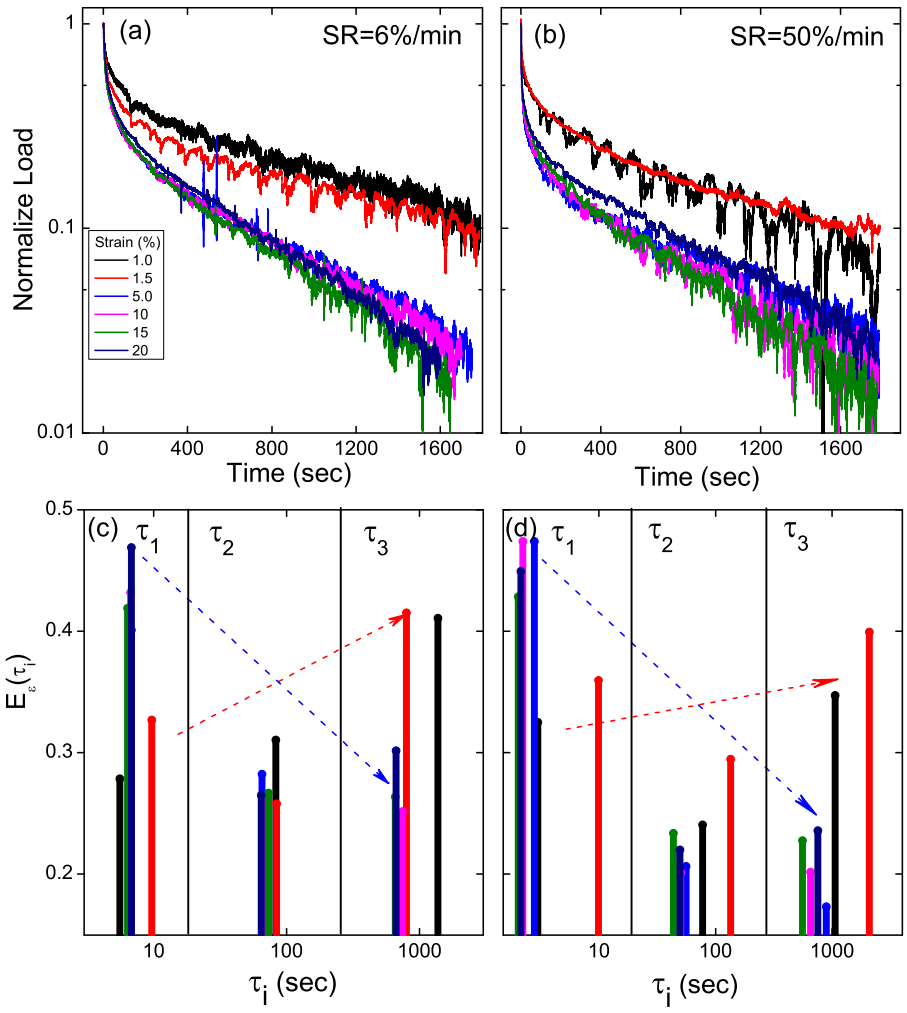

Figure 4.2: **Stress Relaxation at Fixed Strains**. Panel (a) and (b) show the stress relaxation profiles at different strains($\epsilon = 1, 1.5, 5, 10, 15$ and 20%). The stress relaxation experiments were performed under two stretching rates $6\%/min$(a) and $50\%/min$(b). Panel (c) and (d) display the characteristic RTs τ_i by the colored columns within the three sections from left to right. $E_\epsilon(\tau_i)$ denotes the portion of each RT τ_i. The red and blue dashed arrows display a general ascending and descending trend of the $E_\epsilon(\tau_i)$ at relaxing strains $\epsilon = 1, 1.5\%$ and $\epsilon = 5, 10, 15, 20\%$.

4.3 *In-situ* Stress Relaxation of Silk

4.3.1 Introduction to *In-situ* Stress Relaxation

To unravel the structural factors affecting the stress relaxation of silkworm silk, step-relaxation experiments were designed and implemented to monitor the stress relaxation throughout the extendable strain range. Different from the previous work imposing the stepwise strain control to minimize the transient influence of viscosity on mechanical measurements[110], we are more interested in the behavioral manners of stress relaxation in moderate and high strain region. Fig. 4.3(a) shows an illustrative stress-strain profile derived from the step-relaxation experiments, and it exhibits a typical saw-tooth pattern where the vertical "drop" of each "saw tooth" represents the stress relaxing at a fixed strain. Analogous to the relaxation index n defined for the stress relaxation in the linear response region[144], a quantity, referred to as the Differential Relaxation Index(DRI) $n(\epsilon)$, was defined in Eq. 4.3:

$$n(\epsilon) = \frac{\sigma'(\epsilon + d\epsilon) - \sigma'(\epsilon)}{\sigma(\epsilon + d\epsilon) - \sigma'(\epsilon)}, \tag{4.3}$$

where $\sigma(\epsilon + d\epsilon)$ denotes the instantly monitored stress when a material sample is stretched from strain ϵ by $d\epsilon$ in its relaxed state; $\sigma'(\epsilon)$ denotes the residual stress at strain ϵ. The DRI indicates the level of stress relaxation at a certain strain, within the range 0 to 1. It is 0 for an ideal elastomer with no damping, and it is 1 for a pure viscous material.

4.3.2 The DRI vs Strain Profile of *Bombyx mori* Silk

Fig. 4.3 (b) shows the dependence of DRI $n(\epsilon)$ on strain ϵ for an ensemble of samples, and Fig. 4.3(c) presents their statistical relation. The result presented a monotonic ascending trend of DRI against the tensile strain before the strain reaches $\epsilon \approx 3\%$, and it stayed at a plateau of $n \approx 0.9$ subsequently. We found that the transition from the increase to a plateau of DRI arises at the strain close to the yield point, which implies that the silkworm silk experienced a relatively more viscous environment under high tension.

One probable reason of the increased DRI may be attributed to the decreased post-yield modulus, as is widely observed in the conventional stress-strain profile of silkworm silk. The reduction of the elastic energy will relatively enlarge the portion of viscous energy thus increase DRI. However, contrary to the previous works claiming that the viscosity was merely a minor contributor to the silk strength, an extreme high level of stress relaxation at moderate and high tensile strain region was observed, and DRI reached as large as 0.9 measured in our experiments although our stretching rate $(0.1\%/sec)$is relatively low comparing to that in the conventional mechanical tests.

The exciting finding tells that the large viscous contribution of the silk strength gives rise to high instant moduli in the post-yield region, despite the majority of the viscous energy dissipation during a finite-rate stretching process. This is because the increased stress within the strain interval $(\epsilon_0, \epsilon_0 + d\epsilon)$ is counteracted by the dissipation of the stress loaded during previous steps. Therefore, on one

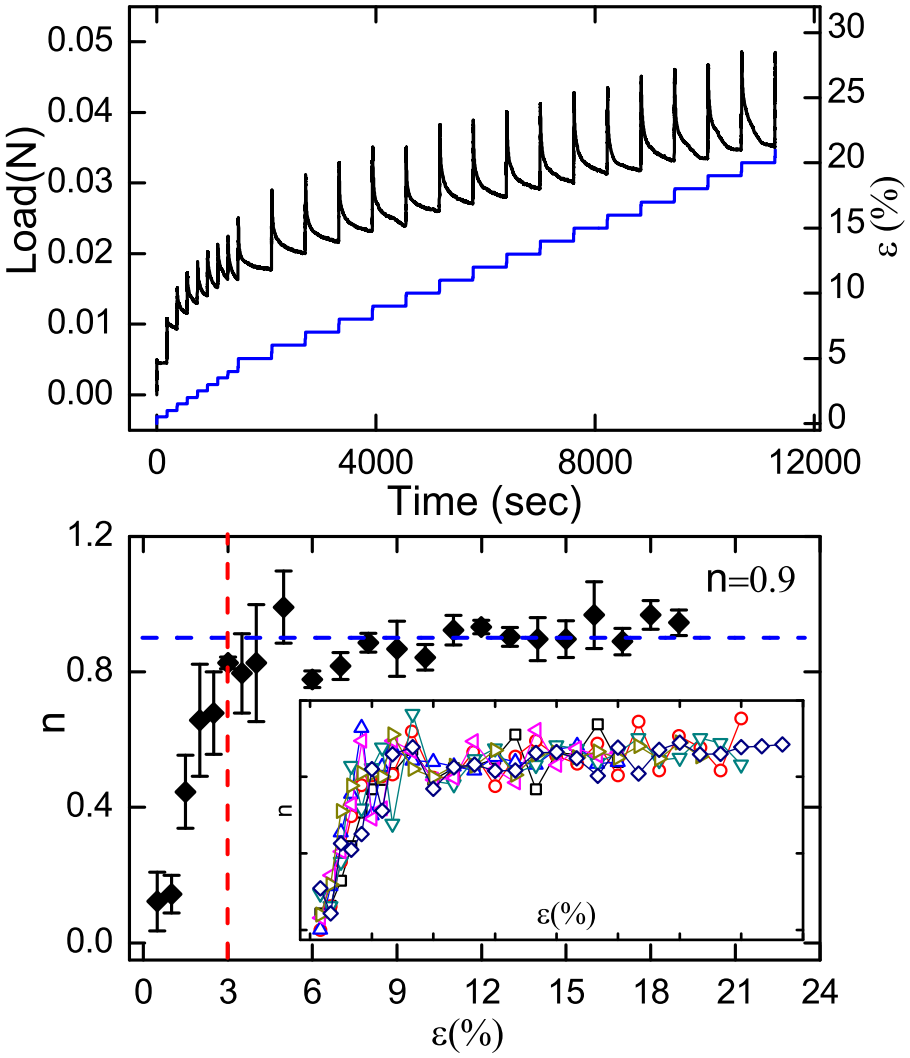

Figure 4.3: **DRI Dependence on Strain of Silkworm Silk**. The upper panel is an illustrative diagram of stress-strain profile under a stepwise strain control; The lower panel is statistical relation between DRI $n(\epsilon)$ and strain ϵ, and the inset of the lower panel shows the relation for 7 silkworm silk samples.

hand, silkworm (*Bombyx mori*) silk may be a potential candidature for new proof-vest material, resisting high-rate thrust by taking use of its viscous energy. On the other hand, by performing the step-relaxation experiment, we were able to approach the lower limit of the stress at certain strains in the stress-strain profile, which was referred to as the "quasi-static" mechanical profile, and reflects the intrinsic elasto-plastic behavior of silk.

4.4 Local Strain induced Thickening of Silk

4.4.1 Mechanism of Abnormal Stress Relaxation of Silk

Although we have observed a high level of dissipation of the silkworm silk strength in moderate and large stain region, as well as an increasing trend of viscosity in small strain region, the nature of this phenomenon with respect to the nano-structures of silk remain unrevealed.

Hence, we proposed a model to uncover the underlying mechanism of the stress relaxation of silk. Conventional stress-strain profile of silkworm silk was studied in our previous work by introducing the "inter-molecule β-sheet splitting" mechanism to explain its softening transition from rubbery to glassy state[99, 143]. It is known that there are only molecular shearing and deformation without the destruction of inter-molecular structures in the linear response region of silk.

However, the time-resolved behaviors may not be simply depicted by considering solely the variation of the silk elasticity and presuming a newtonian fluid-like matrix with constant viscosity. According to the large Poisson Ratio (~ 0.4) of silkworm silk[67], the macromolecule segments within become better aligned along the longitudinal axis while they become more squeezed in the transverse cross-section when being stretched, as shown in Fig. 4.4. To precisely characterize the abnormal stress relaxation phenomenon, we introduce the "local strain induced thickening" mechanism to replace the newtonian fluidic approximation, in order to describe the viscosity variation of silkworm silk under deformation. This mechanism tells that stretched molecules have more inter-molecular contact due to the better alignment than their relaxed state. Besides, the transverse shrinkage of the cross-section area induces additional friction of molecular segments.

4.4.2 Modeling of Silk Stress Relaxation

Based on this understanding, a linear assumption of local viscosity $\mu_x(\epsilon_x^+, \epsilon_x^-)$ was proposed with respect to the local strain in the linear response region as,

$$\mu_x(\epsilon_x^+, \epsilon_x^-) = \gamma(\epsilon_x^+ + \epsilon_x^-), \tag{4.4}$$

where ϵ_x^+ and ϵ_x^- represents the local strain of the crystallite located at the position x(normalized by the gauge length of silk samples) by its left(+) and right(−) neighboring adjacency. And the equation of motion for the crystallite at x yields,

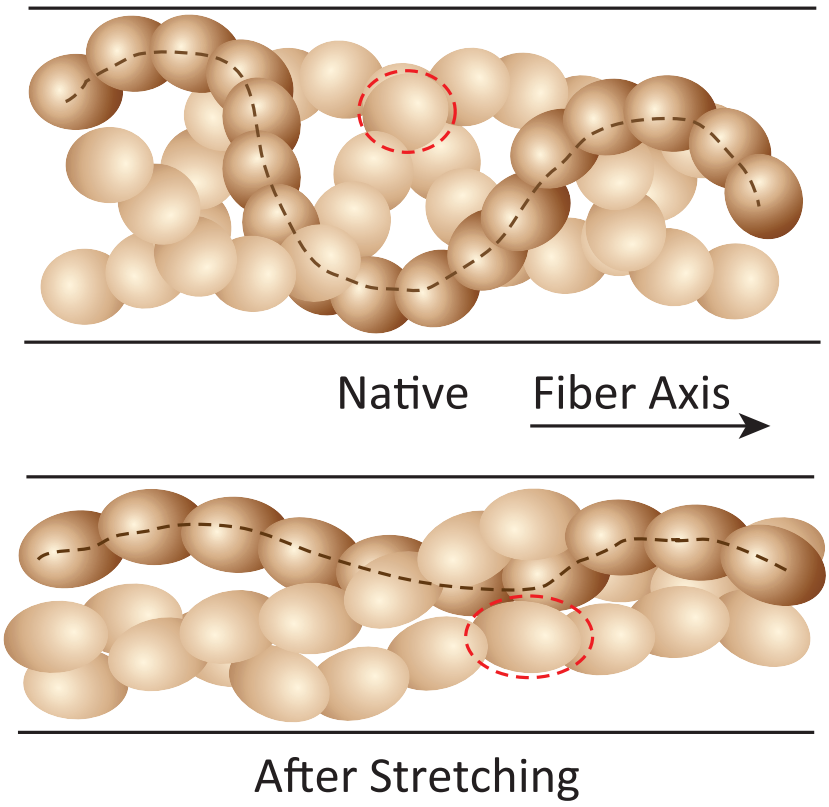

Figure 4.4: **Illustration of "Strain-Induced Thickening" Mechanism**. The upper panel is the conformation of the fibrils within a strand of silkworm silk fiber in its relaxed state; the fibrils are loosely coiled, and the inter-fibrilar contact is week due to a small internal transverse pressure. The lower panel shows the fibril conformation of silkworm silk when stretched; the fibrils are more squeezed and aligned, which gives rise to more inter-fibrilar contact and larger frictional force due to an increased internal pressure.

$$m\ddot{\epsilon}_x = F(\epsilon_x^+) + F(\epsilon_x^-) - \mu_x(\epsilon_x^+, \epsilon_x^-)(\dot{\epsilon}_x - xv), \tag{4.5}$$

$F(\cdot)$ follows Eq. 2.3 by taking into account the "inter-molecule β-sheet splitting" mechanism. It indicates that there exist threshold forces $F_{th}(\epsilon_x)$, beyond which the inter-protein β-sheet crystallites within silk fibrils start to split. v denotes the stretching rate, and xv is the velocity of a matrix under uniaxial extension along the fiber axis. Extensive molecular dynamic simulations were carried out to mimic the step-relaxation experiment, and to explore the relation between DRI and strain. Fig. 4.5 shows that simulated DRI-strain relation is in good accordance with the experimental one, which presents an increasing slope of DRI when the strain is below the yield point and a plateau about 0.9 when above it. The consistency of the results implies that the increased viscosity in linear response region is caused by deformation of protein macromolecular segments where the "local strain induced thickening" mechanism was quantitatively implemented, and that the "inter-protein β-crystallite splitting" remains the dominant mechanism in post-yield region.

4.5 *In-situ* Stress Relaxation of Polymers

In Section 4.3, we have observed an abnormal stress relaxation characteristics of silkworm silk that most plasto-elastic energy ($\sim$ 90%) are dissipated, showing its great energy absorbability. Besides, from Fig. 4.3, the DRI reaches the high value plateau very steeply at strain around 3%. The mechanism we proposed in

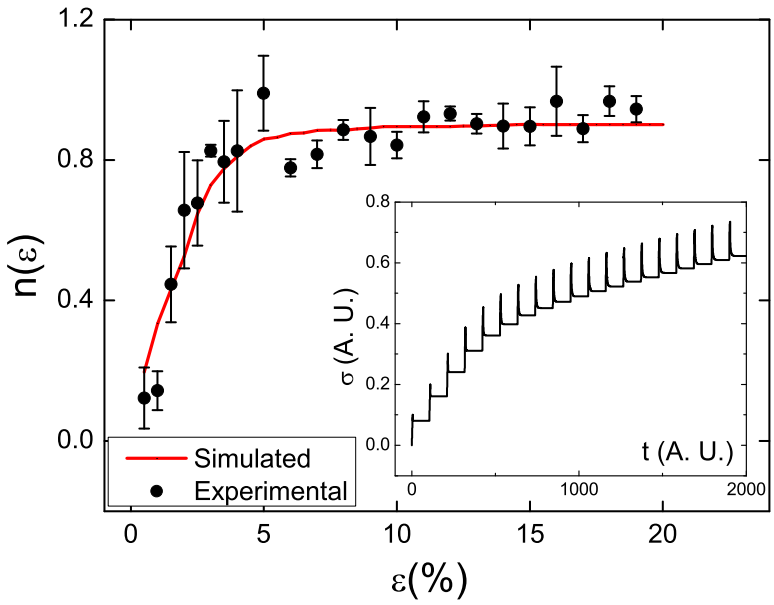

Figure 4.5: **Comparison of Computed and Measured DRI vs Strain Relation**. The main panel shows the relation between DRI $n(\epsilon)$ and strain ϵ derived by both experiment and simulation. Inset is the stress profile with time evolution for the step-relaxation simulation, and the $n(\epsilon)$ was calculated in each step when the stress reached a plateau.

Section 4.4 for the increase of viscosity is the "local strain induced thickening". Here without loss of generality, we carried out similar experiments mentioned in Section 4.3 for two typical polymeric material: 1). Kevlar; 2). rubber, in order to distinguish their stress relaxation behavior on one hand, and verify the proposed mechanism on the other.

From Fig. 4.6, it is found that there is a large linearly increasing region of the DRI vs strain relation, and the relation starts deviating from the linear relation only at very large strains comparing with their breaking strains. Conventional mechanical measurements under strain rate $6\%/min$ give the values of breaking strain of $\sim 4.5\%$ for Kevlar and $\sim 250\%$ for black rubber. Hence, our proposed mechanism "local strain induced thickening" is valid for both materials though their strength and extensibility are dramatically differently from each other. The deviation from the linear relation of DRI vs strain can be interpreted by its structural destruction at high strain range due to its brittleness. Meanwhile, we also notice that black rubber experiences work-hardening region for strain greater than 150%, and previous works show that the strain induced better alignment of polymeric chains of rubber leads to a "crystallization" within rubber strand, which give rises to a dramatic increase of its elasticity. This effect will bend the DRI value down due to the increased value of elasticity of black rubber. In general, the internal viscosity of materials, with absence of high level structural change, will increase with the local strain due to an externally applied force, which is termed as "local strain induced thickening" mechanism.

Meanwhile, we observed the maximum of DRI values are 0.39 for Kevlar and 0.67 for black rubber, much lower than that of *Bombyx mori* silkworm silk. Besides, the

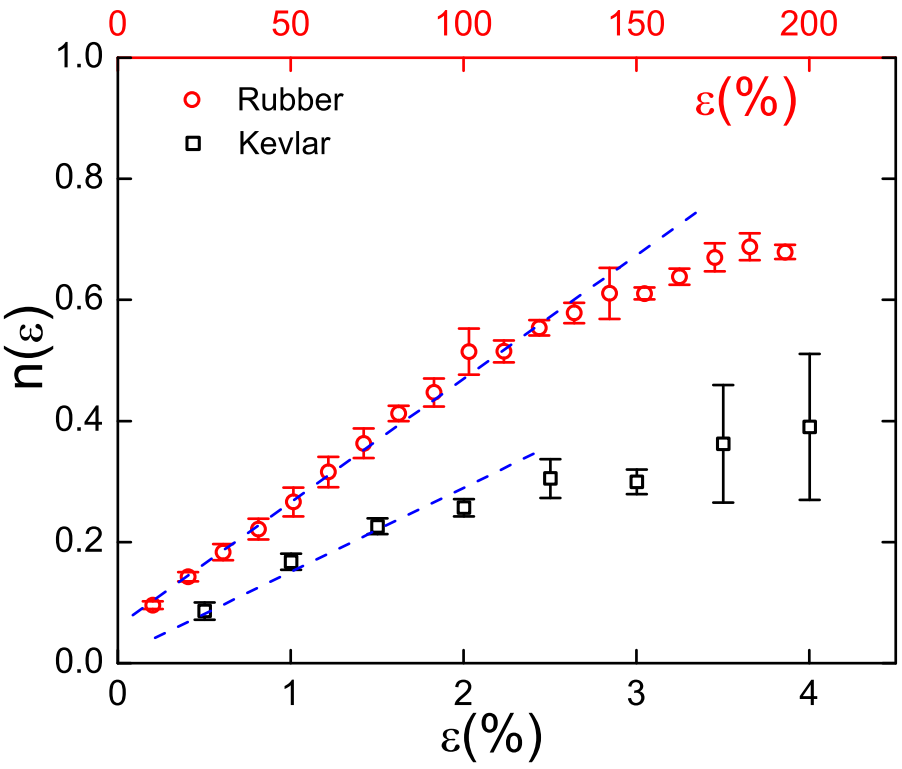

Figure 4.6: **DRI vs Strain Relation of Kevlar and Rubber**. The black hollow squares denote the DRI $n(\epsilon)$ values of Kevlar at different strains ϵ, and the strain ranges from 0.5% to 4% with 0.5% interval for each measurement. The red hollow circles denote the DRI values of black rubber at different strains, and its strain ranges from 1% to 191% with an interval of 10%. The error bars show the standard deviation calculated from 7 samples for Kevlar and 5 samples for black rubber respectively.

relative strains (comparing with the breaking strain) of silkworm silk is far earlier than that of Kelvar and black rubber. This finding shows that the silkworm silk is a good energy dissipating materials, and the energy absorption is much better comparing with typical polymeric materials which also have been wide used, and have their respective applications. It provides the potential that silkworm silk can be a great candidate for resisting high-speed thrusts or bulletproof vest materials.

4.6 Envelop of Mechanical Profile of Silk

Having known as good energy absorbing material, the mechanical profile of silkworm silk under different rate stretching and the amount of energy it can dissipate during the stretching process turns out to be an immediate question. In this section, we aim to address the above mentioned issues. In order to the extent of the energy dissipation, we purposed to reconstruct the quasi-static mechanical profile based on the derived strain-dependent DRI $n(\epsilon)$ in the first place. By distinguishing strength contribution by the elasticity and viscosity, the quasi-static stress $\sigma_{qs}(\epsilon)$ and the stress $\sigma(\epsilon)$ for finite stretching rate v write:

$$\sigma_{qs}(\epsilon) = \int_0^{\epsilon} (1 - n(\epsilon'))d\sigma_0(\epsilon') \tag{4.6}$$

$$\begin{aligned} \sigma(\epsilon) &= \sigma_{qs}(\epsilon) \\ &+ \int_0^{\epsilon} n(\epsilon')d\sigma_0(\epsilon') \int_0^{\infty -} L^*_{\epsilon'}(\tau) e^{\frac{-(\epsilon-\epsilon')}{v\tau}} d\tau \end{aligned} \tag{4.7}$$

where $L^*_{\epsilon}(\tau)$ is the RT spectrum of stress relaxation at strain ϵ, and $d\sigma_0(\epsilon)$ is a

tiny increment of stress at strain ϵ without the dissipation of the stress loaded at the previous stages. $L^*_\epsilon(\infty) = \delta(0)(1 - n(\epsilon))$ is extracted to the first term on the right of Eq. 4.7 to avoid the singularity. Considering the 10-fold difference of RTs as was analyzed in Fig. 4.2 despite the strains, it is rational to simplify Eq. 4.7 by replacing the spectrum expansion in the stress relaxation express with a mono-exponential function of RT τ_0 for a rough estimation, as shown in Eq. 4.8

$$e^{-(\epsilon-\epsilon')/v\tau_0} = \int_0^{\infty-} L^*_{\epsilon'}(\tau)e^{-(\epsilon-\epsilon')/v\tau}d\tau. \tag{4.8}$$

In practice, we reconstructed the quasi-static mechanical profile by discretizing Eq. 4.6 and 4.7 in the following: set the sampling rate to be $1/\Delta$, and strain ϵ under finite stretching rate v is $\epsilon(m) = vm\Delta$, where m is the number of the sampled data. Thus, notations could be abbreviated as $\sigma(\epsilon) \to \sigma^m$, $\sigma_{qs}(\epsilon) \to \sigma^m_{qs}$, $d\sigma_0(\epsilon) \to \sigma^j_0$ and $n(\epsilon) \to n^m$, for the stress by finite-rate stretching, the stress by quasi-static process, the increment of stress solely by extending silk from $\epsilon(j-1)$ to $\epsilon(j)$ and the DRI at strain $\epsilon(m)$, respectively. σ^j_{ob} is defined as the experimentally observed stress increment$(\sigma^j - \sigma^{j-1})$ for strain from $\epsilon(j-1)$ to $\epsilon(j)$. Hence, a recursive relation was derived from Eq. 4.7 that:

$$\sigma^{m+1}_0 = \sigma^{m+1}_{ob} - e^{-\frac{\Delta}{\tau_0}}\sigma^m_{ob} + \sigma^m_0(n^m + e^{-\frac{\Delta}{\tau_0}}(1 - n^m)). \tag{4.9}$$

The quasi-static stress σ^m_{qs} can be calculated following the relation that $\sigma^m_{qs} = \sum_{j=0}^m (1 - n^j)\sigma^j_0$(Fig. 4.7(a)). Herein we fitted the DRI-strain relation in a continuous form: $n(\epsilon) = 0.3\epsilon$ for $\epsilon < 3(\%)$ and $n(\epsilon) = 0.9$ for $\epsilon \geq 3(\%)$.

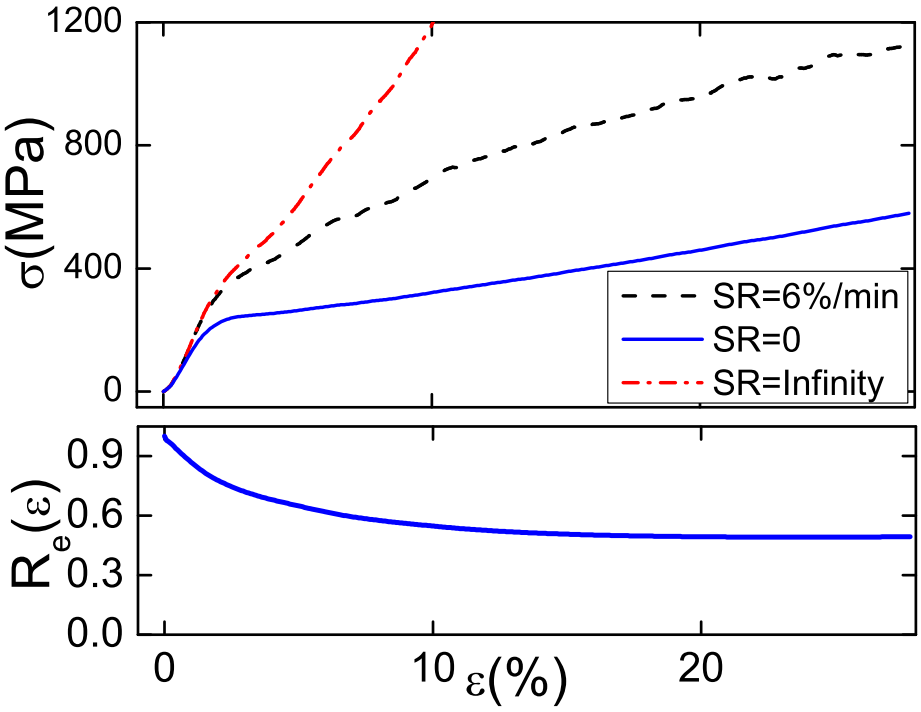

Figure 4.7: **Envelop of Stress-strain Profile of Silkworm Silk**. The upper panel shows the stress-strain profile of silkworm silk for stretching rate(SR)= 0(solid blue line), $6\%/min$(black dashed line) and ∞(red dotted dashed line) respectively, indicate the quasi-static process, conventional stretching and high-speed thrust in order; the lower panel shows the dependence of the elastic energy ration $R_e(\epsilon)$ on the strain of silk.

Accordingly, the elastic energy ratio $R_e(\epsilon)$, defined as proportion of the area under the stress-strain profile by the quasi-static process to that by a finite stretching rate process, can be derived once we obtained the quasi-static mechanical profile (Fig. 4.7(b)). We found that for stretching rate as low as $0.1\%/sec$, there were about 50% out of the silk toughness at strain about 25% contributed by its viscosity. It arises the precaution for the durable or sustainable applications of silkworm silk that the strength requirement need to be lower than the quasi-static strength of silk. This precaution is also necessary to be extended to other viscoelastic materials despite their different viscosity-to-elasticity ratio.

Besides, the stress-strain profile by infinite rate stretching indicates an adiabatic process, during which plasto-elastic energy does not have time to be dissipated. Therefore, the stress at strain ϵ can be calculated by summing over the stress increment at each $d\epsilon$ interval without dissipation, following Eq. 4.10.

$$\sigma_{inf}^{m} = \sum_{j=0}^{m} \sigma_0^j, \tag{4.10}$$

Herein, we do not take the creep effect into account which may cause locally structural destruction due to the localized stress distribution. Either the defect-dominant rupture of materials at ultra-fast stretching is not considered. The omittance of these effects will lead the practical mechanical profiles under ultra-fast rate stretching deviate from the ideally computed case. However, it can still be regarded as a reference of the strength limit of silkworm silk, as it provides the upper-bound of the stress-strain profiles of native silkworm silk under various strain rate. The high post-yield modulus of silkworm silk, as can be seen from Fig. 4.7, is

comparable to the elastic modulus in linear response region, revealing its potential of high-speed resistivity.

4.7 Summary

We studied the stress relaxation of silkworm silk under various experimental conditions and revealed the structural origins of such abnormal relaxation behavior through theoretical modeling. We found a bipartite pattern of stress relaxation throughout the strain region, which acquired distinguishable characteristic RT spectrum in the first place. More importantly, an extremely high level of stress relaxation at moderate and high extensions was observed, resulting in much higher instant moduli than the post-yield moduli measured in conventional finite-rate stretching. The structural factors were also revealed by our modeling that the "local strain induced thickening" mechanism provided a highly viscous environment of silkworm silk under tension, and the "inter-protein β-crystallites splitting" took effect to soften the silk when it was extended beyond the yield point.

The mechanism of "local strain induced thickening" is also verified by the step relaxation experiments of Kevlar and black rubber although their mechanical properties deviates significantly. Comparing with Kevlar, black rubber and silkworm silk, the energy absorbability of silkworm silk is extremely high, which gives rise to its potential applications, acting as a candidate of proof vest materials resisting high-speed thrust.

Additionally, mechanical profiles for two limiting cases, indicating the infinite-rate and quasi-static stretching process respectively, were derived based on the dependence of stress relaxation degree on the extension of silk. The two limiting cases not only present the upper and lower limits of the mechanical profiles under various stretching rates, but also grant valuable references for the time-resolved applications of silkworm silk[1].

[1]The experiments of stress relaxation at various fixed strain of *Bombyx mori* silkworm silk, and the experiments of step-relaxation measurement of silkworm silk were conducted by Mr Yang Li. The experiments of step-relaxation measurement of Kevlar and black rubber were conducted By Tan Chek Kiang Joel.

4.8 Methods

4.8.1 Experimental Procedures

Stress Relaxation at Various Fixed Strain:

All the mechanical measurements of *Bombyx mori* silkworm silk were performed by using an Instron Microtester 5525X (Instron. Inc, Singapore, force resolution 0.5% (unit of indicated load), position resolution $0.02\mu m$, mounted load cell 0.5N, sampling rate $50ms^{-1}$) under room condition ($23°C$ & RH 50%). The diameter of the cocoon silkworm silk chosen is $\sim 11\mu m$. Before each experiment was performed, all samples were subjected to $5 \sim 10$ cycles of 1% strain followed by a return to their original gauge length and relaxed for $30mins$.

Silk fiber was stick to the paper frame with $20mm$ gauge length before mounted to Instron Microtester. A degummed cocoon silkworm (degumming procedure can be found in Section 3.5) silk fiber sample is stretched to the strain 1%, 1.5%, 5%, 10%, 15% and 20% at constant strain rates $0.1\%/sec$ and $0.83\%/sec$ respectively, and hold for 1800 seconds at each set of experiments.

Step Relaxation of Silk:

The step relaxation shown in Fig. 4.3 was realized by repeated cycles composed of a stretching process with constant rate $0.1\%/sec$ and a stress relaxation period.

For strain less than 4%, silk samples were strained for 0.5% in the stretching process of each circle, followed by a period of 180 seconds holding for stress relaxation. For strain greater than 4%, silk were strained for 1.0% in the stretching process of each circle, followed by a period of 600 seconds holding for stress relaxation.

Step Relaxation of Kevlar:

Single stranded Kevlar fibres with an average diameter of $13.6362\mu m$ were chosen for this experiment. Kevlar fibre samples were affixed to a paper frame. The gauge length of the samples was $20mm$. Step-relaxation experiments were performed using an Instron 5848 Microtester(Instron. Inc, Singapore, force resolution 0.5% (unit of indicated load), position resolution $0.02\mu m$, mounted load cell 0.5N, sampling rate $50ms^{-1}$), under room condition ($23^{\circ}C$ & RH 50%).

The step relaxation experiment of kevlar was performed by repeated cycles composed of a stretching process with constant rate $0.1\%/sec$ and a stress relaxation period. Kevlar fiber samples were strained for 0.5% in the stretching process of each circle, followed by a period of 180 seconds holding for stress relaxation. The time, stress and strain were recorded during this process with preset machine resolutions. The strain rate is $0.1\%/sec$.

Step Relaxation of Rubber:

Rubber strips with average dimensions of $1.8x0.8mm^2$ were sampled from a sheet of natural black rubber. Diameters of the rubber strips were measured before and

after the experiment with a pair of vernier calipers. The gauge length used in the tensile tests was $10mm$. The gauge length of the samples was $10mm$. Step-relaxation experiments were performed using an Instron 5848 Microtester(Instron. Inc, Singapore, force resolution 0.5% (unit of indicated load), position resolution $0.02\mu m$, mounted load cell 5N, sampling rate $50ms^{-1}$), under room condition ($23°C$ & RH 50%).

The step relaxation experiment of black rubber is was performed by repeated cycles, which is composed of two sub-cycles within each cycle. In the first sub-cycle, termed as "step cycle", the black rubber strip samples were strained for 1.0% in the stretching process of each circle, followed by a period of 2400 seconds holding for stress relaxation. In the second sub-cycle, termed as "stride cycle", the black rubber strip samples were strained for 9.0% in the stretching process of each circle, followed by a period of 2400 seconds holding for stress relaxation.

The time, stress and strain were recorded during the entire process with preset machine resolutions for all the above conducted experiments.

4.8.2 Theoretical and Computational Mehtods

Stress Relaxation Analysis: The stress in Fig. 4.2 (a) and (b) is normalized in the following:

$$\sigma(t) = (\sigma_{exp}(t) - \sigma_{exp}(\infty))/(\sigma_{exp}(0) - \sigma_{exp}(\infty)), \tag{4.11}$$

where $\sigma_{exp}(t)$ denotes the experimental values of stress at time t, which is recorded when the stress relaxation happens. $\sigma_{exp}(\infty)$ denotes the residual stress when $t \to \infty$.

The RT spectra are expanded in the third-order exponential form in Eq. 4.12:

$$\sum_{i=1}^{3} E_\epsilon e^{-t/\tau_i}, \tag{4.12}$$

where the determining parameters are E_ϵ and τ_i for a give stress relaxation profile at fixed strain ϵ. These parameters are best fitted under the restrictions that $E_\epsilon \geq 0$ and $\tau_i \geq 0$ for any component i at any strain ϵ. If the order of the exponential function is equal or greater than 4, the non-negative values E_ϵ and τ_i are no longer valid. The RTs range in the magnitudes of $10sec$, $100sec$ and $1000sec$, respectively for stress relaxation at the corresponding strains, which is consistent with the separation of characteristic relaxation time discussed in Ref [147].

MD Simulation: In the MD simulation of *Bombyx mori* silk, Velocity Verlet algorithm was used. The modeling parameters are shown in Table 4.1.

Table 4.1: Parameters in the Modeling of Silk

Parameter Name	Notation	Value
Size	N	100
Original Inter-crystallite Distance	L_0	1.0
Time Step	Δt	0.01, 0.005, 0.001
Stretching Rate	$\Delta \dot{x}$	$0.1\%/sec$
Scaling Constant	S_c	400[a]
Step Cycle	N. A.	$0.5\%/step$
Maximum Strain[a]	ϵ_{max}	25%
Viscosity	μ	0.04
Mean Threshold Force	$\langle F_{th}(\epsilon_x)\rangle$	0.03
Spread of F_{th} [c]	σF_{th}	$0.2\langle F_{th}(\epsilon_x)\rangle$

[a] The mass of crystallites is set to be sufficient small to make the inertia of crystallites little, by maintaining its impact in the stress imbalance within the system. The equations of motion were scaled by the mass in practical simulation.

Chapter 5

Impact of Twisting on Mechanical Strength of Silk

In this chapter, we extensively examined the mechanical properties of silkworm silk and spider dragline silk under twisting in order to investigate the effect of twisting on the mechanical response in longitudinal direction, as well as the cross-dimensional coupling. It was found that the modulus of silk increased with increasing twisting, and an optimal modulus of silkworm silk was detected. Despite the structurally inferior rupture properties for silks under twisting, the strategy is still beneficial to reinforce the energy absorbability in the low-strain region. Such observed properties are attributed to the elastomeric structural origin, combined with the secondary structure destruction for silk under a high level of twisting. Our results open the mechanical investigation along the cross-axis dimension, and the enhanced initial rigidity gives rise to the potential to fulfill certain biomedical

applications.

5.1 Introduction to Silk Torsion

5.1.1 Silk Response of Torsional Motion

The longitudinal mechanical responses of silks, including silkworm silk and spider dragline silk, have been extensively studied, and their extraordinary properties attracted considerable attention in scientific, engineering and biomedical disciplines for decades[6, 7, 11–14].

However, the torsional mechanical responses are little known till the discovery of the "shape memory effect" of spider dragline silk[40, 41]. These studies show that the torsional motion of spider draglines has two features. 1), A very fast oscillatory decay of the torsional angle when silk is suddenly released from a torsional confinement; this oscillatory motion of silk lasts up to several tens of seconds, but the pseudo-equilibrium where it stops is deviated from its actual equilibrium position. 2), A slow multi-exponential decay to the initial equilibrium occurs. A general torsional relaxation profile of spider dragline silk can be seen in Fig. 5.1(a). Such unrivalled natural quality of spider draglines prevents spider from a rapid spinning and the slow process of the self-recovery nature is rarely seen in other materials, demonstrating that spider draglines experience no torsional plastication during this process.

Similar torsional experiment for *Bombyx mori* silkworm silk was conducted, as shown in Fig. 5.1(b). The relaxation profile of silkworm silk has no speciality, exhibiting an under-damping relaxation mode, where the amplitude of the oscillation decays exponentially and the oscillation follows a harmonic manner with a fixed frequency[148]. The relaxation profile of silkworm silk is relatively conventional, as can be widely seen in other viscoelastic materials. A torsional elastomer model was then applied, which yields the equation of motion:

$$I\frac{d^2\theta}{dt^2} + C\frac{d\theta}{dt} + \kappa\theta = \tau(t), \tag{5.1}$$

where I is the moment of inertia of the suspending article, C is the torsional viscosity, κ is the torsional elasticity, and $\tau(t)$ is the time-dependent torque applied. The time dependence of torsional angle $\theta(t)$ can be solved given initial conditions($\theta(0) = \theta_0$, $\dot{\theta}(0) = 0$ and $\tau(t) = 0$). The torsional rigidity was calculated to be $\sim 20kgm/s^2$. It turns out to be the first characterized quantity in the torsional motion of silk.

Compared to spider draglines, the relaxation of silkworm silk does not follow a two-component decaying pattern. It suggests that the composition of this material is not the only cause of the unique "shape memory effect", rather the hierarchical structure is responsible to such properties. Accordingly, the above studies are the start of the understanding of the mechanical behavior in the cross-sectional plane of silk fibers. Currently the focus in this investigation is on the "kinetics" rather than "mechanics". Hence, the torsional properties of silks have yet been well understood.

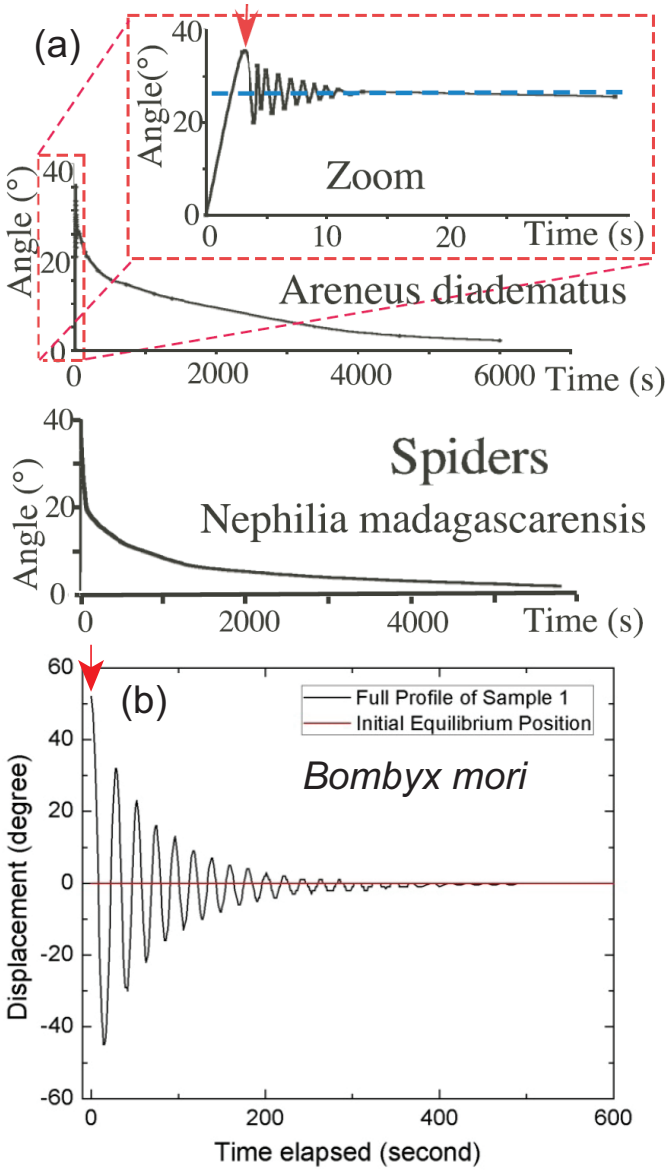

Figure 5.1: **Experimental Torsion Pendulum Relaxation Dynamic Profiles**. Red arrows denote the time point the applied torque is released. (a) Profiles for types of spiders - *Araneus diadematus* and *Nephila madagascarensis*[41]; the inset is the zoom of the beginning of the relaxation profile. (b) Profile of *Bombyx mori* silkworm silk[148].

5.1.2 Motivation and Objective

Great efforts have been dedicated to the improvement of silk quality. Mechanical properties such as strength, elasticity, and toughness raise the most widely concern. As mentioned in Section 1.2.2, chemical, physical, and biological methods have been adopted to achieve greater strength of silk. Among these methods, the physical ways, such as change in reeling styles in silk spinning process, are preferential, due to their low-cost, environmental friendliness and great potential in industrialization.

The torsional relaxation patterns of silks have been characterized, as shown in Fig. 5.1, where the pattern of silkworm silk can be interpreted by conventional linear torsional elastomer. However, the effect of twisting on silk strength remains unknown. Hence, the aim of this study is to investigate the influence of torsion on the longitudinal mechanics, as well as the coupling between fiber axis and cross-axis direction.

5.2 Impact of Twisting on Longitudinal Mechanical Properties

5.2.1 Mechanical Profiles of Twisted Silk Fibers

In order to investigate the effect of torsion on the mechanical strength of silk, mechanical measurements of twisted silk fibers were conducted. *Bombyx mori*

silkworm cocoon silk and *Nephila Pilipes* spider major ampullate dragline silk were chosen as representative samples in this study.

Mechanical profiles of silkworm silk and spider draglines are shown in Fig. 5.2(a) and (b). For both types of silk fibers, the curves from the twisted samples are similar to the untwisted profiles, and all stress-strain curves locate within the stress envelop in respective cases. Here the extent of twisting is quantified by the torsional angle, and is referred to as "*twisting angle*". To be more rigorous, the twisting angle needs to be scaled by the sample length and cross-sectional area. The scaling was omitted because the same sample length was taken and comparison was conducted within each species. These mechanical profiles can serve as evidence that the twisted silk fibers subject to various twisting angles did not suffer from severe structural variation, and that little local structural destruction occurred which might induce considerable mechanical differences.

Particular concerns were then put into the inter-species difference of mechanical responses under different twisting angles. In Fig. 5.2(a), various stress-strain profiles cross at the strain about 7.5%. The silk fibers under higher twisting angle acquire higher stress values before this crossover point, but they acquire lower stress values after that. The stress-strain profiles of spider dragline silk under twisting are always above the untwisted ones throughout the strain range, but they reach a rupture at a lower strain. For both silks, the ultimate strengths of the twisted silk are inferior to the untwisted ones.

To explore the structural origin, the different content of crystalline region could cause such mechanical difference. As is widely accepted, the crystallinity of *Bombyx*

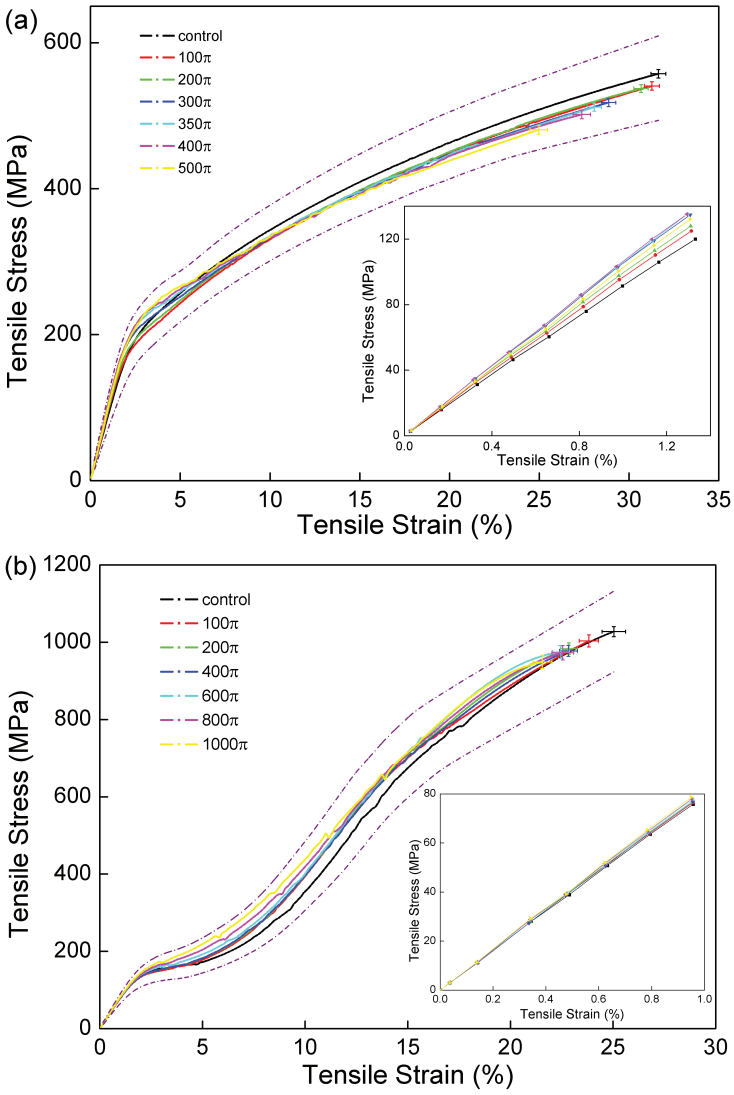

Figure 5.2: **Stress-strain Profiles of Twisted Silks**. (a) and (b) denotes the stress-strain profiles for *Bombyx mori* silkworm silk and *Nephila Pilipes* spider draglines ilk respectively. Different colors represent different extent of twisting, as indicated in each panel. Each stress-strain profile is derived by averaging over more than 40 samples. The error bars at one end of every stress-strain profile denote the standard deviation of the breaking points, and the dashed line is the envelop of stress deviation of untwisted silks along the strain range. The insets are the magnification of the linear threshold region.

mori silk is about 40% while that of *Nephila Pilipes* spider draglines is lower than 20%. Crystallites act as molecular junctions connecting protein macromolecules, a higher crystallinity leads to a more rigid and larger molecular network, which will be distorted or destroyed at weak junctions or defects under twisting. Hence, the internal protein molecular network within silkworm silk is largely deformed, subject to bending, twisting and elongating tension under twisting. The cross point occurs after the yield point where the β-sheet crystallites start to split massively. The twisted silk fibers are subjected to a relatively larger tension than the native silk, and they become inferior once the larger content of split crystallites dominate. However, a lower value of crystallinity of spider dragline silk makes smaller and more elastic molecular network. Due to the good elasticity of the inter-molecular network, the twisted spider dragline silk behaves like typical twisted elastomer.

5.2.2 Characteristic Quantities of Twisted Silks

To understand the effect of twisting on the mechanical properties in detail, the dependence of the mechanical quantities on twisting angle was analyzed.

The effect of twisting on the elastic modulus of silkworm silk is shown in Fig. 5.3(a). An optimal value of elastic modulus was found at the twisting angle about $300\pi \sim 400\pi$, with an enhancement about 20% of the original modulus of silkworm silk. Evidence of microfibrillar structure in silkworm silk has been reported in previous studies[34, 35]. Nano-fibrils will entangle together to form a spinning structure under twisting. Entanglement between small fibrils can act as obstacle for axial movement during tensile deformation.

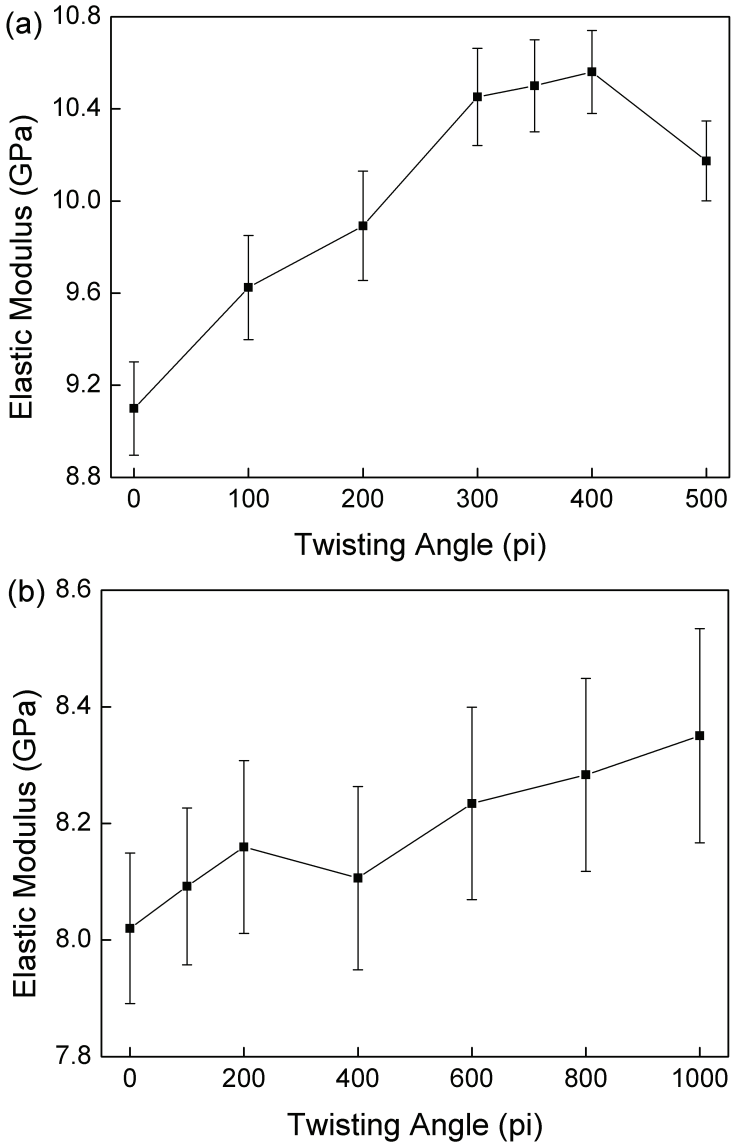

Figure 5.3: **Dependence of Moduli on Twisting Angle**. (a) Silkworm silk; (b) Spider dragline silk. The error bars in respective panels represent the standard deviation of the moduli under different twisting angles.

A simple calculation based on an elastomeric model was carried out, by setting the optimal modulus at twisting angle $\theta = 300\pi$. It was found that silk fibers needed to be strained for $\sim 2\%$ to maintain their length during the twisting process, which coincided with the strain where the yield point located. The breakage of the β-sheet crystallites after the yield point would destroy the original backbone of silkworm silk, which in turn softened the initial modulus of silk. Detailed calculation can be found in Section A.3 in the appendix chapter.

On the other hand, no significant change was found in the elastic modulus of spider silks for various twisting angles (Fig. 5.3(b)), and the slight increase may be caused by the tightened amorphous matrix or intra-protein β-sheets. The occurrence of such elastomeric behavior of longitudinal strengthening is obvious, because the massive breakage of the β-sheet crystallites happens at very high stress and strain, which causes the softening after the work-toughening region. The detailed mechanism was verified in Chapter 2.

From Fig. 5.4, the mechanical strength and extensibility of both silks became worse for higher twisting angles. The inferiority shows that twisting cannot further strengthen and enlarge the extensibility of silk, which originally possesses extraordinary strength and toughness. To this end, this method is not engineering applicable in the limiting cases when the breaking points need to take response.

In this section, we observed the dependence of mechanical properties of silkworm silk and spider dragline silk under various twisting angles. The strength and extensibility of the twisted silk fibers are inferior to the native ones, and a high level of twisting causes negative effect in these two quantities. However, an optimal

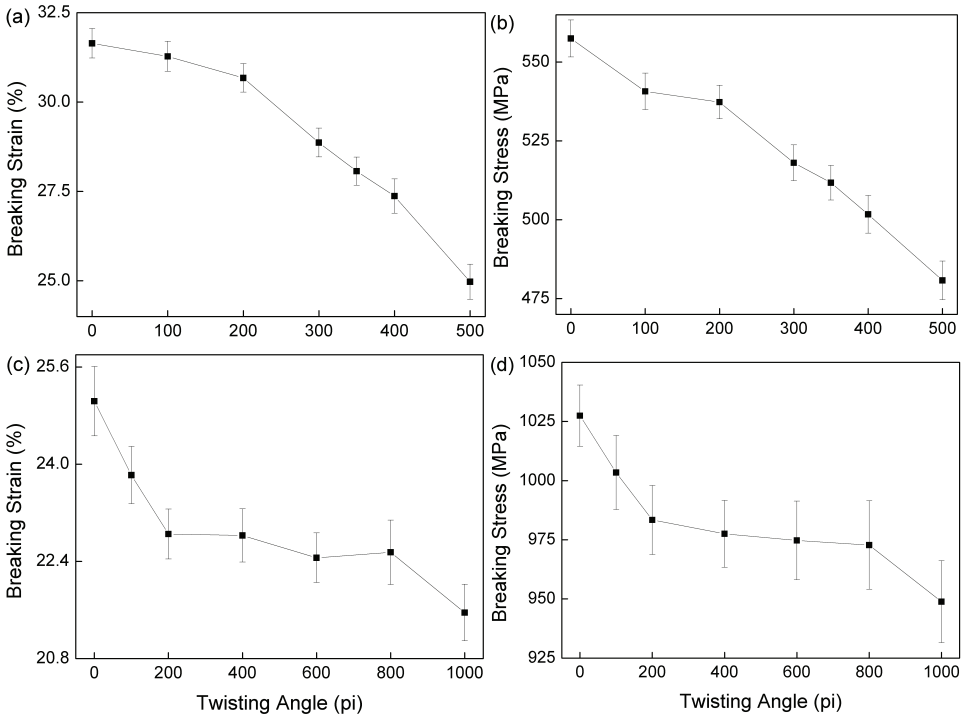

Figure 5.4: **Dependence of Silk Failure on Twisting Angle**. (a) and (b) Dependence of breaking strain and stress of silkworm silk on twisting angle. (c) and (d) Dependence of breaking strain and stress of spider dragline silk on twisting angle.

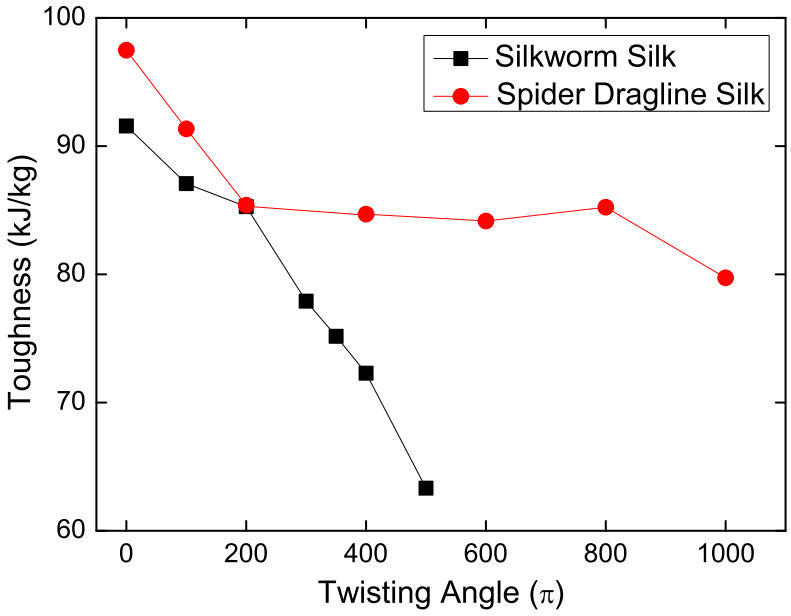

Figure 5.5: **Silk Toughness vs Twisting Angle**. Black solid squares: silkworm silk; Red solid circle: spider dragline silk.

elastic modulus was detected for twisted silkworm silk, and elastomeric behavior was detected of spider dragline silk.

5.3 Toughness and Engineering Implication

Toughness, defined as the material energy absorbance before its failure, was calculated for silkworm silk and spider dragline silk, as can been seen from Fig. 5.5. The inferiority of silk strength and extensibility by twisting was discussed in the last section, and the inferiority of toughness is straightforwardly understood.

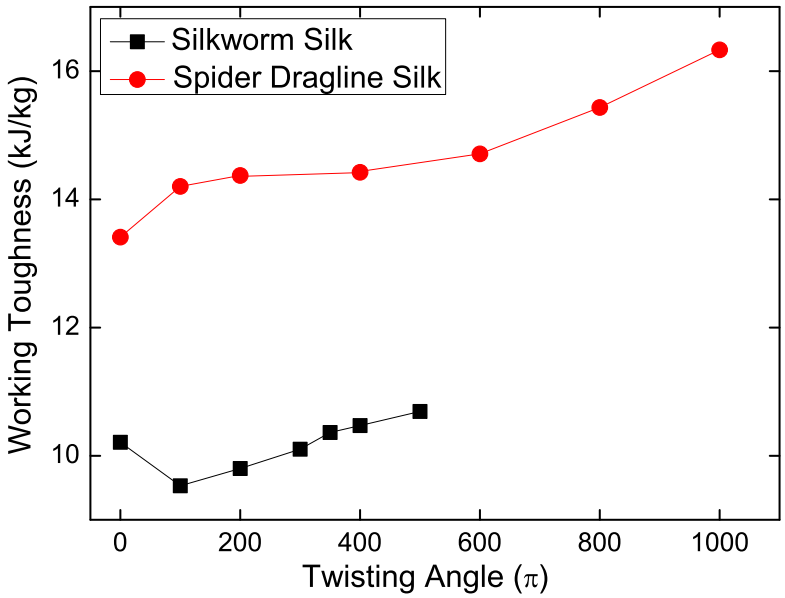

Figure 5.6: **Working Toughness of Twisted Silks**. Black solid squares: silkworm silk; Red solid circle: spider dragline silk. The calculation of the working toughness of respective silks is based on Eq. 5.2 and 5.3, where the strain bond were chosen to 7.5% for silkworm silk and 10.0% for spider dragline silk.

The strength, extensibility, and toughness are highly related to the breaking point of material. However, due to the variety of applications of silk, it is known that not all applications require the silk working in their extreme conditions. For instance, the strength of silk at low extension is of more concerns when it serves as surgical sutures, tendon repair and scaffold supporting materials. It is reasonable we reconsider the energy absorbability in low extension region, as shown in Fig. 5.6.

Here we define the "working toughness" of silkworm silk and spider dragline silk,characterizing

the low-strain energy absorbability, in the following:

$$E_w^{silkworm} = \int_0^{7.5\%} \sigma^{silkworm}(\epsilon)d\epsilon \tag{5.2}$$

$$E_w^{spider} = \int_0^{10.0\%} \sigma^{spider}(\epsilon)d\epsilon, \tag{5.3}$$

where $E_w^{silkworm/spider}$ denotes the working toughness of silkworm silk and spider dragline silk; $\sigma^{\cdot}(\epsilon)$ denote their respective stress at strain ϵ. The strain range we define for working toughness is chosen to be $\sim 1/3$ of the breaking strain(7.5% for silkworm silk and 10.0% for spider dragline silk). From Fig. 5.6, the working toughnesses of both silks increase with the increased twisting angle, although some of the working toughnesses of silkworm are lower than the untwisted one. This is because twisted silkworm silk is softened before reaching the unbiasedly chosen strains. Despite the slight increase of the Young's Modulus of spider dragline silk, the working toughness is enhanced for $\sim 25\%$, originated from the left-shift/early occurrence of the work-toughening process.

Therefore, in view of applications, silks acquire a higher rate of energy absorbability over low-strain range despite their softening and brittlement due to the large extent of twisting. Such properties may benefit them in some applications where the initial rigidity is more concerned.

5.4 Summary

This chapter discussed the effect of twisting on the longitudinal mechanical properties of silk. The Young's modulus, breaking stress, breaking strain and toughness were experimentally measured and compared among silk samples under various extent of twisting. It is found that there was an optimal twisting angle providing a highest modulus of silkworm silk. This was interpreted by the β-sheet crystallite breakage around the yield point. However, both types of silk become inferior under twisting with respect to their breaking point. The findings showed that silk materials did not fully behave like pure elastomers, but the high-level structures, especially the secondary structures, *i. e.*, the β-sheet crystallites, amorphous matrices and the molecular networks were dominant in shaping their mechanical behavior.

Besides, working toughness was defined by counting energy absorption in low-strain range, and a high extent of twisting gave rise to an increased working toughness for both silks. This result provided the engineering insight that silk could offer better rigidity for surgical sutures, scaffolds and other padding substrates. Overall, the study is indicative of the basic mechanical behavior of silk along cross-axis dimension, although there are yet no structural examination carried out for detecting the internal structural change during the twisting process[1].

[1]This work is collaborated with Qinqiu Deng, who conducted the experiments mentioned in Section 5.5.

5.5 Experimental

Sample Preparation:

The silkworm silk samples were reeled from Bombyx mori(B. mori) cocoons submerged in water at about $60°C$. All the silk reeled from silkworms was degummed by washing the fibers for 30 minutes in a $2wt\%$ solution of Marseille soap and $0.5wt\%$ of Na_2CO_3 in water at about $95°C$, followed by rinsing with deionized water. The process was repeated several times with fresh solutions and the degummed silk fibers were air dried.

Adult female *Nephila pilipes* spiders were anaesthetized by CO_2 and fixed to a black hard cardboard with tape. A plastic column attached to the computer controlled motor was used to collect the single major ampullate (MA) silk at a constant speed of $10mm/sec$. The temperature and relative humidity were kept at $25°C$ and RH 55%.

Twist Experiments

The silk sample mounted on the paper frame was fixed onto the wheel by the clip and paper slit. The motor-driven wheel was to control the desired twist angle. The spinning speed of the motor is $2\pi/sec$. The platform with adjustable height was to avoid causing unnecessary over-stretch of the silk sample. The twisted sample was then mounted carefully to a new paper frame for further tensile test.

Mechanical Measurements

To obtain the mechanical properties of the silk sample, Instron Micro Tester (Model 5848) was used to measure their stress-strain profiles. The force resolution is 0.5% of indicated load, position resolution is $0.02\mu m$, and strain rate is 50% per minute. The whole tests were performed at $22°C$ and the Relative Humidity is 60%.

Chapter 6

Conclusions and Outlook

Natural silk fibers attract extensive attention from scientific and engineering field due to their combination of good properties and increasingly widened applications. One of the main obstacles which inhibits the further development in biomimetic engineering is the unknown mechanism whereby silks possess high strength with respect to their structures. Hence, the ultimate goal of my research project is to reveal the intrinsic correlation between the structural features and the mechanical properties of natural silks. Several closely relevant topics, as discussed in respective chapters, uncover a facet of the structure-property relation of silk. Chapter 2 to Chapter 5 interpret the super-strength, mechanical profiles, and the energy absorbability of silk fibers in different domains and dimensions, from the view of their hierarchical nano-structures. Besides, Some feasible orientations of the silk study where further dedication of endeavor is worthwhile will be pointed out in this chapter, including their potential and currently encountered difficulties.

6.1 Conclusive Remarks

The investigation of correlation between the mechanical properties and nano-structures of silk fibers was discussed from Chapter 2 to Chapter 5.

In Chapter 2, the mechanical profiles of the silkworm silk and spider dragline silk were well interpreted by two major mechanisms. The massive splitting of the inter-protein β-sheet crystallites softens the mechanical strength of silkworm silk after the yield point, which also occurs at the high-strain end of the spider dragline silk. Nevertheless, the intra-protein β-sheets, solely observed in spider dragline silk, split at lower threshold forces due to their low compactness. The limited size makes the intra-protein β-sheets being fully dissolved into the amorphous matrix under certain stress, and the molecular network is tightened afterwards. The tightening of the amorphous matrix gives rise to an enhanced modulus, and is reflected as the work-toughening region in the mechanical profile of the spider dragline silk. The two mechanisms in our model were illustrated in the MD simulation, and the numerical results agree with the experimental measurement when properly setting the adjustable parameters.

In our modeling of the structures of silks, we confined the crystallites along the axis, and omitted the impact in the cross-axis direction. This simplification made the transverse structural factors into the modeling parameters as threshold forces and proportional constants E_i (i=0,1).

The issue raised by the oversimplification of the model in Chapter 2 was addressed in Chapter 3. A series-connected parallel-responsive model was proposed in order

to examine the influence of crystallite properties. The sizes of crystallites in each dimension, the crystallite orientation and crystallinity were incorporated in this model and the mechanical strength was discussed. Predicted relation shows that the breaking stress of silkworm silk is highly dependent on the crystallite orientation, which is quantified by the orientation function f. A dramatic increase of silk strength was observed when crystallites approaching the perfect alignment. Besides, the crystallinity has sub-linear relation with the breaking stress, consistent with the statement that crystallites act as the molecular junctions and reinforce the backbone of silk fibers.

Experimentally, we imposed the reeling fashion of varying reeling speeds, since it was proved to be an effective way to change the mechanical profiles of silks, thus the strength and toughness. Variations of the initial conformations of crystallite structures were detected. An increased reeling speed led to a higher crystallinity, a better crystallite orientation, as well as an nearly unchanged crystallite size in all dimensions. The mechanical strength by experimental measurements is in good accordance with that by the modeling of crystallite properties when the crystallite properties are substituted.

This work provided the upper limit of the silk strength tuned by solely changing the reeling speed, and it was predicted to be 1.2GPa, close to the strength of spider dragline silk. Moreover, the study developed a new inverse engineering method to design ultra-strong material by implementing the guideline extracted from our proposed theoretical model. This guideline-destination protocol gives rise to an efficiency leap in functional semi-crystalline material design in the future development along side the achievement of ultra-strong silk design by the combined

theoretical prediction and effective experimental strategy.

Chapter 4 reported the mechanical behavior of silkworm silk in the time domain. Stress relaxation experiments throughout the strain range were conducted, and a bipartite multi-exponential decaying pattern of the stress relaxation profiles was observed for various strains, which were grouped by the separation of the yield point. We designed the "step-relaxation" experiment to probe the viscoelastic behavior of silkworm silk for detailed analysis. By quantifying the energy dissipation ratio of silkworm silk with "Differential Relaxation Index", silkworm silk is found to have an extremely high level of energy dissipation compared with the conventional polymeric materials, *e. g.* Kelvar and rubber, making it a potential candidate as energy absorption material.

The structural factors were also revealed by the modeling proposed in this work. The "local strain induced thickening" mechanism provides a highly viscous environment of silkworm silk under tension. The "inter-protein β-crystallite splitting" takes effect to soften the silk when it is extended beyond the yield point. For Kelar and rubber, since there are no semicrystalline domains, only the mechanism of "local strain induced thickening" is applicable, leading to its good linearity of the positive relation between relaxation index and applied strain.

Additionally, an envelope of the mechanical profiles of silkworm silk was identified. The upper and lower limits of the stress-strain profile were derived from that under infinite or zero strain rate. Although the aging and creeping effects are not taken into account in the envelope characterization, the mechanical envelop still grants valuable information for the time-resolved application of silkworm silk.

Chapter 5 turned to considering the motion in the cross-axis dimension, and extensively investigated the influence of twisting on the longitudinal mechanical properties of silk. This is the first study on the coupling between different dimensions of silk materials. Twisting strategy was adopted in the experiments, and the Young's modulus, breaking stress, breaking strain and toughness were experimentally measured and compared among silks under various extent of twisting.

An optimal twisting angle was observed to maximize the Young's modulus of silkworm silk, which was interpreted as the β-sheet crystallite breakage around its yield point by a simplified elastomer model. However, no positive influence was found for strength and extensibility of both silkworm silk and spider dragline silk. The finding shows that silk materials do not fully behave like elastomers, but the high-level structures, especially the secondary structures, *i. e.*, the β-sheet crystallites, amorphous matrix and the molecular networks composed of them dominates their mechanical behaviors in different dimensions. Working toughness was defined to quantify the energy absorption in low-strain range. High energy absorbability at low strain range ($\sim 1/3$ of the breaking strains for respective silks) were achieved by a high extent of twisting, which gave rise to the engineering insight that twisted silk could offer better rigidity for durable biomedical applications, such as sutures, scaffold and other padding substrates.

From the above studies I have undertaken, it is evident to conclude that the secondary structures of silk materials have significant impact on their mechanical behavior. Protein macromolecules form semicrystalline domains. The β-sheet crystallites provide the high strength of silk while the amorphous molecular network offers good extensibility as well as a viscoelastic internal environment for its

extraordinary energy absorbability. By having a comprehensive understanding of the structural origin of silk's super strength, a bright perspective of the improvement of silk quality and the broadening of their applications can be foreseen in the near future.

6.2 Outlook to Future Research Perspective

Based on my results and the methods developed in my works, several directions remain open and they are worthwhile to undertake further studies.

6.2.1 Single Molecule Force Spectroscopy of Silk Proteins

Single Molecule Force Spectroscopy (SMFS) has been developed to be a sophisticated technique, allowing the study of nano-mechanical properties of natural bio-macromolecules and synthetic polymers since last decade. This technique is based on the instrument of atomic force microscopy (AFM). The SMFS technique is advanced for its high force sensitivity to pico-Newton and high space resolution down to sub-nanometer. It is not only used in exploring the random coiling structures which behave like elastomers, but also in the change of high-order structure in complicated structural domains. Due to these advantages, SMFS may catch some specific fingerprint information of nano-mechanical properties of polymer chains that cannot be achieved by conventional mechanical measuring methods.

Zhang and Oroudjev carried out the SMFS experiments for *Bombyx mori* fibroin

and recombinant spidroin[135, 149]. In the SMFS experiments of *Bombyx mori* fibroin, three types of force-extension curves were found, two of which could be fitted by the modified freely jointed chain (MFJC) model. Oroudjev's work provided an rough estimation of a minimal unfolding module size to be around 14 nm, which corresponded to the extended length of a single repeated module, 38 amino acids long. Both of the findings demonstrated the novel features of SMFS, distinguishing the different conformations of macromolecule chains.

However, the theoretical approaches available for analyzing the information or reproducing the force spectrum are few. One of the conventional model is the Worm-like Chain Model, which is suitable for polymeric chains with fitted persistence length; Another model proposed by J. M. Fernandezis's group, concerns the folding and unfolding rates of secondary structures, and a set of parameters are need for practical simulation. Molecular simulation is available with various choices of MD simulation packages designed specially for polymeric material. Current molecular simulation can handle millions of atoms at most, and the simulation speed is significantly elevated due to the advance of computer technology. Without giving many artificial parameters, the simulation can be done only with the information of topology (pdb files) and force fields (embedded in most packages).

Molecular simulation is capable of obtaining the conformation of macromolecules under given conditions, and the dynamics when the molecule is subject to external forces. This method may provide conformational insight of the macromolecules, and the dynamic insight of the structural change under stress. The difficulty of this approach is the time scale. The simulation time scale is down to the unit of picoseconds, while the unfolding rate ranges from mili-seconds or seconds. Another

issue is the "crowding" effect. If there are more than one macromolecules on neighboring sites, crowding may lead to the actual situation different from the simulated case.

6.2.2 Multiscale Modeling of Silk

The molecular simulation by recently developed force field packages is powerful, but the huge number of atoms or residues of macromolecules, together with the incompatible time scales, makes the simulation handled only for very few macromolecular chains. However, specifically for silk study, the development of such "bottom-up" method is crucial for revealing the mechanism of silk strength, because of the less assumptions needed in simulating their mechanical behavior, and more realistic conformation in reproducing the multiscale structures.

Up to the most recent progress through this path, it is yet evident to fully mimic the structural hierarchy of silk materials by a single crystallite, a confined amorphous region, or their simple combinations[91, 102]. Nova recently set a good example of connecting the crystalline and amorphous domain in series according to their content percentage, although such simple assembling of the secondary structural elements may not meet their realistic arranging manner[91].

The above modeling yields the assumption that the mechanical behavior of the lower-level structure has impact on that of the higher-level structure, but not vice versa. To this end, for investigating the structural origin in the scale of the whole fiber, an elastomeric network model can be adopted, with all structural "elements"

well defined, such as links and joints of the network. The multiscale modeling method has just been launched into the study of silk. But its bright prosperity can be foreseen since more intrinsic underlying "physics" and "mechanism" are expected to be revealed with concrete evidence.

Appendix A

A.1 Discrete Forms of Stress Calculation

In Chapter 2, integral forms were given of the stress calculation in Eq. 2.3 and 2.4, by calculating the exact values of effect elastic constant k_{eff} and the effect strain $\Delta x - \sum_{i=0}^{N} \Delta L_i$. The stress was analytically and numerically unsolvable, due to the quantity F appears in the upper limit of the integral while a parameter-dependent definite gaussian form integral can not be solved.

In practice, we considered the equation of motion for each confined crystallite. For instance, concerning a crystallite within the silkworm silk matrix, with two ends connected by its neighboring crystallites by amorphous chains. Since the mathematical form of the external stress causes the β-sheet crystallite in Eq. 2.1, the stress applied at each end F_i^+ and F_i^- can be calculated as follows:

$$
\begin{aligned}
F_i^{\pm} &= \frac{k_0}{1+\Theta(F_i^{\pm}-F_{th}(i))\frac{F_i^{\pm}-F_{th}(i)}{E_0 L_0}} \\
&\times \quad ((\Delta x_{i\pm1}-\Delta x_i)-\Theta(F_i^{\pm}-F_{th}(i))\frac{F_i^{\pm}-F_{th}(i)}{E_0}).
\end{aligned}
\tag{A.1}
$$

where L_0 is the original length of between crystallites, which is set to 1 in all simulations in Chapter 2. $\Theta(x)$ yields,

$$
\Theta(x) = \begin{cases} 0 & x \geq 0 \\ 1 & x < 0. \end{cases}
\tag{A.2}
$$

Hence, $F_i^{\pm}$ can be solved for individual crystallites by a self-consistent procedure as:

$$
\begin{aligned}
F_i^{\pm} &= \Theta(F_{th}(i)-F_i^{\pm})k_0(\Delta x_{i\pm1}-\Delta x_i) \\
&+ \quad \Theta(F_i^{\pm}-F_{th}(i)(\frac{F_{th}(i)}{2}-\frac{k_0 L_0}{2}-\frac{k_0^2 L_0}{2E_0} \\
&+ \quad \sqrt{(k_0 L_0+\frac{k_0^2 L_0}{E_0}-F_{th}(i))^2+4(\frac{F_{th}(i)k_0^2 L_0}{E_0}+k_0^2 L_0(\Delta x_{i\pm1}-\Delta x_i)))}
\end{aligned}
\tag{A.3}
$$

Thus, the equation of motion for crystallite i of mass m_i writes:

$$
m_i \Delta\ddot{x}_i = (F_i^{+}+F_i^{-})-\mu\Delta\dot{x}_i,
\tag{A.4}
$$

The series of Eq. A.4 was then simulated using Velocity Verlet Algorithm. The

stress responses were recorded as $F = F_N^-$ when the stress was almost balanced within the system ($\Delta\dot{x}_i \approx 0$).

The splitting process of β-sheet crystallites of spider dragline silk is similar to that of silkworm silk. However, the splitting process of intra-protein β sheets is slightly different. The additional item in conditional expression Eq. 2.3 represents the full destruction of the β sheets due to their small size and low compactness.

$$\begin{aligned} F_i^{'\pm} &= \Theta(F_{tr}(i) - F_i^{'\pm})\tilde{F}_i^{'\pm} \\ &+ \Theta(F_i^{'\pm} - F_{tr}(i))(\frac{k_0}{1 + \frac{F_{tr}(i) - F_{th}(i)}{E_1 L_0}} \\ &\times ((\Delta x_{i\pm1} - \Delta x_i) - \frac{F_{tr}(i) - F_{th}(i)}{E_1})), \end{aligned} \tag{A.5}$$

where $\tilde{F}_i^{'\pm}$ yields the form of Eq. A.7 by replacing E_0 with E_1. In analogy with Eq. A.4, Eq. A.6 is solvable for each intra-protein β-crystallite by writing down the similar equations of motion. For the spider dragline silk, we chose the percentage of the β-sheet crystallites is 50% out of the whole content of β-sheeted structures, which is consistent with the crystallinity of about 20% out of totally the 40% β-sheeted structures.

The most complicated case is the contact between intra-protein β sheets and β-sheet crystallites, which have different responses. In this situation, the elongation by splitting of β-sheeted structure is $\Delta L_{i/i+1}^{total} = \Delta L_{i+1}^- + \Delta L_i^{'+}$. For instance, in the case of $F_{tr}'(i) > F_i^{'+} > F_{th}'(i)$ and $F_{i+1}^- > F_{th}(i+1)$, the equation for stress calculation reads:

$$
\begin{aligned}
F_i^{+\prime}/-F_{i+1}^{-} &= \frac{k_0}{1+\frac{F_i^{\prime+}-F_{th}^{\prime}(i)}{2E_1L_0}+\frac{-F_{i+1}^{-}-F_{th}(i+1)}{2E_0L_0}} \\
&\times \ ((\Delta x_{i+1}-\Delta x_i)-\frac{F_i^{\prime+}-F_{th}^{\prime}(i)}{2E_1L_0}+\frac{-F_{i+1}^{-}-F_{th}(i+1)}{2E_0L_0}).
\end{aligned} \tag{A.6}
$$

where Newton's Third Law needs to be fulfil that $F_i^{\prime+} = -F_{i+1}^{-}$. Hence, the equations of motion writes in similar forms (distinguished by notation of "prime"), respectively for inter-protein β-sheet crystallites and intra-protein β sheets. The equations headed with "prime" are those for intra-protein β sheets.

$$
\begin{cases}
m_i\Delta\ddot{x}^{\prime}{}_i = (F_i^{\prime+}+F_i^{\prime-})-\mu\Delta\dot{x}^{\prime}{}_i \\
m_i\Delta\ddot{x}_i = (F_i^{+}+F_i^{-})-\mu\Delta\dot{x}_i.
\end{cases} \tag{A.7}
$$

Velocity Verlet Algorithm was applied for simulating the motion of crystallites subjecting to a constant rate strain. The stress responses were recorded as $F = F(')_N^-$ when the stress was almost balanced within the system ($\Delta\dot{x}(')_i \approx 0$).

A.2 Inverse Laplace Transform Analysis

The original Laplace Transform writes:

$$
F(s) = \mathcal{L}\{f(t)\} = \int_0^{\infty} e^{-st}f(t)dt, \tag{A.8}
$$

where s is a complex number, and $F(s)$ is the Laplace Transform of function $f(t)$ in t domain.

The stress relaxation function, with the consideration of non-aging materials, can be expanded be the Dirichlet series , which has the form:

$$R(\xi) = \sum_{i=0}^{N} E_i e^{-\xi/\tau_i} d\tau, \tag{A.9}$$

where ξ is time lag after the system is fixed to certain extension/strain. τ_i is the relaxation time and E_i is the corresponding weight of the relaxation component of characteristic relaxation time τ_i. For a infinite long Maxwell-like Chain, a continuous form of stress relaxation can be re-cast as:

$$R(\xi) = \int_0^{\infty} L^*(\tau) e^{-\xi/\tau} d\tau. \tag{A.10}$$

Herein, $L^*(\tau)$ is the continuous distribution of E_i in Eq. A.9. In practice to determine the weight coefficient E_i, an empirical choice of uniform distribution of τ_i in logarithmic scale is one of the good ways to deal with this ill-conditioned problem[150].

Set $L(\tau) = L^*(\tau) \times \tau$, and $\tau = 1/\zeta$, Eq. A.10 can be transformed to

$$R(\xi) = \int_0^{\infty} \zeta^{-1} L(1/\zeta) e^{-\xi\zeta} d\zeta. \tag{A.11}$$

Comparing with the Laplace Transform formulism (Eq. A.8), one can see that $R(\xi)$ is exactly the laplace transform of $\zeta^{-1}L(\zeta^{-1})$, and $\zeta^{-1}L(\zeta^{-1})$ can be regarded as the laplace coefficient. To solve $\zeta^{-1}L(\zeta^{-1})$, Inverse Laplace Transform is necessary to be carried out as:

$$\begin{aligned} f(t) &= \mathcal{L}^{-1}\{F(s)\} = \frac{1}{2\pi i}\lim_{T\to\infty}\int_{\gamma-iT}^{\gamma+iT} e^{st}F(s)ds \\ &= \lim_{k\to\infty}\frac{(-1)^k}{k!}(\frac{k}{t})^{k+1}f^{(k)}(k/t), \end{aligned} \tag{A.12}$$

where the integration is done along the vertical line $\Re e\{s\} = \gamma$ in the complex plane such that γ is greater than the real part of all singularities of $F(s)$, ensuring the contour path located in the region convergence. In the asymptotic form, $f^{(k)}(\cdot)$ is the kth derivative of function $f(\cdot)$.

In that sense, the weight coefficient distribution function can be written as:

$$L^*(\tau) = \lim_{k\to\infty}\frac{(-k\tau)^k}{(k-1)!}R^{(k)}(k\tau)/\tau. \tag{A.13}$$

Substituting to the discrete form in Eq. A.9, the weight coefficient yields:

$$E_i = \lim_{k\to\infty}\frac{(-k\tau_i)^k}{(k-1)!}R^{(k)}(k\tau_i)\ln 10\Delta, \tag{A.14}$$

where Δ is the resolution of the logarithm of relaxation time τ, *i. e.*, $\ln\tau$. From Eq. A.14, one can see that E_i is highly dependent on the values of every order

of derivative of function $R(\xi)$. However, noise level is not negligible from the experimental data in Fig. 4.2.

Therefore, we only adopt the principle of the method, by expanding the time series of stress relaxation function into multi-exponential form and determine the limited number of coefficients, τ_i and $E_\epsilon(\tau_i)$, as was conducted in Section 4.2.2.

A.3 Prediction of Optimal Modulus of Silk

I proposed a simple elastomeric model for silkworm at zero extension, because experimentally the gauge length was maintained during the twisting process. Several parameters are neglected in this model, as it was found in our later calculation that the bending and self-twisting of each fibril is not essential affecting the final results. Hence in this model, the Poisson Ratio, bending rigidity and twisting rigidity of each fibril are set to be 0.

The model is illustrated in Fig. A.1, so as the meanings of the physical quantities that will be used in later calculation. The shape of the cross section of silk fibril is set to be circle in my calculation for simplicity.

Hence, $L = \sqrt{\theta^2 r^2 + L_0^2}$, and the average extension can be calculated as follows:

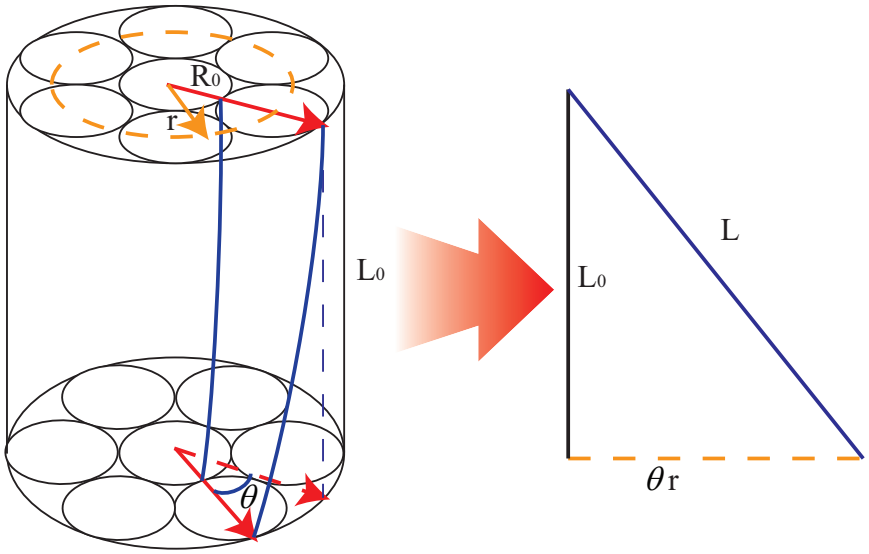

Figure A.1: **Simplified Elastomeric Model**. The left part demonstrates a segment of a twisted elastomer with twisting angle θ, and the radius of this elastomer is R_0. The elastomer fiber is constituted of fibril bundle(7 fibrils shown in the bundle is for display purpose). The fibril is original set to be aligned to the fiber axis, and the distance from the marked fibril by solid blue line to the central axis of fiber is r. The right part is the unfolded cylindrical surface of radius r, and the final length of the fibril after twisting is L.

$$\begin{aligned}\langle \Delta L \rangle &= \langle L - L_0 \rangle \\ &= \langle L \rangle - L_0 \\ &= \frac{1}{\pi R_0^2} \int_0^{R_0} \sqrt{\theta^2 r^2 + L_0^2} 2\pi r dr - L_0 \\ &= \frac{2}{3} \frac{-L_0^3 + L_0^2 \sqrt{L_0^2 + R_0^2\theta^2} + R_0^2\theta^2 \sqrt{L_0^2 + R_0^2\theta^2}}{R_0^2\theta^2} - L_0.\end{aligned} \tag{A.15}$$

Herein in the situation of silkworm silk studied, $L_0 = 20mm$, $R_0 = d/2 = 5.5\mu m$ and $\theta = 300\pi \sim 400\pi$. The twisted silk, maintaining its original gauge length is strained about $1.7\% \sim 2.9\%$ in average. This strain range coincide with that of yield point, after which β-sheet crystallites start to split massively.

Therefore, by implementing this simple elastomeric model, the optimal value of the Young's modulus of silkworm can be predicted to locate in the range of twisting angle between 300π and 400π. At least, it is confirmed that the Young's modulus is inferior for twisting angle larger than 400π. Before the twisting angle of 400π, silkworm silk behaves like pure elastomer. Spider dragline silk also behaves in an elastomeric way, but throughout all twisting angles, which is consistent of its breakage of β-sheet crystallite splitting in high strain range.

References

[1] D. Porter, *"Group Interaction Modelling of Polymer Properties"*, Marcel Dekker Inc, New York(1995).

[2] R. F. Foelix, *Biology of Spiders*(2nd Edition), Oxford University Press, Inc. and Georg Thieme Verlag, New York(1996).

[3] D.A. Parry and J. M. Squire, *Adv. Protein Chem.* **70**, 1(2005).

[4] T. D. Sutherland, P. M. Campbell, S. Weisman, H. E. Trueman, A. Sriskantha, W. J. Wanjura, and V. S. Haritos, *Genome Res.* **16**, 1414(2006).

[5] J. Shi, S. Lua, N. Du, X.-Y. Liu, and J. Song, *Biomaterials* **29**, 2820(2008).

[6] P. M. Cunniff , S. A. Fossey, M. A. Auerbach, J. W. Song, D. L. Kaplan, W. W. Adams, R. K. Eby, D. Mahoney and D. L. Vezie, *Polym. Adv. Technol.* **5**, 401(1994).

[7] D. A. Tirrell, *Science* **271**, 39(1996).

[8] C. Y. Hayashi, N. H. Shipley, and R. V. lewis, *Int. J. Biol. Macromol.* **24**, 271(1999).

[9] M. B. Hinman, J. A. Jones, and R. V. Lewis, *Trends Biotechnol.* **18**, 374(2000).

[10] N. Du, X. -Y. Liu, J. Narayanan, L. Li, M. L. M. Lim, and D. Li, *Biol. J.* **91**, 4528(2006).

[11] H. Heslot, *Biochimie* **80**, 19(1998).

[12] T. Asakura and D. L. Kaplan, *Encyclop. Agric. Sci.* **4**, 1(1994).

[13] G. H. Altman, F. Diaz, C. Jakuba, T. Calabro, R. L. Horan, J. Chen, H. Lu, J. Richmond, and D. L. Kaplan, *Biomaterials* **24**, 401(2003).

[14] U. J. Kim, J. Park, H. J. Kim, M, Wada, and D. L. Kaplan, *Biomaterials* **26**, 2775(2005).

[15] R. E. Marsh, R. B. Corey and L. Pauling, *Biochimica Et Biophysica Acta*, **16**, 1(1955).

[16] B.Fraser and T.P.MacRae, *"Conformations of Fibrous Proteins and Related Synthetic Polypeptides"*, Academic Press, New York(1973).

[17] C -Z. Zhou, F. Confalonieri, M. Jacquet, R. Perasso, Z -G. Li and J. Janin, *Proteins: Structure, Function, and Genetics*, **44**, 119(2001)

[18] S -W. Ha, H. S. Gracz, A. E. Tonelli and S. M. Hudson, *Biomacromolecules*, **6**, 2563(2005).

[19] H. M. Peters, *"Ecophysiology of Spiders"* (Ed. W. Nentwig), Springer, Berlin, 203(1987).

[20] H. M. Peters and J. Kovoor, *Zoomorphol.*, **111**, 1(1991).

[21] M. Xu and R. V. Lewis, *Proc. Natl. Acad. Sci. USA*, **87**, 7120(1990).

[22] Simmons, A. E. Ray and L. W. Jelinski, *Macromolecules*, **27**, 5235(1994).

[23] S. J. Lombardi, D. L. Kaplan, *Arachnol.*, **18**, 297(1990).

[24] D. J. strydom, T. Haylett, R. H. Stead, *Biochem. Biophys. Res. Commun.*, **79**, 932(1977).

[25] F. Vollrath and D. P. Knight, *Nature*, **410**, 541(2001).

[26] A. E. Terry, D. P. Knight, D. Porter and F. Vollrath, *Biomacromolecules*, **5**, 768(2004).

[27] E. Atkins, *Nature*, **424**, 1010(2003).

[28] H -J. Jin and D. L. Kaplan, *Nature*, **424**, 1057(2003).

[29] X. Chen, Z. Z. Shao, D. P. Knight and F. Vollrath, *Proteins-Structure Function and Bioinformatics*, **68**, 223(2007).

[30] C. W. P. Foo, E. Bini, J. Hensman, D. P. Knight, R. V. Lewis and D. L. Kaplan, *Appl. Phys. A-Mater. Sci. Process.*, **82**, 223(2006).

[31] R. E. Marsh, R. B. Corey and L. Pauling, *Biochim. Biophyis. Acta.*, **16**, 1(1955).

[32] Y. Takahashi, M. Gehoh and K. J. Yuzuriha, *J. Polym. Sci. Pt. B: Polym. Phys.*, **29**, 889(1991).

[33] L. K. Nicholson, T. Asakura, M. Demura and T. A. Cross, *Biopolymers*, **33**, 847(1993).

[34] Y. Shen, M. A. Johnson and D. C. Martin, Yu Shen, Michael A. Johnson, and David C. Martin, *Macromolecules*, **31**, 8857(1998).

[35] D. T. Grubb and L. W. Jelinski, *Macromolecules*, **30**, 2860(1997).

[36] A. Simmons, E. Ray and L. W. Jelinski, *Macromolecules*, **27**, 5235(1994).

[37] J. Kummerlen, J. D. van Beek, F. Vollrath and B. H. Meier, *Macromolecules*, **29**, 2920(1996).

[38] R. W. Work, *Textile Res.*, **47**, 650(1977).

[39] F. I. Bell, I. J. McEwen and C. Viney, *Nature*, **416**, 37(2002).

[40] O. Emile, A. Le Floch and F. Vollrath, *Nature*, **440**, 621(2006).

[41] O. Emile, A. Le Floch and F. Vollrath, *Phys. Rev. Lett.*, **98**, 167402(2007).

[42] S. Osaki, *Int. J. Biol. Macromol.*, **24**, 283(1999).

[43] J. M. Gosline, M. W. Denny and M. E. Demont, *Nature*, **309**, 551(1986).

[44] J. M. Gosline, M. E. Demont and M. W. Denny, *Endeavor*, **10**, 37(1986).

[45] M. A. Wilding and J. W. S. Hearle, in *"Polymeric Materials Encyclopaedia"*, Vol. **11**(Ed. J. C. Salamone), CRC, Boca Raton, Florida, (1996).

[46] Z. Shao and F. Vollrath, *Nature*, **418**, 741(2002).

[47] H. Paul, *"The Book of the Spider"*, Random House, New York(1994).

[48] J. C. Zemlin, *"Technical Report "*, **TR-69-29-CM**(AD 684333)(1968).

[49] G. Zhou, Z. Shao, D. P. Knight, J. Yan and X. Chen, *Adv. Mater.*, **21**, 366(2009).

[50] J. Yan, G. Zhou, D. P. Knight, Z. Shao and X. Chen, *Biomacromolecules*, **11**, 1(2010).

[51] M. Tsukada, G. Freddi, N. Kasai and P. Monti, *J. Polym. Sci.: Part B: Polym. Phys.*, **36**, 2717(1998).

[52] T. Kameda, K. Kojima, E. Togawa, H. Sezutsu, Q. Zhang, H. Teramoto and Y. Tamada, *Biomacromolecules*, **11**, 1009(2010).

[53] C. Jiang, X. Wang, R. Gunawidjaja, Y. -H. Lin, M. K. Gupta, D. L. Kaplan, R. R. Naik and V. V. Tsukruk, *Adv. Funct. Mater.*, **17**, 2229(2007).

[54] H. Baldassarre, B. Wang, C. L. Keefer, A. Lazaris and C. N. Karatzas, *Reproduction, Fertility and Development*, **16**, 465(2007).

[55] A. Lazaris, S. Arcidiacono, Y. Huang, J. -F. Zhou, F. Duguay, N. Chretien, E. A. Welsh, J. W. Soares and C. N. Karatzas, *Science*, **295**, 472(2002).

[56] S. -M Lee, E. Pippel, U. Gösele, C. Dresbach, Y. Qin, C. V. Chandran, T. Bräuniger, G. hause and M. Knez, *Science*, **324**, 488(2009).

[57] K. M. Parthasarathy, M. D. Nash, V. Arurnugam, V. Subramaniam and R. Sanjeen, *J. Appl. Polym. Sci.* **59**,2049(1996).

[58] V. Arumugam, M. D. Naresh, N. Somanathan and R. Sanjeevi, *J. Mater. Sci.* **27**, 2649(1992).

[59] D. L. Kaplan, S. J. Lombardi, W. S. Muller and S. A. Fossey, *Biomaterials: Novel Materials from Biological Sources*(Ed. D. Byron), Stockton Press, New York,(1991).

[60] *http://en.wikipedia.org/wiki/Silk*

[61] N. Hyde, *National Geographic*, **165**, 2(1984).

[62] T. J. Bunning, H. Jiang, W. W. Adams, R. L. Crane, B. Farmer and D. Kaplan, "Chapter: Applications of Silk" in in *Silk Polymers: Materials Science and Biotechnology* (Ed. D. Kaplan, W. W. Adams, B. Farmer and C. Viney), American Chemical Society, Washington D. C.(1994).

[63] D. H. Hollander, *Med. Hypotheses*, **43**, 155(1994).

[64] R. L. Moy, A. Lee and A. Zalka, *Am. Fam. Physician*, **44**, 2123(1991).

[65] N. Minoura, S. Aiba, Y. Gotoh, M. Tsukada and Y. Imai, *J. Biomed. Mater. Res.*, **29**, 1215(1995).

[66] K. Inouye, M. Kurokawa, S. Nishikawa and M. Tsukada, *J. Biochem. Biophys. Meth.*, **37**, 159(1998).

[67] G. H. Altman, R. L. Horana, H. H. Lu, J. Moreaua, I. Martinb, J. C. Richmondc and D. L. Kaplan, *Biomaterials* **23**, 4131(2002).

[68] M. G. Dunn, A. J. Tria, P. Kato, J. R. Bechler, R. S. Ochner, J. P. Zawadski and F. H. Silver FH, *Am. J. Sports. Med.*, **20**, 507(1992).

[69] M. G. Dunn, L. D. Bellincampi, A. J. Tria and J. P. Zawadski, *J. Appl. Polym. Sci.*, **63**, 1423(1997).

[70] J. Beard, *New Scientist*, **1847**, 18(1992).

[71] BBC News, http://news.bbc.co.uk/2/hi/science/nature/379338.stm (1999).

[72] D. V. Mahoney, D. L. Vezie, R. K. Eby, W. W. Adams and D. Kaplan, "Chapter: Aspects of the Morphology of Dragline Silk of *Nephila Clavipes*" in *Silk Polymers: Materials Science and Biotechnology* (Ed. D. Kaplan, W. W. Adams, B. Farmer and C. Viney), American Chemical Society, Washington D. C.(1994).

[73] R. Pachter, R. L. Crane and W. W. Adams, "Chapter: Approaches to Modeling and Properties of Model Peptides", in *Silk Polymers: Materials Science and Biotechnology* (Ed. D. Kaplan, W. W. Adams, B. Farmer and C. Viney), American Chemical Society, Washington D. C.(1994).

[74] N. Ganesh, W. Zhang, P. C. Mathias, E. Chow, J. A. N. T. Soares, V. Malyarchuk, A. D. Smith and B. T. Cunnigham, *Nature Nanotechnology*, **2**, 515(2007).

[75] W. Zhang, N. Ganesh, P. C. Mathias, and B. T. Cunningham, *Small*, **4**, 2199(2008).

[76] J. Zi, X. Yu, Y. Li, X. Hu, C. Xu, X. Wang, X. Liu and R. Fu, *Proc. Natl. Acad. Sci. USA.*, **100**, 12576(2003).

[77] O. Kratky, *Trans. Faraday Soc.*, **52**, 558(1956).

[78] S. S. Zimmerman, M. S. Pottle, G. Nemethy and H. A. Scheraga, *Macromolecules*, **10**, 1(1977).

[79] K. C. Chou, G. Nemethy, S. Rumsey, R. W. Tuttle and H. A. Scheraga, *J. Mol. Biol.*, **188**, 641(1982).

[80] S. A. Fossey, G. Nemethy, K. D. Gibson and H. A. Scheraga, *Biopolymers*, **31**, 1529(1991).

[81] G. Nemethy, M. S. Pottle and H. A. Scheraga, *J. Phys. Chem.*, **87**, 1883(1983).

[82] S. Keten and M. J. Buehler, *Appl. Phys. Lett.*, **96**, 153701(2010).

[83] B. R. Brooks, R. E. Bruccoleri, B. D. Olafson, D. J. States, S. Swaminathan and M. Karplus *J. Computat. Chem.*, **4**, 187(1983).

[84] D. Van Der Spoel, E. Lindahl, B. Hess, G. Groenhof, A. E. Mark, H. J. Berendsen, *J. Computat. Chem.*, **26**, 1701(2005).

[85] D. A. Case, T. E. Cheatham III, T. Darden, H. Gohlke, R. Luo, K. M. Merz Jr, A. Onufriev, C. Simmerling, B. Wang and R. Woods, *J. Computat. Chem.*, **26**, 1668(2005).

[86] J. C. Phillips, R. Braun, W. Wang, J. Gumbart, E. Tajkhorshid, E. Villa, C. Chipot, R. D. Skeel, L. Kale and K. Schulten, *J. Computat. Chem.*, **26**, 1781(2005).

[87] W. L. Jorgensen and J. Tirado-Rives, *J. Am. Chem. Soc.*, **110**, 1657(1988).

[88] T. Yamane, K. Umemura and T. Asakura, *Macromolecules*, **35**, 8831(2002).

[89] S. Keten, Z. Xu, B. Ihle and M. J. Buehler, *Nat. Mater.*, **9**, 359(2010).

[90] S. Keten and M. J. Buehler, *J. R. Soc. Interface*, DOI: 10.1098/rsif.2010.0149(2010).

[91] A. Nova, S. Keten, N. M. Pugno, A. Redaelli and M. J. Buehler, *Nano Lett.*, DOI: 10.1021/nl101341w(2010).

[92] H. Yoshimizu and T. Asakura,*J. Appl. Poly. Sci.*, **40**, 127(1990).

[93] J. Magoshi, Y. Magoshi and S. Nakamura, *J. Poly. Sci., Appl. Polym. Symp.*, **41**, 187(1985).

[94] L. R. G. Treloar, *"The Physics of Rubber Elasticity"*, Oxford University Press, Oxford(1975).

[95] L. Mullins, *"The Mechnical Properties of Biological Materials"* (Eds. J. F. V. Vincent and J. D. Currey), Society for Experimental Biology, Cambridge(1980).

[96] Y. Termonia, *Macromolecules*, **27**, 7378(1994).

[97] Y. Termonia, *Macromolecules*, **22**, 3633(1989).

[98] H. Zhou and Y. Zhang, *Phys. Rev. Lett.* **94**, 028104(2005).

[99] D. Porter, F. Vollrath, and Z. Shao, *Eur. Phys. J. E* **16**, 199(2005).

[100] F. Vollrath and D. Porter, *Appl. Phys. A: Solid Surf.*, **82**, 205(2006).

[101] F. Vollrath and D. Porter, *Soft Matter*, **2**, 377(2006).

[102] S. Xiao, W. Stacklies, M. Cetinkaya, B. Markert and F. Gräter, *Biophys. J.*, **96**, 3997(2009).

[103] M. A. Wilding and J. W. S. Hearle, *Polymeric Materials Encyclopaedia* **11**, 8307(1996).

[104] M. Kumar, K. J. Sanford, W. A. Cuevas, M. Du, K. D. Collier, and N. Chow, *Biomacromolecules* **7**, 2543(2006).

[105] C. Zhou, B. Leng, J. Yao, J. Qian, X. Chen, P. Zhou, D. P. Knight, and Z. Shao, *Biomacromolecules* **7**,2415(2006).

[106] Y. Wang, H. J. Kim, G. Vunjak-Novakovic, and D. L. Kaplan, *Biomaterials* **27**, 6064(2006).

[107] C. Vendrely and T. Scheibel,*Macromol. Biosci.* **7**, 401(2007).

[108] J. Kopecek, *Biomaterials* **28**, 5185(2007).

[109] M. Tuskada, Y. Gotoh, M. Nagura, N. Minoura, N. Kasai, and G. Freddi, *J. Polym. Sci.: Part B: Polym. Phys.* **32**, 961(1994).

[110] I. Krasnov, I. Diddens, N. Hauptmann, G. Helms, M. Ogurreck, T. Seydel, S. S. Funari, and M. Müller, *phys. Rev. Lett.* **100**, 048104(2008).

[111] D. Wilson, R. Valluzzi, and D. L. Kaplan, *Biophys. J.* **78**, 2690(2000).

[112] E. Bini, D. P. Knight, and D. L. Kaplan, *J. Mol. Biol.* **335**, 27(2004).

[113] J. Gatesy, C. Hayashi, D. Motriuk, J. Woods, and R. Lewis, *Science* **291**, 2603(2001).

[114] J. O. Esteivkrt, *J. Mol. Biol.* **2**, 350(1960).

[115] A. H. Simmons, C. A. Michal, and L. W. Jelinski, *Science* **271**, 84(1996).

[116] C -Z. Zhou, F. Confalonieri1, N. Medina, Y. Zivanovic1, C. Esnault, T. Yang, M. Jacquet, J. Janin, M. Duguet, R. Perasso and Z -G. Li3, *Nucleic Acids Res.* **28**, 2413(2000).

[117] F. Vollrath, B. Madsen, and Z. Shao, *Proc. R. Soc. Lond. B* **268**, 2339(2001).

[118] D. T. Grubb, *Macromolecules* **30**, 2860(1997).

[119] R. J. Young and S. J. Eichhorn, *polymer* **48**, 18(2007).

[120] C. Viney and F. I. Bell, *Current Opinion in Solid State and Materials Science*, **8**, 165(2004).

[121] J. P. O'Brien, S. R. Fahnestock, Y. Termonia and K. H. Gardner, *Adv. Mater.*, **10**, 1185(1998).

[122] F. Teule, A. R. Cooper, W. A. Furin, D. Bittencourt, E. L. Rech, A. Brooks and R. V. Lewis, *Nat. Protocols*, **4**, 341(2009).

[123] A. Seidel, O. Liivak and L. W. Jelinski, *Macromolecules*, **31**, 6733(1998).

[124] C. Holland, A. E. Terry, D. Porter and F. Vollrath, *Polymer*, **48**, 3388(2007).

[125] *"The Mechanical Properties of Biological Material"*(Eds. M. W. Denny, C. J. F. Vincent and J. D. Currey,), Cambridge University Press, Cambridge, UK(1980).

[126] T. Lefevre, M. E. Rousseau, and M. Pezolet, *Biophys. J.*, **92**, 2885(2007).

[127] J. D. van Beek, S. Hess, F. Vollrath and B. H. Meier, *Proc. Natl Acad. Sci. USA*, **99**, 10266(2002).

[128] B. L. Thiel, K. B. Guess and C. Viney, *Biopolymers*, **41**, 703(1997).

[129] L. D. Miller, S. Putthanarat, R. K. Eby and W. W. Adams, *Intl. J. Biol. Macromol.*, **24**, 159(1999).

[130] J. Perez-Rigueiro, C. Viney, J. Llorca and M. Elices, *Polymer*, **41**, 8433(2000).

[131] O. Liivak, A. Flores, R. Lewis and L. W. Jelinski, *Macromolecules*, **30**, 7127(1997).

[132] C. Riekel, B. Madsen, D. Knight and F. Vollrath, *Biomacromolecules*, **1**, 622(2000).

[133] M. Khan, H. Morikawa, Y. Gotoh, M. Miura, Z. Ming, Y. Sato and M. Iwasa, *Intl. J. Biol. Macromol.*, **42**, 264(2008).

[134] S. Cocco, J. Yan, J.-F. Léger, D. Chatenay and J. F. Marko, *Phys. Rev. E*, **70**, 011910(2004).

[135] W. Zhang, Q. Xu, S. Zou, H. Li, W. Xu, X. Zhang, Z. Shao, M. Kudera and H. E. Gaub, *Langmuir*, **16**, 4305(2000).

[136] L. F. Drummy, B. L. Farmer and R. R. Naik, *Soft Matter*, **3**, 877(2007).

[137] J. Pérez-Rigueiro, C. Viney, J. Llorca and M. Elices, *J. Appl. Polym. Sci.*, **70**, 2439(1998).

[138] D. Porter and F. Vollrath, *Adv. Mater.*, **21**, 487(2009).

[139] B. D. Cullity and S. R. Stock, *"Elements of X-ray Diffraction"*, Addison Wesley, Waltham, Massachusetts(1959).

[140] Junisbekov, T. M., Kestelman, V. N. & Malinin, N. I. "*Stess Relaxation in Viscoelastic Materials*", Science Publishers, Inc., Enfield, NH(2003).

[141] Gul, E. E. & Kuleznev, V. N. "*structure and Mechanical Properties of Polymers*", Vysshaya Shkola, Moscow, Russia(1972)

[142] Findley, W. N. *et al.* "*Creep and Relaxation of Nonlinear Viscoelastic Materials*", Dover Publications, New York(1989).

[143] X. Wu, X. -Y. Liu, N. Du, G. Xu and B. Li, *App. Phys. Lett.*, **95**, 093703(2009).

[144] V. K. Kothari, R. Rajkhowa and V. B. Gupta, *J. Appl. Polym. Sci.*, **82**, 1147(2001).

[145] A. V. Tobolsky and K. Murakami, *J. Polym. Sci.* **XL**, 443(1959).

[146] N. W. Tschoegl, *"The Phenomenological Theory of Linear Viscoelastic Behavior"*, Springer Verlag(1989).

[147] G. Zi, Z. P. Bažant, *J. Engr. Mech.*, **128**, 1331(2002).

[148] D. Ye, X. Wu, Y. Li, J. C. K. Tan and X. -Y. Liu, *"Torsional Relaxation and the Effect of Twisting in Enhancing the Tensile Strength of Silkworm Silk"*, UROP Report, National University of Singapore, Singapore(2010).

[149] E. Oroudjev, J. Soares, S. Arcidiacono, J. B. Thompson, S. A. Fossey and H. G. Hansma, *Proc. Natl. Acad. Sci. USA*, **99**, 6460(2002).

[150] Z. P. Bažant and S. Prasannan, *J. Eng. Mech.*, **115**, 1704(1989).

PHYSICAL MECHANISM OF SILK STRENGTH AND DESIGN OF ULTRA-STRONG SILK

WU XIANG

NATIONAL UNIVERSITY OF SINGAPORE

2010